Eindhoven University of Technology

MASTER

DC upset resistance welding

Modelling and control of a weld process

Naus, G.J.L.

Award date:
2005

DC upset resistance welding
Modelling and control of a weld process

G.J.L. Naus

TU/e Master Thesis
2004-2005

Supervisors:
prof. dr. ir. M. Steinbuch (TU/e)
dr. ir. W.J.A.E.M. Post (TU/e)
ir. R. Meulenberg (Fontijne Grotnes B.V.)

Engineering thesis committee:
prof. dr. ir. M. Steinbuch (Chairman, TU/e)
dr. ir. W.J.A.E.M. Post (TU/e)
ir. P.C. Teerhuis (TUD)
dr. ir. R.H.B. Fey (TU/e)
ir. R. Meulenberg (Advisor, Fontijne Grotnes B.V.)

University of Technology Eindhoven (TU/e)   Fontijne Grotnes B.V.
Department of Mechanical Engineering   Research and Development group
Division Dynamical Systems Design
Control System Technology group

Abstract

Fontijne Grotnes B.V. produces wheel rim production lines for the automotive industry. The DC upset resistance weld process is part of these lines. Coiled sheets are welded to a cylinder, which are used as basis for the final wheel rims. The control and the present theoretical basis of this weld process are mainly based on practical experience. It is difficult to define the quality of a weld with respect to the weld process or to influence the quality of a weld. Temperature progress during the weld process is not defined nor measured and the position is not actively controlled although these are the most important variables of the weld process.

Consequently a theory, based on the equilibria present in the systems of the weld process, is developed. Experiments are performed to validate this theory. The various parts of the weld process are modelled and combined to a simulation model for off-line simulation of the process. This model is validated by comparing the resulting pressure, electrical current and position progress to experimental results. Special attention is given to the modelling and control of the hydraulic system. This has resulted in a relatively easy model-based controller design and a paper on the modelling and control of hydraulic systems focussing on position control.

Based on the renewed and extended insight in the weld process, a new control strategy has been developed. A MIMO feedback tracking controller is developed based on an on-line temperature calculation using classic control actions. The temperature, pressure and position progress during the weld process now are user-defined by means of reference trajectories. To facilitate working with the MIMO control problem, MCDesign, a tool for MIMO controller design is developed. The new control strategy is implemented and tested successfully.

Samenvatting

Fontijne Grotnes B.V. produceert productie straten voor de fabricage van velgen. Het gelijkstroom weerstand stuik lasproces is onderdeel van deze straten. Rond gebogen metalen platen worden tot cylinders gelast. Deze cylinders vormen de basis voor de uiteindelijke velg. De beheersing van het lasproces en de huidige theoretische basis hiervan, zijn voornamelijk op trial and error gebaseerd. Het is lastig om de kwaliteit van een las te benvloeden en deze te relateren aan het lasproces. De proces temperatuur en het verloop van de positie zijn de belangrijkste proces variabelen. De proces temperatuur is echter niet gedefinieerd en wordt ook niet gemeten. Daarnaast wordt de positie niet actief geregeld.

Daarom is een theorie ontwikkeld die gebaseerd is op de evenwichten van de in het lasproces aanwezige systemen. Experimenten zijn uitgevoerd om deze theorie te onderbouwen. De verschillende onderdelen van het lasproces zijn gemodelleerd en gecombineerd tot een simulatiemodel, waarmee het proces off-line gesimuleerd kan worden. Het model is gevalideerd door het verloop van de druk, de elektrische stroom en de positie te vergelijken met experimentele resultaten. De modellering en regeling van het hydraulische systeem hebben speciale aandacht gekregen. Dit heeft geresulteerd in een relatief eenvoudig model-gebaseerd ontwerp van een regeling. Daarnaast is een paper geschreven over het modelleren en regelen van een hydraulisch systeem, waarbij de focus ligt op positie regeling.

Een nieuwe regelstrategie is ontwikkeld op basis van het vernieuwde en uitgebreide inzicht in het lasproces. Gebaseerd op een on-line temperatuur berekening is een MIMO feedback regelaar ontworpen, waarbij gebruik is gemaakt van klassieke regeltechniek. Het verloop van de temperatuur, de druk en de positie tijdens het lasproces wordt nu voorgeschreven door middel van referentie trajectories. Om het ontwerp van MIMO regelaars te vergemakkelijken, is MCDesign ontwikkeld. De nieuwe regel strategie is gemplementeerd en succesvol getest.

Contents

Nomenclature and parameters

The parameters defined in this list of nomenclature correspond to the setup at Fontijne Grotnes B.V. and the material used in the experiments described in section 2.3.

a_o radius of a circle (m), eq. 2.14

A cross section of a (coiled) sheet (mm^2)

A_c contact surface between the sheet ends (m^2)

A_{eff} effective cylinder surface (m^2), $(= 1.57 \cdot 10^{-3} \ (\text{m}^2)$ in the setup)

A_p cross section surface of the piston (m^2), $(= 2.8 \cdot 10^{-3} \ (\text{m}^2)$ in the setup)

A_r cross section surface of the rod (m^2), $(= 1.3 \cdot 10^{-3} \ (\text{m}^2)$ in the setup)

b diameter of the orifice of the spool valve (m), eq. C.4

c_d compensation factor $(\text{kg}^{-0.5}\text{m}^{1.5})$, eq. C.4

C_o hydraulic stiffness (Pam)

C_p specific heat $(\text{Jkg}^{-1}\text{K}^{-1})$

d damping (Nsm^{-1})

d_{el} elastic damping of the material (Nsm^{-1}), $(= 5.0 \cdot 10^6 \ (\text{Nsm}^{-1})$ in the setup)

d_m damping of the material (Nsm^{-1})

d_p piston diameter (m), $(= 65 \cdot 10^{-3}$ (m) in the setup)

d_{pl} plastic damping of the material (Nsm^{-1})

d_{pr} rod diameter (m), $(= 40 \cdot 10^{-3}$ (m) in the setup)

dx part of L (m), eq. 3.1

$d\dot{x}$ speed of displacement (ms^{-1})

dV volume (m^3)

dy (a part of the) width of a (coiled) sheet (m)

dz (a part of the) height of a (coiled) sheet (m)

E Young's modulus (Pa)

E_{oil} oil stiffness (Pa), $(= 8 \cdot 10^8$ (Pa) in the setup)

F force (N)

F_f friction force (N)

F_{up} upset force (N)

G approximation gain $(-)$, $(= 1 \cdot 10^6$ $(-)$ in the setup), eq. C.14

$G_{F_f 1}$ friction force gain $(-)$, $(= 7.63 \cdot 10^5$ $(-)$ in the setup), eq. 3.15

$G_{F_f 2}$ average friction force $(-)$, $(= 7.63 \cdot 10^5$ $(-)$ in the setup), eq. 3.15

h height of a (coiled) sheet (m)

HB Brinell Hardness (Pa)

HB_r Brinell Hardness at room temperature (Pa), $(= 200 \cdot 10^6$ (Pa) in the setup)

i electrical current (A)

$\dot{i}$ change in electrical current per time unit (A)

i_1 electrical current directed through the material in between the clamps (A)

i_2 electrical current directed through the material outside the clamps (A)

k stiffness(Nm^{-1})

k_{el} elastic stiffness of the material (Nsm^{-1}), $(= 87.5 \cdot 10^6 \ (\text{Nsm}^{-1})$ in the setup)

k_m stiffness of the material (Nsm^{-1})

k_{pl} plastic stiffness of the material (Nsm^{-1}), $(= 0 \ (\text{Nsm}^{-1})$ in the setup)

L	distance between the clamps (m)	Q_i	internal energy (J)
L	maximum stroke of the hydraulic cylinder (m), ($= 30 \cdot 10^{-3}$ (m) in the setup)	Q_l	loss of energy (J)
		Q_r	radiation energy (J)
		Q_s	total, section specific, energy supply (J)
L_d	dead zone per cylinder chamber (m)		
L^*	total inner length of the hydraulic cylinder (m)	Q_y	internal energy of the material deforming into the upset (J)
m	mass (kg), ($= 300$ (kg) in the setup)	$q_{out,i}$	mass flow out of cylinder chamber i (m^{3}s^{-1})
N	number of sections ($-$)		
p	pressure (Pa)	Q_{Rb}	heat generation due to R_b (J)
p_{cl}	clamping pressure (Pa)	Q_{Rc}	heat generation due to R_c (J)
p_e	small variation in p_o ($-$)	$r_{b,i}$	bearing leakage coefficient ($-$), eq. C.24
p_i	pressure in cylinder chamber i (Pa)		
p_n	normalised pressure ($-$)	r_p	piston leakage coefficient ($-$), eq. C.25
p_o	linearisation point of p_n ($-$)		
p_{pump}	pump or supply pressure (equals p_s) (Pa), ($= 10 \cdot 10^6$ (Pa) in the setup)	R_b	bulk resistance (Ω)
		$R_{b,r}$	bulk resistance at room temperature (Ω)
p_s	supply pressure (Pa), ($= 10 \cdot 10^6$ (Pa) in the setup)	$R_{b_{back}}$	bulk resistance of the (coiled) sheet outside the clamps (Ω)
p_{tank}	tank pressure (Pa), ($= 0$ (Pa) in the setup)	$R_{b_{back},r}$	bulk resistance of the (coiled) sheet outside the clamps at room temperature (Ω)
p_{up}	upset pressure (Pa)		
p_y	yield pressure, equals σ_y (Pa)		
$\dot{p}_i$	change in pressure in cylinder chamber i (Pas^{-1})	R_c	contact resistance (Ω)
		R_{cl}	contact resistance between the clamps and the (coiled) sheet (Ω)
$\dot{p}_n$	normalised change in pressure ($-$)		
p_1	pressure in cylinder chamber 1 (Pa)	R_p	normalised piston leakage coefficient (Pam^{-1})
p_2	pressure in cylinder chamber 2 (Pa)		
p_∞	atmospheric pressure (Pa)	R_{tot}	total resistance of a (coiled) sheet (Ω)
P	pressure (Pa)		
P_L	load pressure (Pa)	t	time (s)
P_{ref}	reference pressure (Pa)	t_i	starting time of the weld process (s)
q_i	volume change (m^{3}s^{-1}), eq. C.16	t_h	heating time (s)
$q_{in,i}$	mass flow into cylinder chamber i (m^{3}s^{-1})	t_p	gap-closing time (s)
		t_{tot}	total time of the weld process (s)
q_l	flow from the servo valve to the hydraulic cylinder (kgm^{-3})	t_{tr}	time of the transition from elastic to plastic material behaviour (s)
$q_{Lb,i}$	leakage flow over the bearing out of cylinder chamber i (m^{3}s^{-1}), eq. C.24	t_y	process time at the start of t_{tr} (s)
		T	temperature (K)
		T_e	decrease in yield temperature due to σ_e (K)
q_{Lp}	leakage flow over the piston from cylinder chamber 1 to 2 (m^{3}s^{-1}), eq. C.25		
		T_i	temperature of section i (K)
		T_m	melting temperature (K), ($= 1630$ (K) in the setup)
q_n	normalised flow ($-$), ($= 1.67 \cdot 10^5$ ($-$) in the setup)		
		T_r	room temperature (K), ($= 298$ (K) in the setup)
$Q_{c,h}$	horizontal energy conduction (J)		
$Q_{c,v}$	vertical energy conduction (J)	T_{ref}	reference temperature (K)
Q_h	heat generation (J)	$T_{y,r}$	yield temperature for infinitesimal small σ (K)

$\dot{T}_{cd}$	speed of cooling down (Ks^{-1})		ϵ_T	temperature error (K)
u_i	inverter control signal (mA), ($= 0\ldots1$ (mA) in the setup)		ϵ_y	yield strain (m)
			ϵ_y	position error (m)
u_v	servo valve control signal (mA), ($= -1\ldots1$ (mA) in the setup)		η	linearisation point of x_n ($-$)
			λ	coefficient of thermal conductivity (Jm^{-1}K^{-1})
U	potential difference over the clamps (V)		ξ_{cs}	damping of ω_{cs} ($-$), ($= 0.6$ ($-$) in the setup)
v	speed (ms^{-1})			
V	volume (m^3)		ξ_v	damping of $\omega_{v,o}$ ($-$), ($= 0.7$ ($-$) in the setup)
V_i	volume of cylinder chamber i (m^3)			
$\dot{V}_i$	volume change of cylinder chamber i (m^{3}s^{-1})		ξ_{URW}	compensation factor ($-$), ($= 12$ ($-$) in the setup), eq. 2.20
w	width of a (coiled) sheet (m)		ξ_{Zm}	compensation factor ($-$), ($= 3$ ($-$) in the setup), eq. 2.16
x	distance between the clamps (m)			
x	length of the orifice of the spool valve(m), eq. C.4		ρ	specific mass (kgm^{-3}), ($= 7850$ (kgm^{-3}) in the setup)
x_e	small variation in x_o ($-$)		ρ_i	oil density of cylinder chamber i (kgm^{-3})
x_{in}	displacement of the spool valve (m)			
x_{max}	maximum stroke of the spool valve (m)		ρ_e	electrical resistivity (Ωm)
			ρ_o	oil density at atmospheric pressure (kgm^{-3})
x_n	normalised spool valve displacement ($-$)			
x_o	linearisation point of x_n ($-$)		$\rho_{e,r}$	electrical resistivity at room temperature (Ωm), ($= 3.45\cdot10^{-4}$ (Ωm) in the setup)
x_{out}	displacement of the spool valve (m)			
$\dot{x}$	speed of displacement of the right clamp (ms^{-1})		$\dot{\rho}$	change in oil density (kgm^{-3}s^{-1})
			σ	stress (Pa)
$\dot{x}_n$	velocity of the normalised spool valve displacement ($-$)		σ_e	external stress (Pa)
			σ_y	yield stress (Pa)
$\ddot{x}$	acceleration (ms^{-2})		$\sigma_{y,I-II}$	yield stress at the switch from phase I to II (Pa)
y	displacement of the rod (m)			
y_{ref}	reference position (m)		$\sigma_{y,II-III}$	yield stress at the switch from phase II to III (Pa)
$\dot{y}$	speed of the rod (ms^{-1})			
			$\sigma_{y,r}$	yield stress at room temperature (Pa)

Greek letters

α_{th}	thermal expansion coefficient (K^{-1})		Φ_i	mass flow of cylinder chamber i (kgs^{-1})
α_{rho}	coefficient of thermal resistance (ΩmK^{-1})		ω_{cs}	natural frequency of the converter system (Hz), ($= 1000$ (Hz) in the setup)
ΔP	pressure difference (Pa)			
ΔT	difference in temperature (K)			
Δv	difference in speed (ms^{-1})		ω_o	natural frequency of the hydraulic cylinder (Hz)
$\Delta\sigma$	difference in stress (Pa)			
ϵ	strain (m)		$\omega_{v,o}$	natural frequency of the servo valve (Hz), ($= 200$ (Hz) in the setup)
ϵ	overlap of the servo valve (m), ($= 0$ (m) in the setup), eq. C.7			
ϵ_P	pressure error (Pa)			
ϵ_{th}	emissivity constant (m), ($= 0.56$ (m) in the setup)			

Preface

The assignment discussed in this report was executed at Fontijne Grotnes B.V. in Vlaardingen, within the framework of a Master's Thesis at the department of mechanical engineering of Eindhoven University of Technology. The assignment is a result of the R&D-team of Fontijne Grotnes B.V. examining the DC upset resistance weld process used in their wheel rim production lines. Accordingly, the assignment was performed working in this team.

The weld process involved is driven by a force and an electrical current. The process is divided into 5 phases based on position and time restrictions. The current weld program prescribes a constant force and electrical current in each phase, depending on the measured position and time. Based on understanding the process, a new control strategy has to be developed including continuous control of significant process variables. The original assignment consisted of three parts. The first part was to expand and create a better insight in the weld process, secondly to develop a reliable model of the process to contribute to this insight and finally to develop a new control strategy.

In the first chapter an introduction of the weld process used is given and the assignment is expound and defined. A description of the weld process, including a theoretical approach and an experimental validation is discussed in Chapter 2. In the next chapter a model of the weld process and the various systems is developed, from which a simulation model results. Special attention is paid to the modelling and control of the hydraulic system. In Chapter 4 the development of a new control strategy including the implementation and the results, is discussed. To facilitate the design of the controller, a tool specialised in dealing with MIMO control problems has been developed.

Besides the stated assignment, the goal was to become familiar with working in a medium-sized company like Fontijne Grotnes B.V. A nice cooperation with the other members of the team and fellow students at the company were instructive and pleasant. Furthermore, the experience of a year working at the company and going through the various departments and projects gave a good impression of the company.

Chapter 1

Introduction

1.1 Fontijne Grotnes B.V.

Fontijne Grotnes B.V. [Fontijne, (web)] was established in 2000 by the acquisition of Grotnes Metalforming Systems, Chicago, Illinois, U.S.A., by Fontijne Holland, Vlaardingen, the Netherlands. A company combining nearly 200 years of experience as a manufacturer of metalforming equipment for the wheel industry, sizing equipment, nuclear supercompactors, laboratory platen presses and services was established. Fontijne is a leading European supplier of wheel and rim manufacturing systems, while Grotnes continues to supply other markets, with the two companies working in co-operation to innovate the product line and lead the industry.

Fontijne Grotnes BV
Designers and Manufacturers
of special machinery

Figure 1.1: the company logo of Fontijne Grotnes B.V.

Fontijne develops custom machinery solutions for the expanding, coiling, rotary roll forming and welding of cylindrical metal parts. These parts are utilised in transportation, aerospace, agriculture, petroleum, appliance, and forging industries. Their customers' products range from the simple: wheel rims and pipe couplings, to the sophisticated: missile tubes and jet engine rings and nozzles. Fontijne can carry out an entire forming process or a single production module.

1.2 A rim production line

The wheel rim production lines developed by Fontijne vary in the range of very small spare tire rims for passenger cars to large rims for industrial trucks. So cross section of about 350 mm^2 to 3000 mm^2 and more are involved. Fontijne produces completely automated and hand supported production lines as well as parts of the lines and single machines. Several techniques to produce rims exist like deep drawing and casting (for example for aluminum rims). At Fontijne, however, the rims are made out of a sheet of metal which is coiled, welded and profiled. A production line for this kind of process consists of five main parts, each including various fabrication / production steps and separate machines. In Figure 1.2 an overview of the processes in a complete rim production line is shown.

The rim production line starts with a straightener. The straightener uncoils and cuts the material, which is supplied on big coils. In the preparation line, the cut-to-length sheets are coiled and welded to cylinders. This line ends with the removal of the upset resulting from the welding.
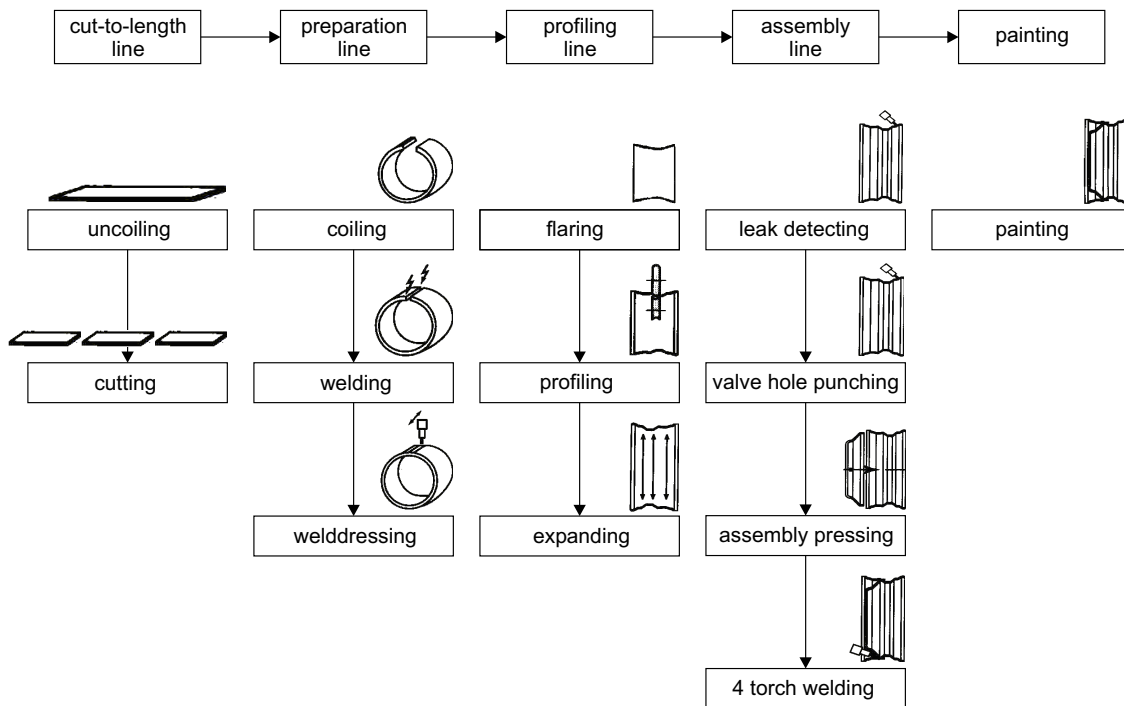
Figure 1.2: overview of the processes in a rim production line.

Next the profile is formed into the rims. Most loss of rims occurs at the flaring process due to cracking at the welding seams or just beside it. In this flaring process two cones are pressed into both sides of the cylinders. The profiling ends with an expanding step to give the rims their final size. The total production line ends with painting, after a leak detection test, the punching of a valve hole and the assembly of a disc into the rims.

The machinery for the rim production line is partly developed by Fontijne itself and partly acquired. One of the machines that Fontijne has developed itself is the direct current (DC) upset resistance welding machine [Fontijne, 2001]. The involved weld process is a butt welding process used in rim production lines and for example spot welding. Two sheet of metal are pushed together sideways with a large amount of force. An electrical current is directed through the sheets and heat is formed due to the resistance to conduct electrical current of the butt-joined material. This resistance is highest at the seam between the two sheets. When the temperature is high enough, the sheet ends start to yield, upset is formed and the sheets are welded together [key-to-steel, (web)]. Commonly used for this kind of weld process are alternating current (AC) welders because of their robustness. Using AC welding, the temperature is increased to the metal's melting temperature. An arc arises over the seam between the two sheets and the melting metal spatters away. In this way the usually polluted sheet ends are burned away. If enough of the metal is burned away, the sheets are welded together. This costs a lot of energy and requires much power, not only because the metal is burned away, but also by the use of alternating current. Using alternating current instead of direct current, the peak currents needed to achieve a certain average (RMS), are much higher. This affects the efficiency of the energy transfer to the welding seam and makes the process more susceptible to abortion. Using DC welding, the metal is only heated to its yield temperature and then welded together. In this way the weld process elapses much smoother and accordingly can be controlled more easily. Shorter weld times, less energy consumption, less loss of material and no spattering, which makes it a much cleaner process, are the main advantages [Kucklick, 1996].

The quality of a weld is defined to be good if the weld survives the imposed deformations

of the following processes in the rim production line. The flaring process is the first significant deformation step after the weld process. At this process up to 2% loss of rims is present due to cracking at the welding seam or just beside it. The quality of the weld is dependent on the temperature progress of the material during the weld process [Mast, 2000], [Put,1999], [NIMR, 2005]. The NIMR (Netherlands Institute *for* Metal Research) [NIMR, (web)] is doing research in this field, which has to result in guidelines for an optimal progress of the weld process. In this way the quality of a weld can be determined from the results of the weld process itself and besides may be influenced willfully.

Fontijne has developed their own welding machine series for the DC upset resistance weld process, the Fontijne Resistance Welders (FRW-series) [Fontijne, 2001]. An overview of the weld process and the welding machine used is given in Chapter 2. The software to control the process, WELD2000 [Fontijne, 2000], is developed by Fontijne itself as well. It is implemented on the FRW-series. Nowadays Fontijne is making a new move by implementing WELD2000 at welding machines of competitors already in the field. Supported by the success of this strategy, control of the weld process has become one of the points of attention of the company. Customers are very interested in new developments in this field since problems exist with current rim production lines that are attributed to the weld process. If the weld process becomes more robust and reliable, not only failure can be diminished, but it also gives sight at shorter welding times. The weld process often is one of the bottleneck processes as for time consuming processes in a automated rim production line. So the benefit of a tenth of a second per produced rim pays off a lot in producing 900 to 1100 rims per hour.

Consequently this study to the DC upset resistance weld process as performed at Fontijne, first of all is aimed at a good insight in the process. This has to result in a more robust and reliable control strategy. Besides, if the process is more robust and reliable, other advantages may be taken advantage of like decrease of the needed upset. At the moment, simply a large upset is used to be sure all the pollution in the welding seam is removed and the resulting weld is airtight. The amount of energy used may be optimised by which energy can be saved. Furthermore the insight in the process may be expanded to other resistance welding principles like spot welding.

1.3   Assignment

The assignment as initially defined by Fontijne consisted of two main parts. Firstly the already available theory and modelling of the DC upset resistance weld process had to be completed. Secondly a new controller for the weld process had to be developed, based on the attained insight in the weld process. The controller would be position or pressure based and eventually parts of the controller might become learning because of the repetitive character of the process.

The available theory and modelling appeared to be too fragmented to simply complete and use as a base for the development of a controller. Consequently the insight in the weld process and modelling part of the assignment are emphasised in the first place. The feasibility of the development of a test setup containing a hydraulic system and nonlinear springs was examined. This was stopped when the damping instead of the stiffness of the material appeared to be most significant in the second part of the process. A simulation model to perform off-line simulations of the weld process has to be developed to contribute to the validity of the resulting theory and modelling. Next the MIMO control problem has to be solved in a way the resulting controller is based on the theory and modelling. In designing the controller the complexity of it has to be taken into account considering implementation of it at welding machines in the field.

A secondary requirement of the assignment was a structured and well documented way of working so that others are able to use the developed tools and performed experiments as well.

Chapter 2

The weld process

Before modelling can take place, a good insight in the weld process is inevitable and needed. Various studies to the weld process are performed already. The most significant studies are Meulenberg [2002], Put [1999] and Legemaate [1997]. In most cases however, only a short overview of the weld process is used as a direct introduction to modelling. Up till now, a lack of insight in the process has resulted in problems further on in the development of a new control strategy. Consequently this study is started with an overview of the systems and the equilibria present during the weld process. This is followed by a discussion of the results of experiments. These experiments are performed to contribute to the insight in the process and validate the theory. To start with, the experimental setup used during this study is discussed and an introduction to the weld process is given.

2.1 Experimental setup

The FRW-series are the welding machines produced and developed by Fontijne [Fontijne, 2001] (see Appendix A). They contain some disadvantages as follows from Appendix A. Their operation may be improved by a redesign of the machine as well as the control strategy. Consequently the experimental setup used in this study was developed [Louter, 1999], [Ledeuil 1998], [Allersma, 1999]. It is called the Fontijne Holland Welder (FHW). The setup is a first model for a possible successor of the FRW-series and has to facilitate the study to this redesign.

In Figure 2.1(a) a picture of the setup is shown. In Figure 2.1(b) a schematic overview of the setup including an indication of the degrees of freedom (DOF) of the structure of the setup, is given. The setup is smaller than the FRW-series, so its weld capacity is limited. Hence two smaller sheets instead of a coiled sheet are used in the welding process. Only one clamping mechanism can move in horizontal direction (see Figure 2.1(b)). The position of the clamping mechanisms is still determined by measuring the displacement of the rod. In this case however, the rod is mounted in line with the clamping mechanisms. Moreover, the movement of the clamping mechanisms is a linear motion instead of a rotation. The pressure difference across the hydraulic cylinder is measured as well. Besides that, the potential over the clamps and the electrical current are measured. The total setup is controlled by a digital dSpace system. This system combines a Simulink model, Controldesk and the data acquisition of the machine to control the weld process. A complete overview of the working of the upset resistance weld process performed on this setup, is given in the next sections.

2.2 DC upset resistance welding

The DC upset resistance weld process is part of the rim production line (see section 1.2). The purpose of the process is to close a coiled sheet of metal by welding the sheet ends together. In the scope of this study, the start of the process is limited to clamping of the sheets of metal.

(a) setup   (b) DOF and labelling
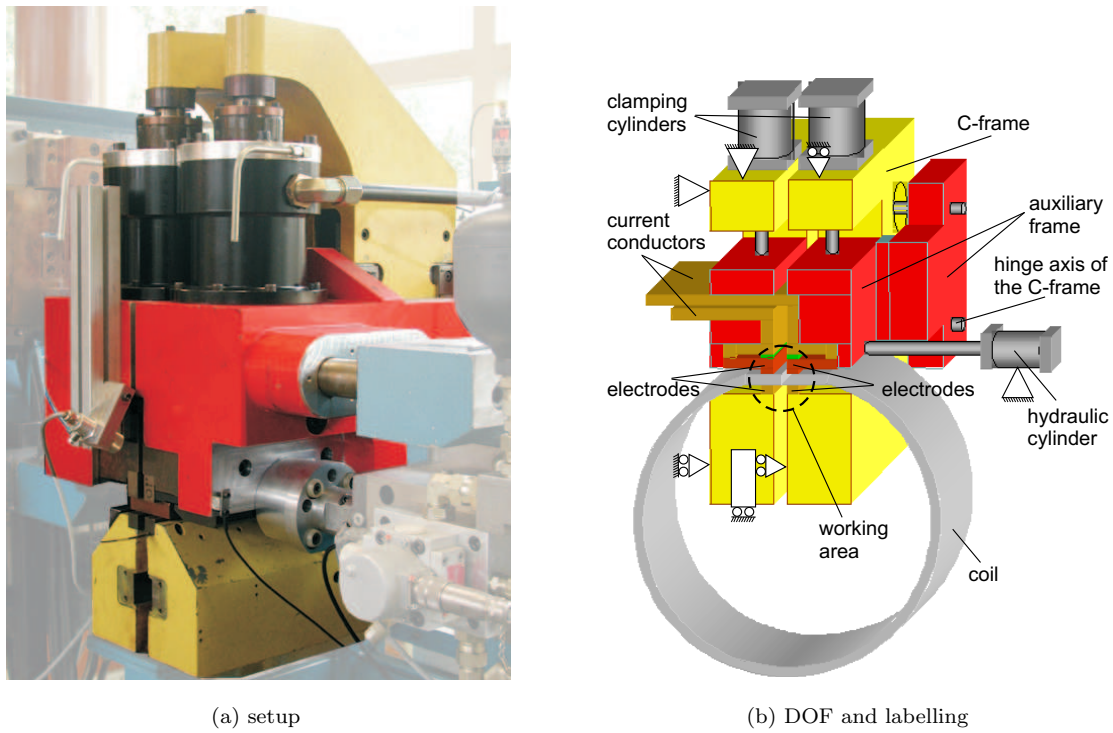
Figure 2.1: (a): picture of the setup (the FHW). (b): schematic representation of the setup, including labelling of the parts, definition of the DOFs and an indication of the working area.

The process is ended by opening of the clamps, thus releasing the sheets of metal. Consequently loading of the welding machine and positioning of the sheets of metal is not taken into account.
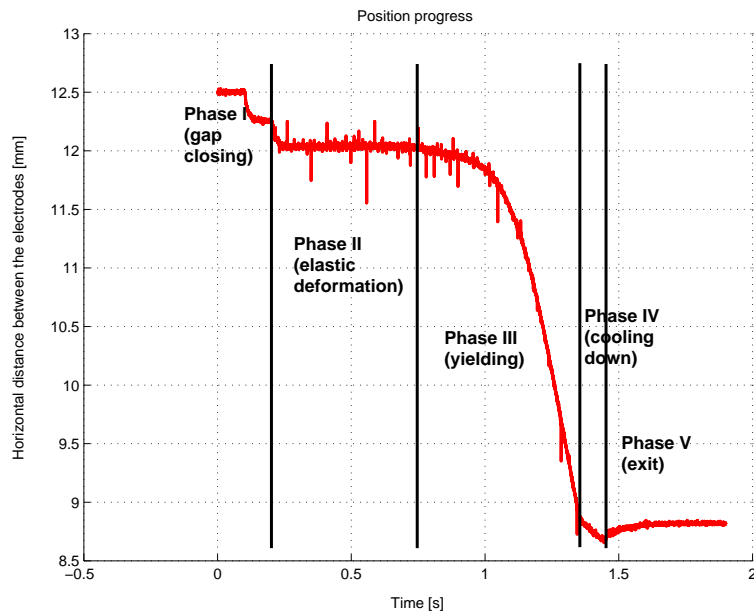

Figure 2.2: characteristic position progress during the weld process.

Till now, the DC upset resistance weld process has been divided into 5 sequential phases. This division is based on the distance between the clamps or electrodes (see also section 3.2). The distance between the electrodes is determined on-line. The weld program uses this distance to steer the electrical current and force, needed in the weld process. A characteristic progress of the displacement during the weld process is depicted in Figure 2.2. First the welding machine is loaded and the coiled sheet is clamped. Secondly the coil ends are pushed together to close the initial gap in between them. Next the material is heated. If it reaches its yield temperature, the actual welding (or yielding) takes place. The amount of displacement determines when a weld is formed. The electrical current is switched off. After a curing time in which the weld cools down and hardens, the pressure is released. Finally the welded coil is removed from the machine.

In developing a theory for the weld process, the emphasis lies on a small part of the welding machine. This so-called working area is shown in Figure 2.3 and also indicated in Figure 2.1(b). The working area involves the metal sheets that are welded together and the electrodes clamping the material.
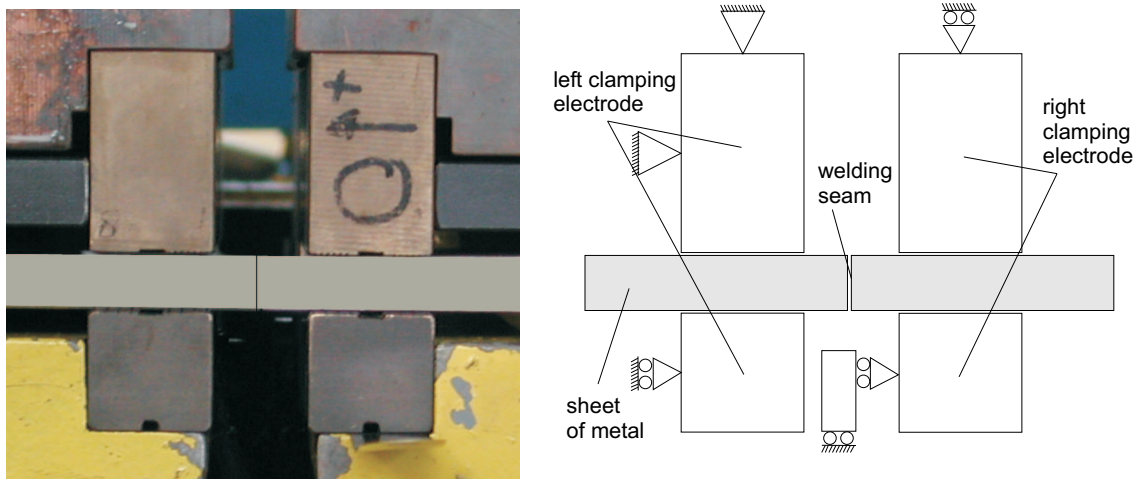

Figure 2.3: close up of the working area of the setup (see also Figure 2.1(b)): the electrodes and the two sheets of metal. In the right figure the degrees of freedom (DOF) of the electrodes are indicated.

The present weld philosophy is based on a division of the weld process into 5 phases. Accordingly, the examination of the weld process is divided into 5 parts as well. The systems and equilibria present in each of these 5 phases are discussed in this section. First a short introduction per phase is given. After that, each phase is discussed point to point and the most important variables are explained in more detail. In this way a theory describing the DC upset resistance weld process is developed. This theory is verified by means of experiments and simulations (see section 2.3 and Chapter 3).

2.2.1 Gap-closing

First the sheets of metal are clamped by two independent clamps. Next the sheet ends are pushed together with a predefined force. This force is applied by means of a hydraulic cylinder mounted to the right clamp, see Figure 2.8. This clamp is the only one with a degree of freedom (DOF) in horizontal direction. The inital gap between the sheet ends is eliminated and a contact surface between the two ends, the welding seam, is created. Loading coiled sheets, in practice also a so-called slip-control is present. Slip-control involves compensation for misalignment of the sheet ends (as far as this is possible). This misalignment originates from the coiler. The coiler can not adept to varying internal stresses in the material, which results in coiled sheets with a varying

initial gap. Using the setup instead of the FRW-series two separate sheets are used and thus no slip-control is needed.
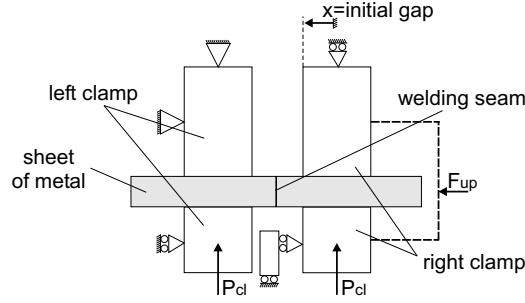

Figure 2.4: phase I: gap-closing

- The sheets are clamped with a predefined clamping pressure p_{cl} of $9 \cdot 10^6$ to $10 \cdot 10^6$ Pa.

- The sheet ends are pushed together with a constant upset force F_{up}. This force is applied at one side by means of a hydraulic cylinder.

- F_{up} is proportional to the pressure of the hydraulic system p_L: $p_L = F_{up}/A_{cyl}$, with A_{cyl} the effective cylinder surface.

- The sheets are initially cut-to-length, which results in a certain surface coarseness of the sheet ends. Due to this coarseness, contact points are formed between the sheet ends by means of the upset force. The total surface of the contact points is summed to a contact surface A_c between the sheet ends. This contact surface is smaller than the cross section of the material.

- The pressure on the contact surface, p_{up}, is proportionally to the size of the surface: $p_{up} = F_{up}/A_c$, so $p_{up} = p_{up}(A_c)$. During the setup of the upset force, the pressure on the contact surface will increase till the yield stress of the material. If it equals the yield stress the deformation of the contact points will become plastic. Till then, elastic deformation of the contact points is present. In this way the cross section of the contact points enlarges. Besides that, the gap between the sheet ends decreases and new contact points are formed. So the size of the total contact suface A_c increases. The deformation of the contact points is catalysed by the upset pressure $p_{up} > \sigma_y$ and will stop when the upset pressure equals the yield stress: $p_{up} = \sigma_y(\epsilon, T, \sigma_{y,o})$. The force due to elastic deformation of the material present in the welding seam, now equals the upset force. To describe this process, the next assumptions are made:

  - The temperature change as a result of the deformation is negligible and is therefore assumed to be constant.
  - After the elastic deformation of the first contact points, the deformation becomes plastic. Because the temperature is taken constant, this is cold deformation. Hence strengthening is present. However, the contact surface A_c increases by means of this plastic deformation. This results again in elastic deformation of material. Consequently as long as the contact surface grows, the deformation can be seen as elastic. The effect of strengthening, $\sigma_y(\epsilon) = \sigma_y$, which is a result of plastic deformation, thus is neglected.

  So now $\sigma_y(\epsilon, T, \sigma_{y,o}) = \sigma_{y,o}$ holds, with $\sigma_{y,o}$ the yield stress of the material at room temperature.

- Phase II starts after an at beforehand given displacement x or time, see section 3.2. These bounds to the displacement and the time are determined by trial and error and normally are about 1.0 mm respectively 0.2 s.

The result is an equilibrium between the contact surface A_c, the upset pressure p_{up} and the upset force F_{up}. With the upset pressure p_{up} equal to the yield stress $\sigma_y = \sigma_{y,o} = \sigma_{y,I-II}$ and at a temperature $T = T_r$.

2.2.2 Heating

When the gap between the sheet ends is closed, an electrical current is switched on over the resulting welding seam. This electrical current is applied using the clamps, with which the coil is clamped, as electrodes. Because of the contact surface between the sheet ends is smaller than the cross section of the sheets, a restriction resistance exists. In literature this is called the contact resistance R_c, which will be used further on. Besides that, the electrical resistance of the material, called the bulk resistance, is present. Combination of the electrical current and these resistances result in heat generation.
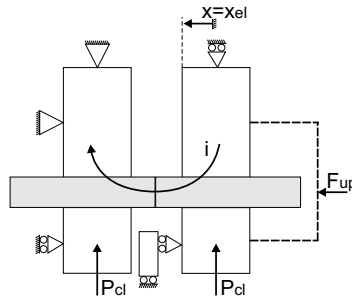

Figure 2.5: phase II: heating

- Apart from the present upset force F_{up}, a constant electrical current i is applied at the welding seam.

- A contact resistance R_c and the bulk resistance R_b of the material are present.

- Combination of the electrical current and the present resistances result in heat generation $Q_h = i(R_c + R_b)$. The total resistance is largest at the welding seam. Consequently heat generation starts at the welding seam. The bulk resistance increases accordingly to the temerature of the material. Hence it is largest at the welding seam and heat generation also proceeds at the welding seam.

- Through for example conduction and radiation, energy Q_l will be lost. The material is heated with the resulting energy.

- The contact resistance, as well as the bulk resistance are temperature dependent and increase at higher temperatures. Besides, R_c is inverted proportional to the contact surface A_c. Consequently it will decrease when A_c increases.

- The yield stress σ_y decreases when temperature increases. This disrupts the equilibrium $\sigma_{y,I-II} = p_{up}$, causing the material to deform. This deformation is the same as described at section 2.2.1. Hence, the upset pressure p_{up} decreases along with the yield stress to keep the process at equilibrium.

- The contact surface A_c increases by this deformation till it equals the size of the cross section of the sheet, $A_c = wh$.

- When $A_c = wh$, the contact resistance R_c vanishes. No restriction in the conducting surface is present anymore, so also no resistance is present. Because of the from now on constant contact surface, the upset pressure becomes linear dependent on the upset force.

- The yield stress at this point equals $\sigma_y = F_{up}/A_c$. The material starts yielding if $p_{up} > \sigma_y$.

The result is a contact surface $A_c = wh$, so the contact resistance R_c becomes zero. The yield stress $\sigma_{y,II-III}$ equals $p_{up} = F_{up}/A_c$. The momentary temperature is called the yield temperature $T_{y,II-III}$. If this temperature is increased, the material starts yielding.

2.2.3   Yielding

The material next to the welding seam is heated to the same temperature as the material in the welding seam. An equilibrium is formed between the speed with which the material reaches the equilibrium temperature and the speed of the plastic deformation. This is catalysed by the upset pressure p_{up} and the electrical current i. This results in yielding, or plastic deformation, forming a weld with upset in the welding seam. By the plastic deformation, the material is pushed out of the welding seam by which the upset is formed. In the modelling, the total displacement by which the upset is formed, is called *upset*.
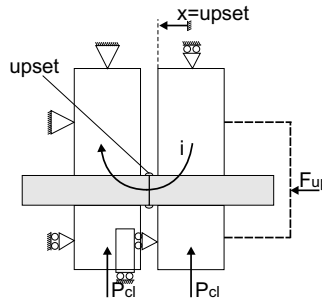

Figure 2.6: phase III: yielding

- The upset pressure p_{up} is linear dependent on the upset force F_{up}) due to the constant contact surface A_c. Due to forming of upset, the cross section at the welding seam increases some more. However p_{up} is assumed to be dependent on the smallest cross section in the material. This now equals $A_c = wh$.

- The magnitude of the bulk resistance R_b depends on the height of the yield temperature at the end of phase II. Depending on the magnitude of R_b and the magnitude of the electrical current, heat generation $Q = R_b i - Q_l$ takes place. The speed of the deformation consequently depends on the magnitude of the electrical current and the height of the yield temperature at the end of phase II. Within limits holds that the higher the yield temperature, the larger the speed of deformation.

- The temperature increases till a stable equilibrium is formed between the amount of energy dissipated by the deformation in the welding seam and the amount of energy applied to the system (see section 3.3.4).

The yielding phase is restricted by a maximum deformation or displacement, proportional to the amount of upset. If the amount of upset is reached, the current is switched off.

2.2.4   Curing

When the demanded amount of upset is reached, the electrical current is switched off. The upset force is released stepwise. The first step is to stop the yielding movement but keep pressure on the newly formed weld so that it can relax. The second step is to prevent a negative force on the weld, which could draw the two sheet ends apart. The material starts cooling down by radiation and mainly conduction.
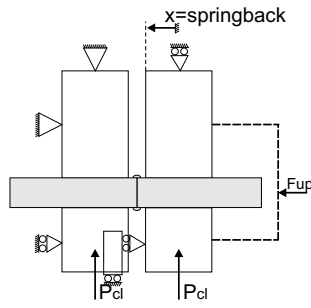
Figure 2.7: phase IV: curing

- When the demanded amount of upset is reached, the electrical current is switched off, $i = 0$.

- The magnitude of the upset force is decreased. Hence the magnitude of the yield stress σ_y becomes larger than magnitude of the the upset pressure p_{up}.

- During heating, energy is stored in the material in the form of heat. This has to be released by radiation and conduction. A large amount of this energy is stored in the upset. The size of the upset thus has significant influence on the duration of the cooling down and the speed of cooiling down, $\dot{T}_{cd}$.

- If for example construction steel is used and the speed of the cooling down is too high, bainiet is formed [Put, 1999]. Bainiet is more brittle than the original material, which is not desirable. So there is a minimum speed of cooling down.

- The upset force is released in 2 steps. The first step resembles the moment the electrical current is switched off. The second moment is when the material has cooled down enough to prevent breaching by elastic springback.

2.2.5 Exit phase

When the temperature of the weld is low enough (bounded by a displacement or time), the clamps open. Finally the coil is transported to the next step in the rim production line where the upset is removed by a trimmer (see Figure 1.2.)
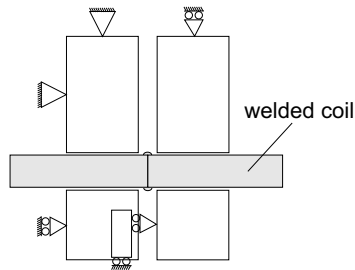

Figure 2.8: phase V: exit

2.3 Experiments

A number of experiments is performed to validate the developed theory of section 2.2. Some of the theoretical assumptions are founded and demonstrated to be correct. Besides that, the results contribute to the theory and the insight in the weld process. This insight in the weld process is later on used in modelling of the process (see Chapter 3).

The experiments are performed on the test setup discussed in section 2.1. Metal sheets with a width of 75 mm and a total cross section of 150 mm^2 are used. The material used is QSTE 460$^{\text{TM}}$ steel for which the characteristic parameters are defined in the Nomenclature. To check the reproducibility of the experiments, some of them were repeated several times.

The position and temperature progress during welding are the most important variables in defining the quality of a weld. The temperature however is not measured. Furthermore, till now no good demands are formulated concerning the temperature progress during welding. Firstly because the temperature is not measured and secondly because the influence of the temperature on the weld quality is not known. The NIMR is doing research in this field, see section 1.2. Consequently the conclusions drawn from the results of the experiments, mainly focuss on the position progress during welding.

A working area with specific combinations of the force and the electrical current in which good welds can be made, is present. Outside this area, the force or electrical current are too high or too low and the welding will fail. The purpose was to get a clear view of the influence of the various parameters on the process and not to set demands for a good weld. Accordingly, the experiments are all performed in this working area. WELD2001 is used to control the weld process (see section 3.2). The weld programs used are based on previous programs, which have already proven to work well. These programs are developed on a basis of trial and error and experience.

Loading the welding machine is not taken into account in this study (see section 2.2). A bad positioning of the metal sheets however, can influence the progress of the weld process negatively. The setup is loaded by hand, so it is taken care of that the positioning is the same for all experiments. Furthermore, the top and bottom side of the sheet ends differ (see Figure 2.10). Hence a proper orientation of the sheets is important as well. When the material is cut-to-length (see section 1.2), part of the material is smoothly cut and the other part is broken (see Figure 2.9).
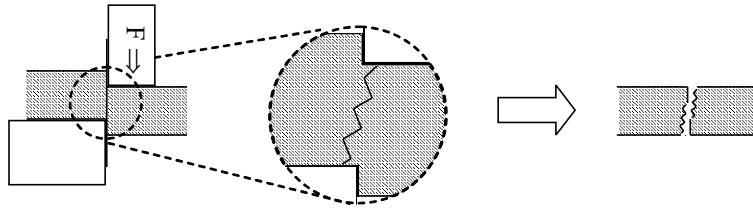

Figure 2.9: side-view of the cut-to-length process of the metal sheets.

When coiling the sheets, these parts exactly match as depicted in Figure 2.10(A). Two separate plates instead of a coiled sheet however are used at the setup. Consequently the sheets may be loaded having the wrong orientation, as depicted in Figure 2.10(B). In that case a relatively large initial gap is present. This results in a far too high initial contact resistance and the results of the experiments will not be representative.

Figure 2.10: side-view of the 2 possible ways of loading the sheets into the welding machine: picture A shows the right way, picture B the wrong way.

2.3.1   Stiffness and damping of the material

The material behaviour is defined as to correspond to the mechanics of a mass-spring-damper system. Modelling the material behaviour in this way, is discussed in section 3.4. The corresponding stiffness k_m and damping d_m are assumed to be temperature dependent. These stiffness and damping obviously represent a combination of several physical parameters that are material-

dependent. At this point however, they are considered to be pure stiffness and damping and determined experimentally.

In phase I and II a constant force is applied. The amount of displacement is very small in this part of the process (see Figure 2.2 of section 2.2). In phase III, a constant force is applied as well. The amount of displacement however, is relatively large. When an equilibrium is settled, the speed of the displacement becomes constant. The amount of displacement in phase IV again is very small. From this can be concluded that the stiffness is dominating in phase I, II and IV, while in phase III the damping is dominating. The stiffness in phase IV and further on, strongly depends on the speed of cooling down and the maximum temperature reached during the process. This is not the main matter in this study. Hence, the attention is concentrated on the stiffness of the material in phases I and II and the damping in phase III. Measured displacement and force characteristics are used to determine their magnitudes.

The influence of the temperature on the stress-strain curve is shown in Figure 2.11. The first linear part of each curve represents elastic deformation. The following nonlinear part represents plastic deformation. The higher the temperature, the lower the stiffness (less steep elastic part). Moreover, the higher the temperature, the lower the yield stress (switch from elastic to plastic deformation) of the material.
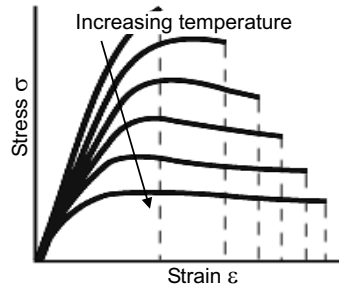

Figure 2.11: influence of the temperature on the stress-strain curve of steel.

With $\sigma_{y,r}$ the yield stress of a material at room temperature and E the Young's Modulus, the yield strain equals

$$\epsilon_y = \frac{\sigma_y}{E} \tag{2.1}$$

(unities are listed in the Nomenclature). Using the thermal expansion coefficient α_{th}, the theoretical yield temperature becomes

$$
\begin{aligned}
T_y &= \frac{\epsilon_y}{\alpha_{th}} \\
&= \frac{\sigma_y}{\alpha_{th} E}
\end{aligned}
\tag{2.2}
$$

Now the influence of an external force, resulting in a pressure σ_e, can be determined

$$\frac{\sigma_e}{\alpha_{th} E} = T_e \tag{2.3}$$

$$
\begin{aligned}
\Delta T &= \frac{\Delta \sigma}{\alpha_{th} E} \\
&= T_y(\sigma_e)
\end{aligned}
\tag{2.4}
$$

with ΔT and $\Delta \sigma$ the remaining temperature respectively the remaining stress before yielding starts. In this specific case the following results
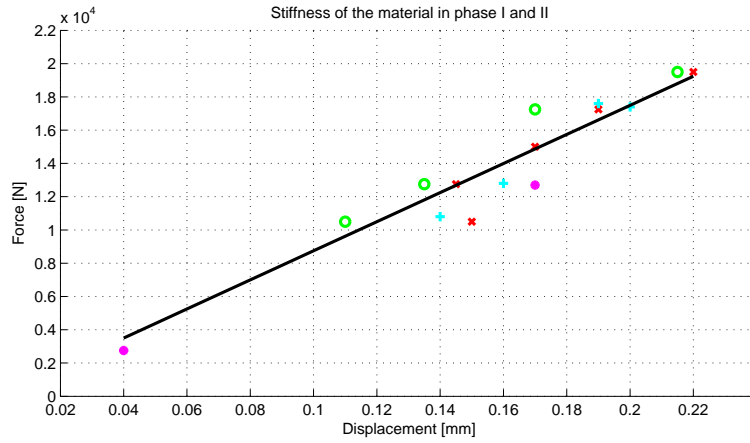
$$\sigma_e = \frac{F_{up}}{A}$$

Figure 2.12: stiffness of the material in phases I and II, calculated using experiments. The experimental data is already compensated for slip and the initial gap (see section 2.3.2).

$$T_y(F_{up}) \quad = \quad T_{y,r} - \frac{F_{up}}{\alpha_{th} E A} \tag{2.5}$$

So the yield temperature will decrease if the upset force is increased and vice versa.

The stiffness in phase I can be determined directly from the force-displacement relations. To determine the stiffness in phase II, several experiments with varying upset-force are performed. Using the elastic springback of the material, the stiffness can be determined as well. This springback occurs when releasing the force. See for example the right grey parts of the plots in the left part of Figure 2.13. The advantage of this latter method is that the displacement due to slip and the initial gap between the sheet ends is not taken into account. Experiments to determine the magnitude of the slip and initial gap are discussed in section 2.3.2.

The stiffnesses of phase I and II are determined using experiments with varying upset force. Experiments using both one and two sheets are compared to be able to exclude the initial gap. In Figure 2.12, the results of these experiments are presented. From these results follows that the stiffness of phases I and II are similar and about 87500 N/mm.

Experimental results show that the magnitude of the upset force does not influence the magnitude of the damping in phase III. The magnitude of the electrical current however does. See for example the result of experiments with varying electrical current shown in Figure 2.13. The speed of displacement $\dot{x}(t)$ in phase III, the steepness of the colored curves, varies with varying magnitude of the electrical current. This speed is linearly dependent on the magnitude of the damping. The speed in the stable part of phase III is calculated and shown in the right part of Figure 2.13.

The electrical current is quadratic proportional to the heat-generating energy term (see equations 3.2 and 3.3). The damping of the material is expected to be dependent on the temperature. If this relation is considered to be linear, the electrical current is quadratic proportional to the speed as well.

$$\begin{cases} T(t) & \propto & i(t)^2 \\ d_{pl}(T) & \propto & T(t) \\ \dot{x}(t) & \propto & d_{pl}(T) \\ \dot{x}(t) & \propto & i(t)^2 \end{cases} \tag{2.6}$$

Consequently a 2nd order curve is fitted over the speed values in Figure 2.13. The good result implies a linear relation between the temperature and the damping of the material in this phase. Modelling and simulations have to point out the exact relation between the damping and temperature. A first indication however is obtained already.
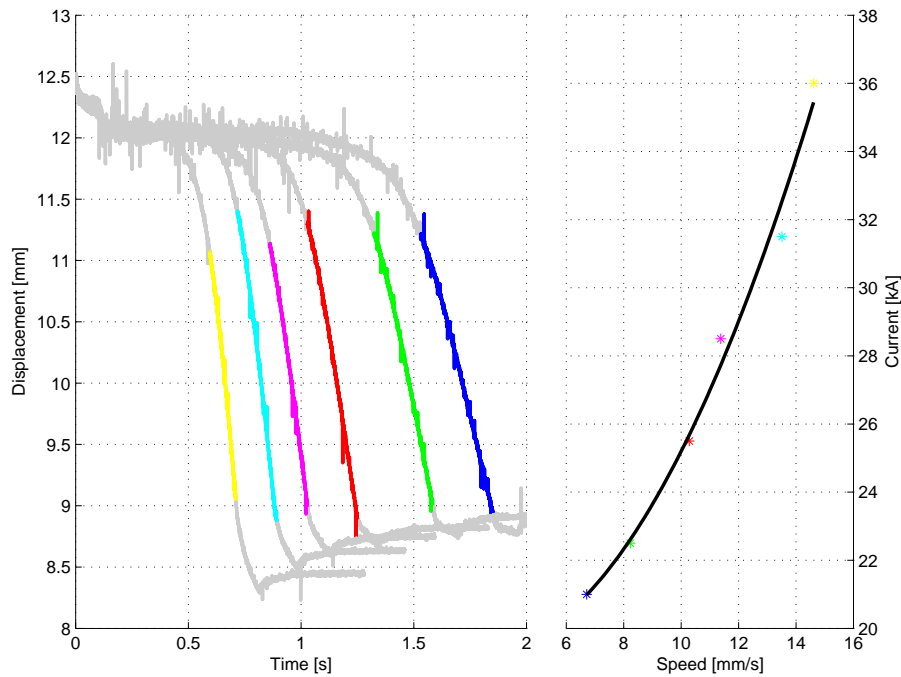
Figure 2.13: displacement and speed of displacement in phase III of the process of experiments with varying electrical current.

The upset force of 12.7 kN used in combination with an average speed of about 12 mm/s, yields a damping d_{pl} of about 1100 Ns/mm. The total variation of the magnitude of the damping varies from 900 to 1800 Ns/mm over the examined region.

2.3.2 Mechanics: slip and initial gap

The force applied to the welding seam is controlled by a feedback loop based on the pressure difference in the hydraulic system. Consequently not only the dynamics of the material and weld but also the dynamics of the hydraulic system and welding machine are included in this measurement. The transfer function estimates of the force show the influence of these dynamics. Exact modelling and measurements are discussed in section 3.6. Yet the time domain responses of the present experiments give some information with respect to the setup already.

In the first place springback is present in the displacement progress. A force dependent springback is present due to the elastic stiffness of the material. A second, smaller displacement, which appears to be constant with respect to the applied force, can be noticed as well. The magnitude of this displacement is about 0.03 mm, see Figure 2.14 (the results of Figure 2.12 are already compensated for this effect). This second displacement may be the result of hysteresis in the motor or the setup.

Secondly, slip between the clamps and the sheets of metal is present. The clamps have to find grip at the beginning of the weld process. Besides that, an initial gap between the sheets of metal is present which is removed in the first phase. The initial gap is a result of loading the setup. To get an idea of the average size of the slip and the initial gap, results of experiments using one and two sheets of metal and applying a varying force, are compared. The influence of this can be seen in the magnitude of the slip or the combination of the slip and the initial gap, see Figure 2.14. From these results can be concluded that an average slip of about 0.05 to 0.1 mm is present and that the size of the initial gap is about 0.15 to 0.2 mm.

Thirdly wave-alike disturbances are present in the measured pressure signal. This may indicate
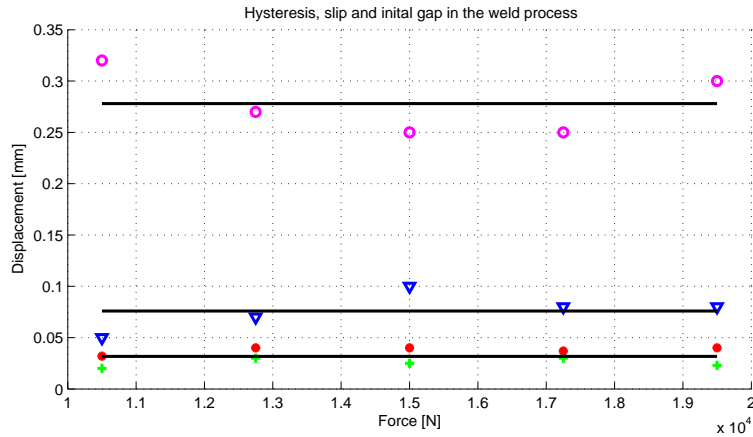
Figure 2.14: constant parts of the measured springback at various experiments. The blue triangles in the middle plot indicate slip between the clamps and the sheets of metal. The magenta circles in the upper plot indicate slip in combination with the initial gap between the sheets. The lower plot indicate the clearance present in the setup.

static friction. Friction is present due to slip between the clamps and the sheets of metal. Besides that, friction is present in the horizontal movement of the clamping device. To examine the influence of the magnitude of the initial gap on these disturbances, the resulting force responses of the same experiments are compared, see Figure 2.15. Figure 2.15(a) shows parts of the resulting force responses from experiments clamping only 1 sheet of metal. Consequently only slip and no initial gap is present. Figure 2.15(b) shows the results of experiments clamping 2 sheets of metal.

The forces at 0.06 s in Figure 2.15 are compared to the forces of the corresponding points in Figure 2.14. The larger the initial gap or the more slip is present, the larger the wave-alike disturbances are. Plot 1 of Figure 2.15(a) for example, corresponds to the blue triangle in Figure 2.14. These results show the highest displacement or largest initial gap and include a lot of disturbances as well. Plot 2 corresponds to the blue triangle with the smallest initial gap. As follows from Figure 2.15(a), this force develops in a very smooth way. The plots in Figure 2.15(b) all include a lot of disturbances. Again the corresponding magenta circles in Figure 2.14 show a relatively large displacement. So the more movement, the more wave-alike disturbances. This can be attributed to on the one hand to the slip between the clamps and the metal. On the other hand it can be attributed to static friction in the movement of the clamping device.

2.3.3 Switching between the phases

The progress of the weld process is determined by the progress of the 5 phases (see section 2.2). Determination of the moments of switching between the phases thus is of importance in controlling the weld process. In this section the main switching moments are discussed.

Phase I to II

Phase II starts when the electrical current is switched on. This switch-on of the electrical current is defined by the bounded displacement and the bounded process time. The first or the latter one is reached depending on the magnitude of the upset force, the material characteristics and the size of the initial gap and slip. So this switching moment is not consistently determined. It may be useful to bound the speed of displacement instead of bounding the displacement and time separately. Experiments show that the speed in the first phase is too small to measure and / or calculate exactly enough. So it can not be used as a bound at this point. Yet it may be used when the measuring and / or calculation of the speed is optimised.
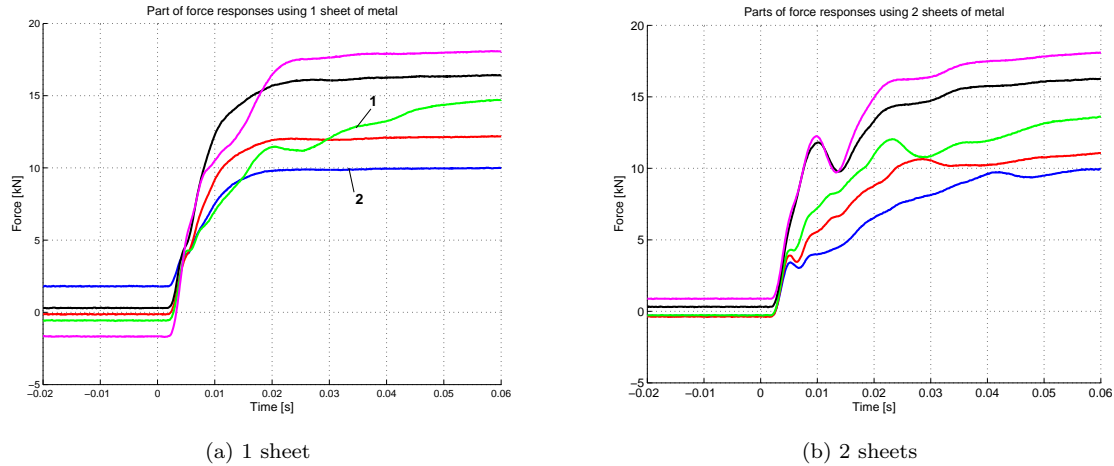
(a) 1 sheet
(b) 2 sheets

Figure 2.15: (a): part of the force response resulting from experiments clamping 1 sheet of metal. (b): part of the force response resulting from experiments using 2 sheets of metal.

If the electrical current is switched on too early and the initial gap is still closing, the result is an enormous heating of the welding seam. This is explained by the large contact resistance R_c, see section 2.3.4. Because of this heating, the material in the welding seam will melt instead of yield. If the start of the second phase is postponed when the gap is already closed, this will only result in some loss of time and the process will not be disturbed. So the conclusion is that simply enough time has to be taken to build up enough pressure in phase I. If the pressure is controlled well, this time is freely adjustable within the limitations of the hydraulic system.

Phase II to III

Phase III should start when the yield temperature is reached and the material starts to yield. Because the stiffness of the material decreases rapidly, the actuator has to move fast to hold the demanded pressure. Normally this doesn't work out very well. Hence an extra pressure boost is imposed on the actuator to keep the resulting pressure relatively constant. If this boost is imposed too late, the pressure drops significantly.

The weld program switches from phase II to phase III when it is obvious the material has started yielding. This is based on the displacement in phase II, which is bounded to for example 0.3 mm. A bound to the time is present as well. In this case however, it is only used for safety. If the maximum displacement is not reached within the given time limit, probably something is wrong and the weld process is aborted. Because of the accuracy of the measured position signal, the displacement bound can not be chosen smaller. The magnitude of the noise in the signal is too high.

As a result of this, phase III is not started until the yielding has already started. A better bound to phase II hence would be to use the temperature of the material and switch to phase III if the yield temperature is reached. The temperature however is not measured. Consequently the progress of the temperature then has to be calculated accurate enough. Another option is to bound the pressure drop. If the yield temperature is reached, the pressure drops significantly. Reaching the yield temperature thus may be indicated by a percentage of pressure drop. The conclusion is that the current definition of this switching moment is not optimal and, if possible, needs improvement.

Phase III to IV

The switching moment between phase III to IV is defined by the demanded amount of upset. If the displacement bound is reached, the electrical current is switched off and the upset force is diminished to stop the yielding of the material. The duration of phase III can be influenced by varying the magnitude of the electrical current $i(t)$ and of the force $F(t)$ (see section 2.3.5). The disadvantage is that the process is not forced to stop yielding. The material has to cool down first. So a fluctuation in the final displacement may occur and most times overshoot in the displacement is present.

2.3.4   Contact and bulk resistance

Both the contact and bulk resistances present in the weld process are temperature dependent. This is shown by equations 2.10 and 2.18, describing both resistances. Large variations in temperature are present during the weld process. Consequently the temperature dependent variables in equations 2.10 and 2.18 are of major importance in modelling the weld process. Therefore a closer look is taken at these resistances. A schematic respresentation of the resistances present, is shown in Figure 2.16. The total resistance of a coil consists of 4 parts (see Figure 2.16):

1. the specific resistance of the material between the clamps, the bulk resistance R_b

2. the contact resistance in the welding seam, R_c, which is present till the material starts yielding

3. the specific resistance of the material at the 'back side' of the coiled sheet, $R_{b_{back}}$. This resistance is not present if two separate sheets are used instead of a single coiled sheet.

4. the specific resistance of the electrodes and the resistances at the transitions from the electrodes to material, R_{cl}. These have to be taken into account because a secondary current before the electrodes is measured instead of the primary current at the material.

R_b and R_c are connected in series. $R_{b_{back}}$ is connected in parallel to R_b and R_c. The total coil, consisting of R_b, R_c and $R_{b_{back}}$, is connected in series to the total resistance of both electrodes, R_{cl} (see Figure 2.16). The experiments are not performed using coiled sheets, so $R_{b_{back}}$ equals zero.
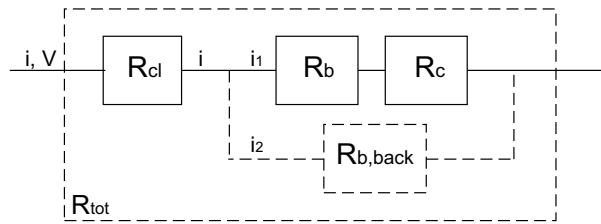

Figure 2.16: schematic representation of the resistances of importance in the setup of the weld process. With the electrical resistance of the material in between the electrodes and outside the electrodes at the 'back side' of the coiled sheet R_b. And with the contact resistance at the welding seam R_c and the contact resistance between the clamps and the sheets as well as the electrical resistance of the clamping material R_{cl}. R_{tot} is the total resistance influencing the measurements.

The total resistance R_{tot} is determined using the measured progress of the electrical current and the voltage, i respectively V:

$$R_{tot} \quad = \quad \frac{i}{V} \tag{2.7}$$

$$= \quad R_b + R_c + R_{b,cl} \tag{2.8}$$

Using one sheet of metal instead of two, the contact resistance R_c in equation 2.8 is eliminated. R_{sub} is defined as the resistance of the sheets and the clamps together. Making use of the same relation as in equation 2.7 the magnitude of this resistance is determined

$$R_{sub} = R_b + R_{cl} \tag{2.9}$$

R_{cl} is constant, while R_b is dependent on the distance L between the clamps. By varying this distance between the clamps and applying a constant force and electrical current, R_b and R_{cl} are determined separately [Bejan, 1993], [Wolfram, (web)]

$$R_b = \rho_e(T)\frac{L}{dydz} \tag{2.10}$$

with $\rho_e(T)$ the temperature dependent electrical resistivity of the material in Ωm [Bejan, 1993],[Wolfram, (web)]

$$
\begin{aligned}
\rho_e &= \rho_{e,r}(1 + \alpha_\rho(T - T_r)) \\
&= \rho_{e,r}\frac{T}{T_r} \qquad \text{for } \alpha_\rho = 3.35 \cdot 10^{-3}
\end{aligned}
\tag{2.11}
$$

With $\rho_e = \rho_{e,r} = constant$ for $T = T_r = 298$ K, $R_b = R_{b,r} = constant$. Consequently $\rho_{e,r}$ can be calculated. In Figure 2.17 the results of experiments with varying distance between the clamps and varying electrical current (with constant distance between the clamps) are presented.
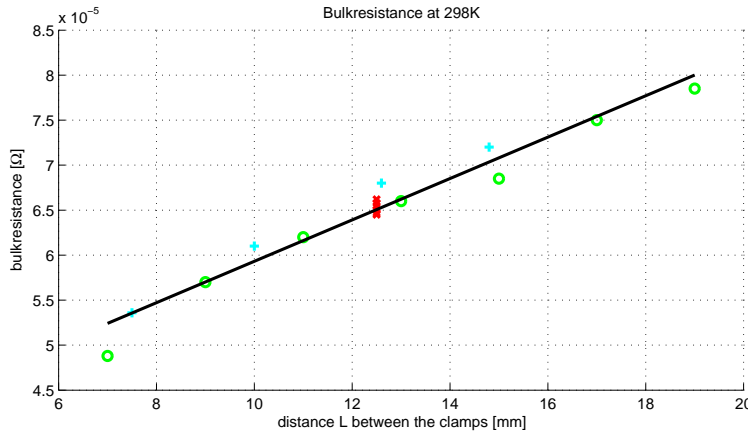

Figure 2.17: bulk resistance of the material at room temperature (298 K) determined from several experiments. The result of the least squares fit is $R_{b,r} = 2.3 \cdot 10^{-6}L + 3.631 \cdot 10^{-5}$ Ω.

From the experimental results presented in Figure 2.17 is concluded that

$$
\begin{aligned}
R_{cl} &= 36.3 \ \mu\Omega \\
R_{b,r} &= 2.3L \ \mu\Omega \\
\frac{\rho_{e,r}}{dydz} &= 2.3 \ \mu\Omega/\text{mm}
\end{aligned}
\tag{2.12}
$$

with $dydz = A = 150$ mm^2 follows for this material

$$\rho_{e,r} = 0.345 \ \text{m}\Omega\text{mm} \tag{2.13}$$

Now using two sheets of metal instead of one, the influence of the contact resistance is determined. The contact resistance actually is a restriction resistance, but is called contact resistance. A restriction exists at the contact surface of the sheet ends. This restriction disappears when yielding starts. It is assumed that the metallic contact formed during yielding is not interrupted

anymore. So once the contact resistance is gone, it does not come back anymore (see also section 3.3.2). Zwolsman [1987] modelled the contact resistance using

$$R_c = \frac{\rho_e}{2a_o} \tag{2.14}$$

with a_o the radius of an imaginary circle describing the metallic contact area in between the two sheet ends. The electrical current and heat flows are assumed to follow the same paths. Next the surface pressure is assumed to be equal to the Brinell Hardness. However this is only true at the breaking stress of the material. Consequently Zwolsman introduces a compensation factor $\xi_{Zm} = 3$

$$\sigma_{surf} = \frac{F}{\pi a_o^2} \tag{2.15}$$

$$= \frac{1}{\xi_{Zm}} HB \tag{2.16}$$

Taking into account the temperature dependency of HB and ρ_e (eq. 2.11), a theoretical model for the contact resistance results:

$$HB(t) = HB_r \frac{T_y - T(t)}{T_y - T_r} \tag{2.17}$$

$$R_c(t) = \frac{\rho_{e,r}}{2} \sqrt{\frac{\pi}{\xi_{Zm}} \frac{HB_r}{F(t)} \frac{T_y - T(t)}{T_y - T_r} \frac{T(t)}{T_r}} \tag{2.18}$$

$$\propto F(t)^{-0.5} \tag{2.19}$$

The total resistance is calculated using the measured voltage and electrical current at the switch-on of the electrical current. In this way the temperature will still be about room temperature and the previous calculated $R_{b,r}$ and R_{cl} can be used to determine $R_{c,r}$. In Figure 2.18 the contact resistance resulting from the theory using equation 2.18 as well as the contact resistance resulting from corresponding experiments are shown (see also section 3.3.2).
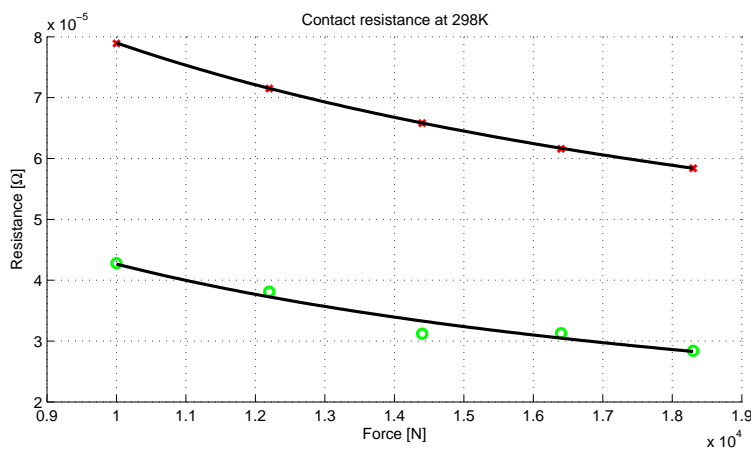

Figure 2.18: contact resistance of the welding seam. The green circles indicate the measurements results, while the red blocks indicate the theoretical values. The result of the least squares fit over the measurements is $R_c = 0.022 F^{-0.68}$ Ω

From the theory it follows that $R_c \propto F^{-0.5}$ (equation 2.19), while the experimentally determined R_c is proportional to $F^{-0.68}$. This is a relatively good comparable result (see Figure 2.18). However the absolute value of the theoretical R_c is about twice as high as the experimental values.

Zwolsman compensates in the derivation of equation 2.18 for some discrepancy between his theory and experimental results using factors based on experiments and making some assumptions. Furthermore the theory is tested with wires of Cu, MnNi and Mo while in this case sheets of steel are used. Hence his compensation factor ξ_{Zm}, used in equation 2.18, is adjusted for this particular process:

$$
\begin{aligned}
\xi_{URW} &= 2^2 \xi_{Zm} \\
&= 12
\end{aligned}
\tag{2.20}
$$

When rims or coils are welded instead of small sheets of metal, $R_{b_{back}}$ will also be present. To examine the influence of this extra resistance on the process, an indication for the magnitude of $R_{b_{back}}$ is calculated. The magnitude of $R_{b_{back}}$ depends on the diameter of the rim and the size of the cross section of the metal used. The larger the diameter or the smaller the cross section, the larger $R_{b_{back}}$ will be and vice versa. Normally, the width of a rim varies from about 200 to 500 mm. The thickness of the material may vary from 2 to 8 mm. And the size of the circumference varies from about 1000 to 1800 mm. The thinnest material off course won't be used for the larger rims and the thickest material not for the smaller rims, so an average of each variable is used. This results in a cross section of 1750 mm^2 and a circumference of 1400 mm. Using equations 2.10 and 2.13 this results in a resistance at room temperature of 0.28 mΩ if the same material as in these experiments is used. The maximum magnitude of the bulk resistance of the weld region at room temperature is assumed to be about 5 μΩ (for this cross section). The maximum magnitude of the contact resistance in the welding seam at room temperature is assumed to be about and 50 μΩ. The contact resistance is independent on the cross section, because of the dependence on the force instead of the pressure. The total resistance of the weld region at room temperature, $R_{b,r} + R_c$, will be about 55 μΩ. Using the following equations which result from Figure 2.16

$$
V = i_1(R_{b,r} + R_c) = i_2 R_{b_{back},r}
\tag{2.21}
$$

$$
\frac{i_1}{i_2} = \frac{R_{b_{back},r}}{R_{b,r} + R_c}
\tag{2.22}
$$

it follows that under these conditions i_1 will be about 5 times as high as i_2. When temperature increases, the resistances increase as well. The weld temperature of the welding seam will become about 1500 K while the temperature of the back side of the coil will only be slightly above room temperature. Combining equations 2.10, 2.13 and 2.22 it follows that i_1 will be about 70 times as high as i_2 under these conditions. So the loss of electrical current through the back side of the coil will be relatively high in the beginning of the weld process. In a later stage of the weld process, when only bulk resistance is present in between the clamps, the loss of electrical current will be small. The result is a minimal increase in temperature of the back side of the coil, which is neglegible.

2.3.5 Time of the weld process

The time the total weld process takes is mainly determined by the duration of the heating and yielding phases. The first one is bounded by reaching the yield temperature of the material. The latter one is bounded by the demanded amount of upset. The height of the yield temperature is influenced by the applied upset force. The smaller the magnitude of this force, the higher the yield temperature (see Figure 2.11). However if too less force is used, the contact resistance will be higher and heat is generated more quickly. The speed of heating of the material is also dependent on the amount of heat generation. This amount is influenced by the magnitude of the applied electrical current. So the duration of phase II depends both on the magnitude of the force and the magnitude of the electrical current.

(a) force vs time   (b) electrical current vs time
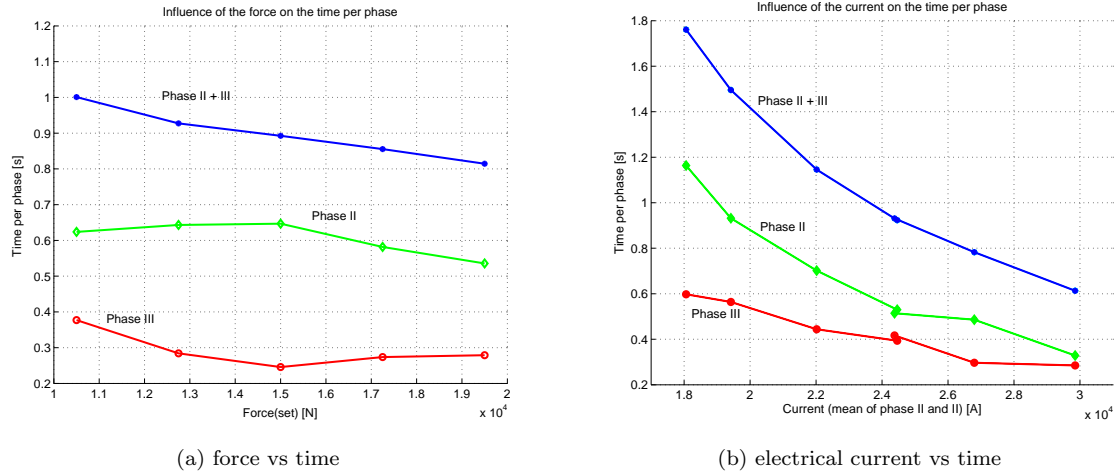
Figure 2.19: (a): Influence of the upset force on the duration of the various phases of the weld process. (b): Influence of the magnitude of the electrical current on the duration of the various phases of the weld process.

The relation between the duration of phase II and the magnitude of the force and the electrical current is examined. Thus experiments with varying force and electrical current are performed. The influence of the upset force on the duration of this phase is depicted in Figure 2.19(a). The middle (green) plot shows the duration of the heating phase for varying magnitudes of the upset-force. As expected, it is nonlinear because of the influence of the upset-force on the contact resistance as well as on the magnitude of the yield temperature. The duration of phase III (the lower (red) plot) on the other hand, is decreased because of the relatively low force. If the force is increased, the yield temperature will decrease. This results in a relatively short heating period, but also in a relatively low temperature during yielding. So the duration of phase II decreases, while the duration of phase III increases. As a result of this, the duration of phase III with respect to the duration of phase II can be manipulated.

Figure 2.19(a) shows that phase II has maximum duration if an upset force of about 15 kN is used. At the same point phase III has minimum duration. If the the magnitude of the upset force is increased, the total weld time decreases (the upper (blue) plot in Figure 2.19(a)). The conclusing is that the influence of the decreased yield temperature is more significant than the influence of the increased contact surface.

The influence of the magnitude of the electrical current on the process time is depicted in Figure 2.19(b). As expected, the larger the magnitude of the electrical current, the shorter the duration of the process. The larger the magnitude of the electrical current, the higher the energy generation and heating of the material. Consequently the yield temperature will be reached sooner and the duration of phase II decreases. Moreover the material can be heated more rapidly to the yield temperature during yielding and the duration of phase III decreases as well.

Figure 2.20 shows an extrapolation of the results of Figure 2.19. The influence of the magnitude of the electrical current on the total process time with respect to that of the upset force is big. Besides that, the duration of phase II with respect to the duration of phase III has to be taken into account in influencing the total process time.
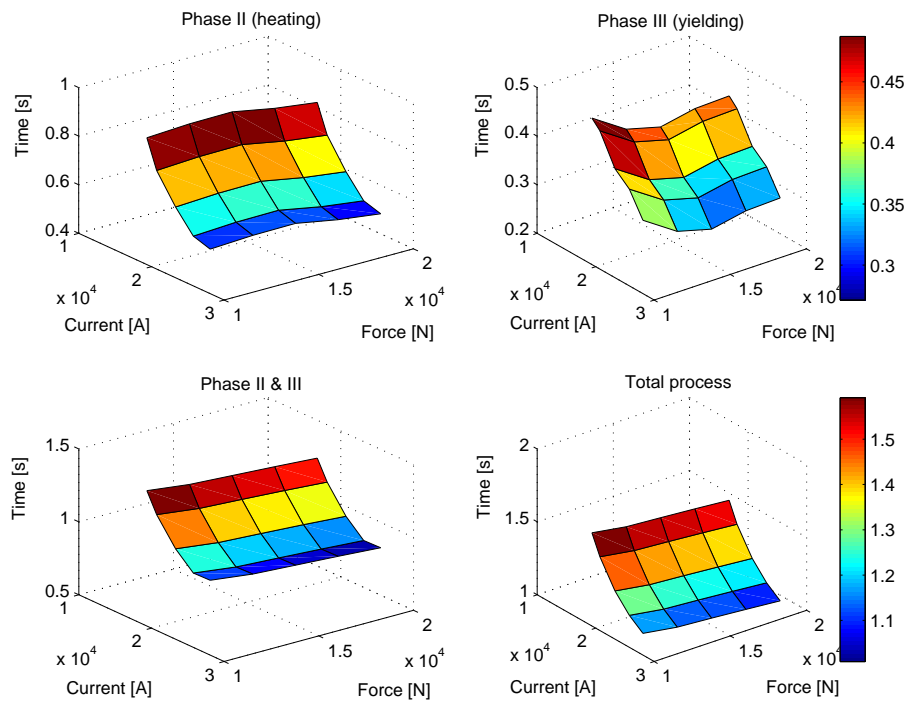
Figure 2.20: influence of the magnitude of the electrical current and the upset force on the duration of the various phases in the process and on the total process time.

Chapter 3

Modelling

3.1 Introduction

The theory of the weld process is validated partly by the experiments as described in section 2.3. To complete the theory, a model of the process is derived. First an inventory of previously performed modelling and the goals in modelling the weld process are discussed. Next the process is divided into several parts. An overview of the modelling per part is given after which they are combined to a single model. In Appendix B a description of the resulting simulation model, which can be used for off-line simulation of the weld process, is included. Finally the derived model is validated by experimental results. Furthermore, the modelling of the hydraulic system is presented in Appendix C. The results are presented in section 3.6.

3.1.1 Previous modelling

A number of studies trying to model the weld process have been performed already. Meulenberg [2002] and Put [1999] both modelled the thermodynamical part of the process for example. Meulenberg [2002] focussed on the heating of the material and Put [1999] paid special attention to the cooling down of the material. Both divided the working area into several distinctive sections. Next they derived a discretisised model of the working area, coupling the sections by the use of the corresponding balance of energy per section. A clear overview of the systems and equilibria present in the weld process as well as the assumptions done in modelling the process, are missing. Consequently parts are missing in their modelling as well. The resulting models do not give a satisfactory representation of (parts of) the weld process. Hence in this study, this is discussed extensively (see section 2.2). Besides that, at Put's work it is very indistinct what his final model looks like due to a lack of structure and overview. Other studies on modelling of the DC upset resistance weld process as performed on the FRW-series are Elassal [1996] and Legemaate [1998]. Studies on resistance spot welding like Feng [1998] are considered also. However these studies contribute more to the insight in the process, than really being a guide for modelling the weld process discussed in this study.

The weld process consists of a thermodynamical and a mechanical part. The thermodynamical behaviour and the mechanical behaviour of the process are coupled and thus influence each other. Consequently both parts have to be considered to gain good insight in the process. Until now most of the performed research was only focussed on the thermodynamical part of the process. Only Elassal [1996] focussed on the mechanics of the welding machine. However he paid little attention to thermodynamical part of the process. Meulenberg [2002] was the first one to start thinking of a mass-spring-damper system describing the mechanics of the weld process. However he didn't succeed in modelling it adequately.

So most of the existing modelling only involves parts of the complete weld process. Besides that, the modelled parts present in previous studies are incomplete due to a lack of insight in the process. Energy loss through yielding for example, has not been used in previous modelling.

However it appears to be of major importance in the total balance of energy. The resulting models are often difficult to interpret or to use. The models lack a clear layout and overview of an underlying theory and assumptions made. Consequently a point by point validation of the models is missing and the results are not satisfactory. One of the goals in (re)modelling the weld process is to do it in an orderly and structured way.

3.1.2   Goals of modelling

The main goal of modelling the weld process is to contribute to the developed theory, getting a good insight in the weld process. The emphasis in modelling lies on the development of a complete model of the process. The progress of variables that can not be measured can be determined by means of a good model. For example a good and reliable temperature calculation is of great interest in determining the quality of a weld. The resulting crystalline structures in the material are dependent on the temperature progress during welding. A simulation model, which can be used for off-line simulations of the weld process is developed too. Till now weld programs could be developed only by experiments and via trial and error. This approach takes a lot of time and is costly. The model has to be clearly structured and set up modular to make it easy to expand and adjust. In this way the model may be used as a base for modelling of the FRW-series for example later on. Finally modelling the weld process is of interest considering the development of a controller. The resulting model or parts of the model may be used as a base for a new control strategy.

3.1.3   Model layout

The theory presented in section 2.2 is used as a base in modelling the weld process. The process is split up into subparts interconnected by the main process variables (see Figure 3.1):

- the weld program WELD2001 generates setpoints for the electrical current and the pressure. These setpoints are based on the time and the displacements at the clamps.

- the converter system delivers the actual electrical current i prescribed by the weld program. The converter system includes a built-in closed loop current controller.

- the hydraulic system delivers the upset force F. This force is related to the pressure in the hydraulic cylinder prescribed by the weld program. The weld program includes a pressure feedback controller generating a control signal u_v to control the servo valve of the hydraulic system.

- the thermodynamics of the working area determine the temperature T of the welding seam. This temperature is used in the mechanics of the working area.

- the mechanics of the working area describe the temperature dependent mechanics of the material. This results in a displacement x at the clamps.

The working area depicted in Figure 3.1 is defined in section 3.3.1 and split up into several subparts. Most of the modelling is performed using Matlab and Simulink.

3.2   Weld program (WELD2001)

At the setup a weld program called WELD2001 is used. WELD2001 is based on WELD2000, which is the weld program used in the current welding machines to control the weld process [Fontijne, 2000]. The operation of WELD2001 is the same as the operation of WELD2000.
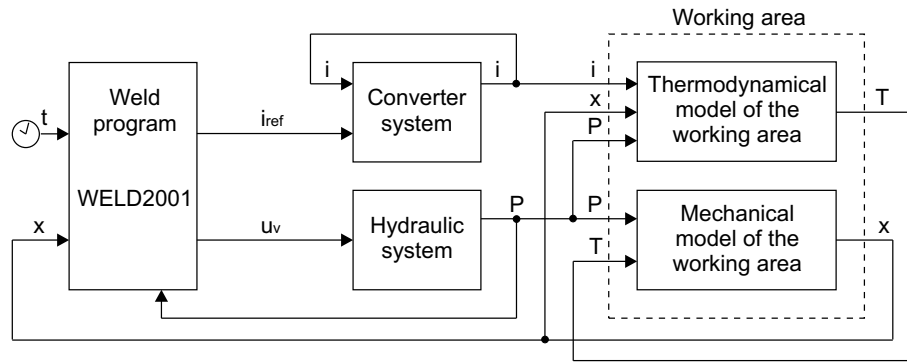
Figure 3.1: schematic overview of the modelling of the weld process. With pressure p, temperature T, displacement x, electrical current i, time t, setpoint current i_{ref} and input signal for the servo valve u_v.

The WELD2001 program is divided into 5 program rules corresponding to the 5 phases the weld process is divided into (see section 2.2). Figure 3.1 gives a schematic representation of how WELD2001 is included in the weld process. For every phase a setpoint for the electrical current and the pressure is defined. The moment of switching between the phases is determined by the time elapsed in every phase and the actual distance between the clamps. Per phase a bound to the time interval and displacement are defined. When one of the bounds is reached, the weld program switches to the next setpoint. Actually, setpoints for the density of the electrical current instead of the electrical current itself are defined. In this way the change over to different plate sizes is facilitated. In the same way setpoints for the compression at the cross section of the material instead of in the hydraulic cylinder are defined. In Figure 3.2 an example of a weld program of WELD2001 is shown.

x \ y	1	2	3	4
1	70	0	1	100
2	80	100	0.3	2000
3	100	100	3	2000
4	75	0	5	100
5	10	0	1	10

Figure 3.2: example of a weld program of WELD2001. Column *1* and *2* represent the density of the electrical current respectively the compression at the cross section of the material. Column *3* and *4* represent the bounds to the displacement and time. The setpoints for the current density and the compression are in kiloamperes per square millimeter respectively in bar. The displacement and time bounds are in millimeters respectively in milliseconds.

The setpoints for the density of the electrical current are transformed to setpoints for the electrical current. The setpoints for the compression at the cross section of the material are transformed to setpoints for the pressure in the hydraulic cylinder. A simplified model of WELD2001 is developed to facilitate simulation of the weld process.

3.3 Thermodynamics of the weld process

The working area of the weld process (see section 2.2) is divided into sections. In this way a discretised model of the thermodynamics is derived. Only a quarter of the working area is modelled. Per section a balance of energy is defined. This results in a set of partial differential

equations. Various kinds of energy generation and losses are present in the weld process and are modelled per section. First the discretisation is discussed. Next the various kinds of energy generation and losses are explained and modelled [Bejan, 1993] and [Wolfram, (web)], [Meulenberg, 2002]. After that, the specific balance of energy per section is discussed.

3.3.1   Discretisation of the working area

The working area is restricted to the material itself, the clamps or electrodes of the welding machine and the surrounding air (see section 2.2). This region of interest, depicted in Figure 3.3 is divided into several parts each having different interactions with its surroundings. These parts are divided into sections except for the surrounding air. The surrounding air is considered as a single section with constant temperature. In Figure 3.3, in each of the 6 distinctive parts one of the sections is shaded. The surrounding air is not indicated as a separate section.
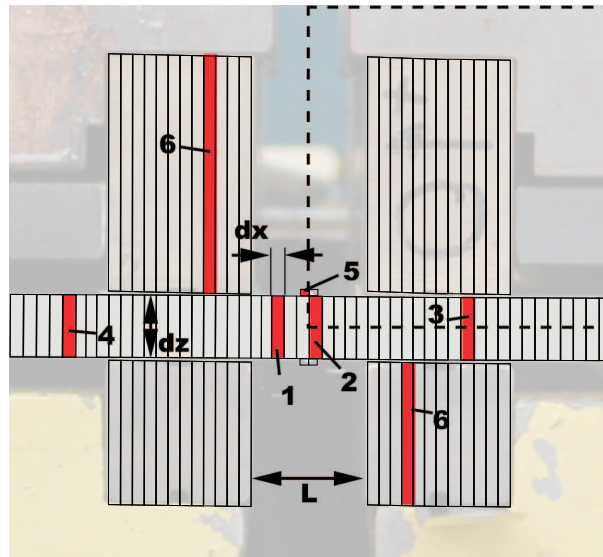

Figure 3.3: schematic representation of the working area, divided into sections. 1 through 5 are parts of the welding material: deformable sections 1, upset sections 2, welding seam sections 3, undeformable sections in between 4 and behind 5 the electrodes. 6 represent the clamping sections.

The material is assumed to be homogenous and the effects at the edges of the material are neglected. Furthermore the influence of the gravity and differences between the upside and down-side of the machine at the working area, are neglected. The shape of the upset, which is obviously influenced by these parameters is not the main goal in this modelling and hence of minor interest. The weld process is assumed to be point symmetric with the middle of the welding seam as the central point. Hence, a 3-dimensional model of a quarter of the total working area is developed. This quarter is indicated by the dotted plot in Figure 3.3.

The choice of the sections and their interactions is of crucial importance to the resulting model. The deformable sections are indicated with 1 in Figure 3.3. These sections involve the base material in between the clamps with exception of the two sections next to the welding seam and the actual upset. The two sections next to the welding seam are the welding seam sections indicated with 2 in Figure 3.3. These sections actually deform into the upset during yielding. Always two of these sections are present in the model. If these sections are completely transferred to the upset, they are replaced by the two adjacent deformable sections. Besides, they are left out from the model for the rest of the simulation. With the material in between the clamps divided into 2N sections,

the initial width of sections 1 and 2 equals

$$dx = \frac{L}{2N} \tag{3.1}$$

with $dx = dx(t)$. The height and length of the sections is equal to the height dz respectively the width dy of the material.

The upset sections can be modelled in many ways. For example as some sort of upset shape-alike curve or rectangular shaped sections as is shown in Figure 3.3. Spread over the 2 welding seam sections or over several deformable sections (including the welding seam sections). The width of a section adapting to the momentary width $dx(t)$ of the welding seam sections or not. The upset section can be divided into several sections or just be seen as 1 section, etc. From simulations a rectangle with a constant width equal to $2dx$ and a height depending on the amount of material that has already become upset appeared to be the best approach. This rectangle is positioned on both the upper and lower side of the welding seam and is divided into two sections each.

The sections indicated with 4 involve the material in between the clamps and the sections indicated with 5 involve the material behind the clamps. The clamps itself are divided into sections indicated with 6 in Figure 3.3. The width of these sections may be larger than dx because far less temperature variations and no deformation are present.

3.3.2 Heat generation

The applied electrical current in combination with the electric resistance in the material and in the welding seam result in heat generation. Energy thus is supplied in the form of heat generation in the welding seam, $Q_{Rb}(t)$ and $Q_{Rc}(t)$ respectively.

$$Q_{Rb}(t) = i(t)^2 R_b(t) \tag{3.2}$$
$$Q_{Rc}(t) = i(t)^2 R_c(t) \tag{3.3}$$

with R_b as in equation 2.10 and R_c as in equation 2.18, taking into account equation 2.20 (see section 2.3.4). Because the voltage over the clamps $U(t)$ is measured, the generation of heat can also be calculated using

$$Q_h(t) = i(t)U(t) \tag{3.4}$$

R_b is the electric resistance in the material and R_c the contact resistance in the welding seam. The contact resistance is only attendant until the yielding starts. At that moment both cross sections of the sheet ends are completely in contact and the contact resistance disappears. In Figure 3.4 the theoretical progress of both resistances is shown. The contact resistance causes heat generation in the heating phase after which the bulk resistance assures that heat still can be generated during yielding.

3.3.3 Conduction, radiation, convection

The sections are either part of the same part of material or clamped to each other. Consequently, they exchange energy by conduction, radiation or convection. To start with the first one, horizontal conduction between the sections is present:

$$Q_{c,h}(t) = \lambda \frac{\partial^2 T(t,x)}{\partial x^2} dx dy dz \tag{3.5}$$

with λ the coefficient of thermal conductivity. The temperature of a section is assumed to be uniform. Now equation 3.5 can be discretised and the horizontal conduction between 2 sections becomes

$$Q_{c,h}(t) = \lambda \frac{T_{i+1}(t) - 2T_i(t) + T_{i-1}(t)}{dx^2} dx dy dz \tag{3.6}$$

(a)   (b)
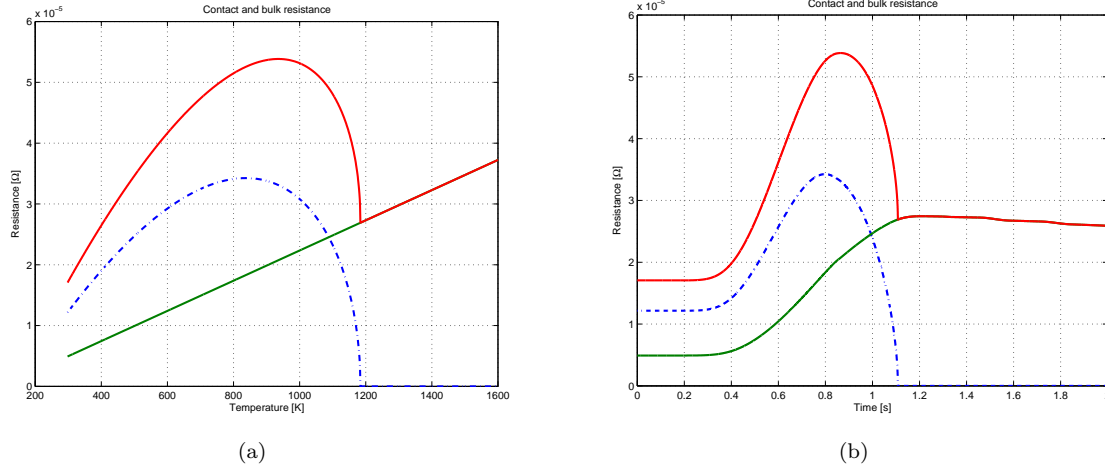
Figure 3.4: (a): theoretical progress of the temperature dependent contact resistance (the blue interrupted line) and bulk resistance for RSt372 steel. The top plot is a summation of both resistances. In (b) a representative temperature progress of the weld process is used.

with T_i the temperature of section i. The numbering i of the sections increases from the welding seam to the left and the right (see also Figure 3.5).

If the material is in contact with the upset or electrodes, vertical conduction $Q_{c,v}(t)$ is present as well. Otherwise energy loss by radiation $Q_r(t)$ is present. The upset is not present until the start of the yielding of the material. Moreover the clamps can open and close. Consequently the energy balance of the deformable sections as well as the balance of the sections between the clamps, switches between $Q_{c,v}(t)$ and $Q_r(t)$.

With the vertical conduction by analogy with the horizontal conduction, the resulting models are

$$Q_{c,v}(t) = \lambda \frac{T_{i+1}(t) - 2T_i(t) + T_{i-1}(t)}{dz^2} dxdydz \tag{3.7}$$

$$Q_r(t) = SB\alpha_\rho(T(t)^4 - T_r^4)dxdy \tag{3.8}$$

with SB the constant of Stefan Boltzmann, α_ρ the temperature resistivity coefficient and T_r the room temperature.

The magnitude of energy loss by convection is assumed to be very small due to negligible air circulation in the working area. Consequently energy loss by convection is neglected.

3.3.4   Internal energy

The internal energy of the material is used in two different ways. The internal energy of the material of the sheets and of the clamps, $Q_i(t)$, is used to convert the balances of energy to a temperature per section. The material in the welding seam that is yielding and actually forming the upset, transports heat into the upset. This heat is represented by the internal energy $Q_y(t)$ of the material. $Q_y(t)$ is used as a loss of energy for the welding seam sections (see section 3.3.1) and a supply of energy for the upset sections. So using the momentary temperature of the material that is yielding, the increase in energy in the upset is calculated by means of the speed of yielding. This loss / supply of energy is called the yielding energy $Q_y(t)$. The models of the internal energy $Q_i(t)$ respectively the yielding energy $Q_y(t)$ are

$$Q_i(t) = \rho C_p \frac{dT}{dt} dV(t) \tag{3.9}$$

$$Q_y(t) = \rho C_p T(t) \frac{dV(t)}{dt} \qquad (3.10)$$
$$= \rho C_p T(t) d\dot{x}(t) dy dz$$

with ρ the specific mass, C_p the specific heat of the material and $d\dot{x}(t) = \frac{dx(t)}{dt}$ the speed of deformation. The specific heat is a temperature dependent parameter. For steel 1010, which is a representative material, holds

$$C_p = 420 + 0,47(T(t) - 273,15) \qquad (3.11)$$

3.3.5 Balances of energy

Six distinctive sections are present in the schematic representation of Figure 3.3. This division is among other things, based on the specific supply of energy $Q_s(t)$ and loss of energy $Q_l(t)$ per section. These supply and loss of energy are used in the specific balance of energy per section. In Figure 3.5 an example of a welding seam section is shown.
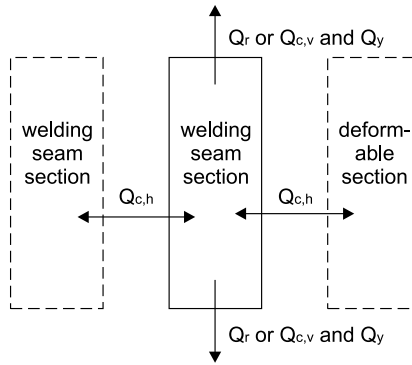

Figure 3.5: schematic representation of a welding seam section.

Analogous to the numbering in Figure 3.3 follows:

section 1 the deformable sections with $Q_i(t)$, $Q_{Rb}(t)$, $Q_{c,h}(t)$ and $Q_r(t)$. If these sections become welding seam sections and start to yield (see section 3.3.1), $Q_r(t)$ changes into $Q_{c,v}(t)$ and $Q_y(t)$.

section 2 the welding seam sections have got the same energy terms as the deformable sections. However, the radiation term $Q_r(t)$ changes to $Q_{c,v}(t)$ and $Q_y(t)$ if yielding starts. Besides, till yielding starts, extra heat generation $Q_{Rc}(t)$ is present (see section 3.3.2).

section 3 the non-deformable sections between the clamps with $Q_i(t)$, $Q_{c,h}(t)$ and till the weld program is ended, $Q_{c,v}(t)$. If the program is ended and the clamps are opened, this latter term becomes $Q_r(t)$.

section 4 the non-deformable sections behind the clamps with $Q_i(t)$, $Q_{c,h}(t)$ and $Q_r(t)$.

section 5 the upset sections include $Q_i(t)$, $Q_{c,v}(t)$, $Q_r(t)$ and $Q_y(t)$. Is is assumed no energy generation $Q_{Rb}(t)$ takes place in the upset.

section 6 the electrode sections include only $Q_{c,v}(t)$. The electric resistance $R_b(t)$ of the electrode material is very low. Consequently the heat generated in the electrodes by means of this electric resistance is neglected. The electrodes are mounted to the rest of the welding machine, which is assumed to stay at room temperature. Hence the heat variation of the electrodes is assumed to be minimal. Most of the heat is conducted to the machine. Energy loss through radiation is neglected because of the relatively low temperatures.

Using the internal energy $Q_i(t)$ and a balance of energy per section, the temperature per section can be calculated:

$$\sum Q(t) \ = \ 0 \tag{3.12}$$

$$Q_i(t) \ = \ \sum Q_s(t) - \sum Q_l(t)$$

$$\frac{dT}{dt} \ = \ \frac{\sum Q_s(t) - \sum Q_l(t)}{\rho C_p dV(t)}$$

$$T(t) \ = \ \int \frac{\sum Q_s(t) - \sum Q_l(t)}{\rho C_p dV(t)} \tag{3.13}$$

Using these equations and the sections as shown in Figure 3.3, a thermodynamical model is developed using Simulink. In this way the temperature of every section is computed and the temperature progress over the complete weld region can be examined (see section 3.7).

3.4   Mechanics of the weld process

The mechanics of the weld process consist of the mechanical behaviour of the welding machine and of the material that is welded. The welding machine includes the hydraulic system, which is discussed in section 3.6. Hence, the mechanics of the welding machine for now are restricted to the moving mass of the welding machine. The mechanical behaviour of the material is described by a mass-spring-damper system with the corresponding spring stiffness k_m and the damping d_m (see section 2.3.1). A schematic overview of the mechanics is given in Figure 3.6. In the next
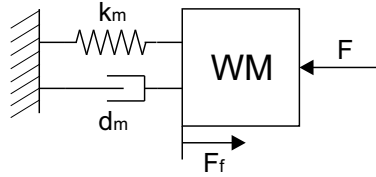

Figure 3.6: schematic representation of the mechanics of the weld process. The welding machine is represented by the moving mass of the welding machine WM, a friction force F_f and the driving force F delivered by the hydraulic system. The mechanics of the metal sheets are represented by a temperature-dependent damping d_m and stiffness k_m.

sections the mechanical behaviour of the material and the mechanics of the welding machine are discussed.

3.4.1   Welding machine

The hydraulic system is not taken into account in the mechanics of the welding machine at this point. Consequently the moving mass of the welding machine of about 300 kg remains. The displacement is driven by the rod of the hydraulic system. A significant amount of friction is present in the movement of this mass (see section 2.3.2). Besides that, an initial gap between the clamped sheets and some slip between the clamps and the material is present, see section 2.3.2.

Static friction is present if the magnitude of the friction force does not depend on the magnitude of the speed. If the magnitude of the friction force does dependent on the magnitude of the speed, Coulomb or viscous friction is present. A combination of both kinds of friction is also possible. Experiments with the moving part of the welding machine driven with a constant speed, are performed. The friction force is the only counteracting force in case no material is clamped. So the mechanical behaviour of the material is left out of consideration. By measuring the pressure difference, the magnitude of the friction force is determined. The magnitude of the Coulomb friction with respect to the magnitude of the static friction is determined by varying the magnitude of the speed in different experiments. In Figure 3.7 the results of these experiments are shown.
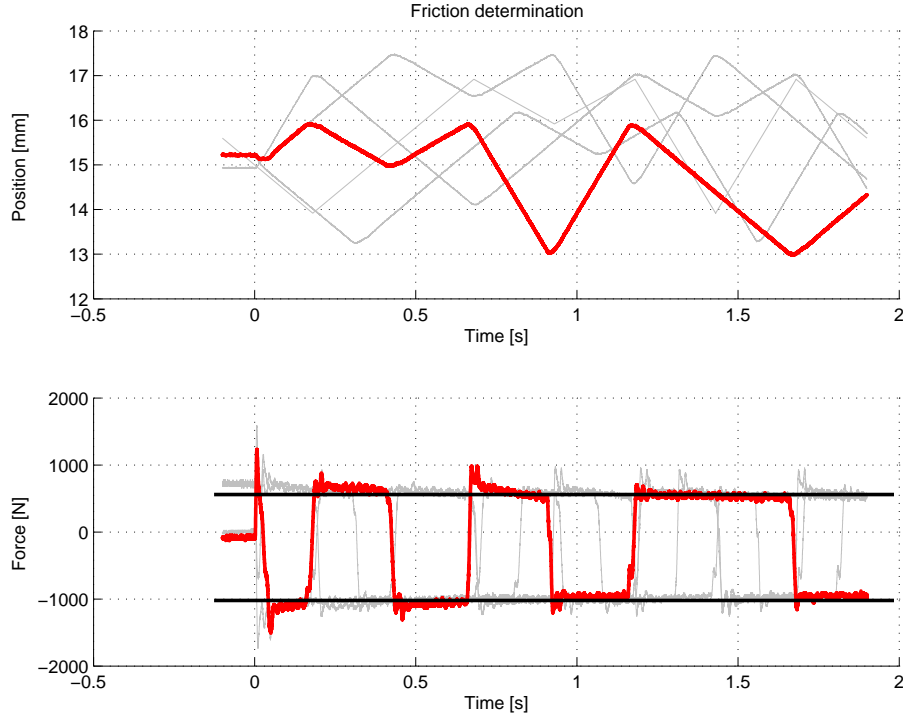

Figure 3.7: results of several measurements to determine the friction in the moving part of the welding machine. For clearness one of the measurements is depicted with a thicker red plot.

The amount of force needed to move the mass, which in this case is equal to the friction force, is substantial. However, the influence of variations in the speed (with respect to the direction of movement) are negligible as can be seen in this figure. Hence the Coulomb friction is assumed to be negligible with respect to the static friction. So only the static friction is taken into account. Using the results of the measurements, the following model for the friction force results

$$F_f = \begin{cases} 550 \ \text{N} & \text{for } \dot{x} > 0 \\ 975 \ \text{N} & \text{for } \dot{x} < 0 \end{cases} \tag{3.14}$$

$$= G_{F_f 1} sign(\dot{x}) + G_{F_f 2} \tag{3.15}$$

with

$$G_{F_f 1} = \frac{550 \cdot 10^3 - 975 \cdot 10^3}{2} \qquad G_{F_f 2} = \frac{550 \cdot 10^3 + 975 \cdot 10^3}{2} \tag{3.16}$$

3.4.2 Mechanical behaviour of the material

In the first part of the weld process, the mechanical behaviour of the material is elastic (see section 2.3.1). This behaviour is modelled with a constant spring stiffness k_{el} and damping d_{el}.

The damping of the material in this part of the process equals about $5.0 \cdot 10^3$ Nsmm^{-1} and the stiffness about $87.5 \cdot 10^3$ Nmm^{-1} (see section 2.3.1). These values are material specific and have to be determined again for a new material or a new cross section.

When the material starts yielding, its mechanical behaviour becomes plastic. The stiffness is reduced to almost zero and the damping determines the speed of displacement during yielding. This damping is dependent on the temperature of the material. The higher the temperature, the smaller the damping. The damping of the sections in the model is coupled in a serial way. Consequently the smallest damping will be significant for the process. The highest temperature is found at the welding seam, so this temperature is used in calculating the damping during yielding $d_{pl}(T)$.

The switch from elastic to plastic behaviour involves a transition region instead of a switching moment. Hence, the switch from a constant k_m and d_m to the almost zero stiffness and temperature dependent d_{pl} involves a transition region as well. The duration of the transition region is calculated and validated by experiments. The friction force present in the welding machine is constant (see section 3.4.1). Compensating the force applied by the hydraulic system for this friction force, the following differential equation results (see Figure 3.6):

$$F(t) = m\ddot{x}(t) + d_{pl,T_y}\dot{x}(t) \tag{3.17}$$

with

$$\begin{cases} \lim_{t \to 0} \dot{x}(t) &= 0 \\ \lim_{t \to \infty} \dot{x}(t) &= \frac{F}{d_{pl}(T)} \\ \lim_{t \to \infty} \ddot{x}(t) &= 0 \end{cases} \tag{3.18}$$

Equation 3.17 is solved for these boundary conditions. This results in an approximation for the displacement $x(t)$ during the transition region and the duration t_{tr} of it. These values are validated using experiments. They give a good indication of the actual displacement and time interval of the transition region.

During the time interval of the transition, k_m and d_m linearly change from elastic to plastic behaviour. With t_{tr} the time interval and t_y the starting time of the transition region

$$t_y = t|_{T(t)=T_y(t)} \tag{3.19}$$

the resulting k_m and d_m become

$$k_m = \begin{cases} k_{el} & \text{for } t \leq t_y \\ k_{el}\left(1 - \frac{t-t_y}{t_{tr}}\right) & \text{for } t_y < t < (t_y + t_{tr}) \\ 0 & \text{for } t \geq (t_y + t_{tr}) \end{cases} \tag{3.20}$$

$$d_m = \begin{cases} d_{el} & \text{for } t \leq t_y \\ d_{el} + \frac{t-t_y}{t_{tr}}(d_{pl(T)} - d_{el}) & \text{for } t_y < t < (t_y + t_{tr}) \\ 0 & \text{for } t \geq (t_y + t_{tr}) \end{cases} \tag{3.21}$$

If the material is at its melt temperature $d_{pl}(T)$ is assumed to be zero. Using a linear interpolation for $d_{pl}(T)$ between the yield and melt temperature, the following holds

$$d_{pl}(T) = d_{pl,T_y}\left(1 - \frac{T - T_y}{T_m - T_y}\right) \tag{3.22}$$

with T_m the melting temperature of the material and d_{pl,T_y} the damping at $T = T_y$.

3.5   Converter system

The magnitude of the electrical current is controlled by a converter system consisting of an inverter and a transformer (see Figure 3.8). First 380 V, 50 Hz alternating current (AC) is rectified to 380 V direct current (DC). The inverter transforms the electrical current at a frequency of

1000 Hz by means of pulswidth modulation. The transformer and rectifier transform the resulting power to 0 to 60 kA DC at a voltage of 0 to 10 V.

The output of the inverter is controlled by a built-in current controller. The controller uses the output current of the inverter and the resulting measured output current of the transformer. In this way the electrical current resulting from the converter system can be controlled in between 0 and 60 kA DC. The control signal of the inverter can be varied in a range of 0 to 1 V, corresponding to this 0 and 60 kA. During this study a maximum of 40 kA instead of 60 kA is used due to a malfunction of the inverter.
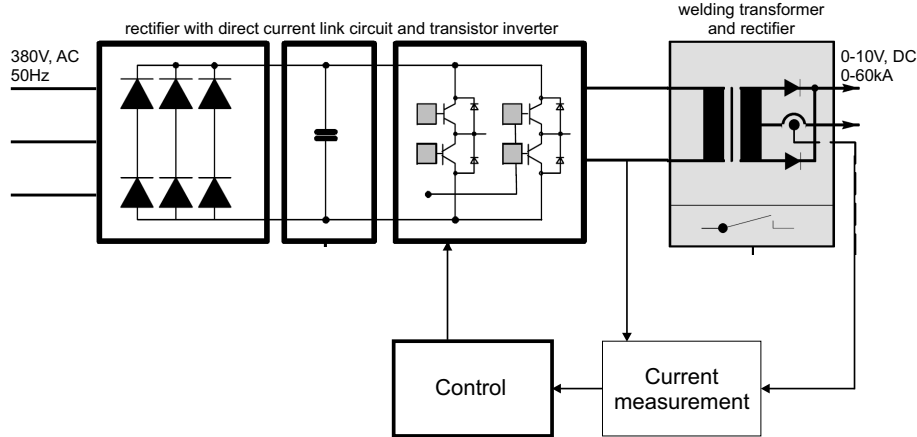
Figure 3.8: schematic overview of the converter system.

Trials to identify the closed loop converter system with the built-in current controller were performed. However this appeared to be hard, so the manufacturer's specifications are used to model this system. Although deficient, the measurement results indicated a bandwidth of 1000 Hz, which corresponds to the specifications. The range of the transformer is 0 to 40 kA, so a 2^{nd}order high frequent filter with a gain $G_{cs} = 40 \cdot 10^3$ is used

$$\omega_{cs,o} = 1000 \ \text{Hz} \tag{3.23}$$
$$\xi_{cs} = 0.6 \tag{3.24}$$

with $\omega_{cs,o}$ and ξ_{cs} the natural frequency respectively the damping of the 2^{nd}order filter.

3.6 Hydraulic system

The hydraulic system is an important part of the setup. The upset force as well as the displacement in the process can be controlled by steering the input signal of the servo valve. Various calculations, measurements and modelling of the hydraulic system have been performed in previous studies. However none resulted in a model good enough to use as a reliable representation of the hydraulic system or the developed models could not be validated because of a lack of good measurements. The controller used at the moment suffices for the purpose it is used for. But because it is partly based on trial and error instead of on theoretical base, the possibilities of the hydraulic system are not utilised to its full potential. Consequently special attention is paid to the modelling and the control of the hydraulic system in this study.

To start with, an overview of hydraulic system is given. Next a parametric white box model of the hydraulic system is developed. This model is linearised so that the results can be verified using the frequency domain. Apart from this model a black box model is fitted, based on measurements performed on the hydraulic system at the setup. These results are also evaluated using the frequency domain. Next the results of the black box model, of the white box model and of the

measurements are compared. A new control strategy for the hydraulic part of the weld process is developed as conclusion. This can be used in the present weld program and may be of use in developing a controller for the total weld process. Most of the white box and black box modelling as well as the performed measurements are presented in Appendix C. The results of this modelling and these measurements are discussed in this section.

3.6.1   Overview of the hydraulic system

The main parts of the hydraulic system present in the setup, are depicted in Figure 3.9. The electric hydraulic servo valve is steered by the control signal u_v. This results in a flow q_L to the hydraulic cylinder. The hydraulic cylinder generates the upset force F_{up}, driving the external mechanics, which results in a displacement y.
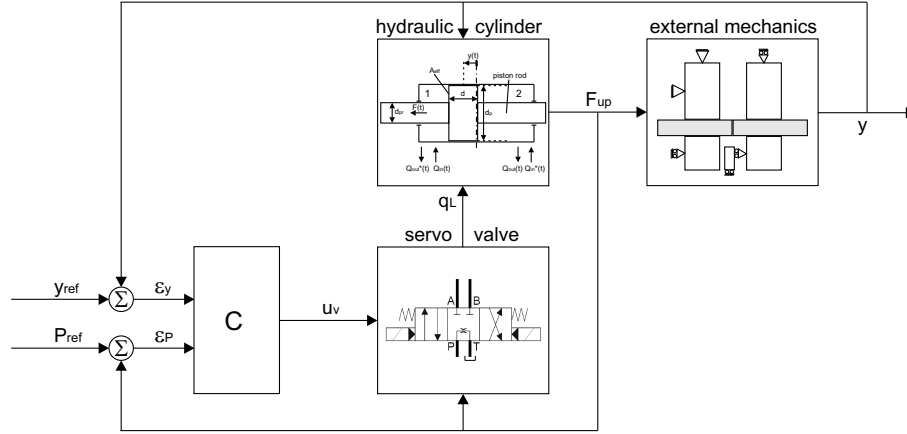

Figure 3.9: schematic representation of the hydraulic system of the setup with C a feedback controller, partly used to control the force $F_{up}(t)$ and partly to control the displacement $x(t)$.

Using this hydraulic system two main purposes can be distinguished. The pressure (or force) resulting from the hydraulic cylinder can be used as a control variable. Or the displacement of the mechanics can be used as a control variable. During the weld process, the pressure is the control variable. In the phases before and after the actual weld process, the horizontal distance between the clamps is the control variable. So in modelling the system both situations have to be taken into account.

3.6.2   White box modelling

A complete overview of the white box modelling and a description of the various parts of the hydraulic system is given in Appendix C. The resulting model [Post, 2005], [Viersma, 1990], [Merrit, 1967], [Wijnheijmer & Naus, 2005], [Kokernak, 1998] (see equations C.40 and C.13) is given by

$$\dot{p}_n(t) = \frac{E_{oil}A_{eff}}{p_s}\left(\frac{1}{V_1(t)} + \frac{1}{V_2(t)}\right)\left(\frac{q_l(t)}{A_{eff}} - \dot{y}(t) - R_p p_n(t)\right) \tag{3.25}$$

$$A_{eff}\dot{y}(t) = -\frac{V_1(t)V_2(t)}{E(V_1(t)+V_2(t))}\dot{p}_L(t) + q_l(t) - R_p A_{eff} p_n(t) \tag{3.26}$$

with

$$q_l(t) = q_n(x_n - \frac{p_n(t)}{2}sign(x_n(t))) \tag{3.27}$$

Both the electric hydraulic servo valve and the hydraulic actuator show nonlinear behaviour (see equations 3.25 to 3.27). The nonlinear, time domain models of the servo valve and hydraulic cylinder are linearised and transformed to the frequency domain. In this way insight in the characteristics of the hydraulic system is expanded. Moreover, validation of the model using measurement data, becomes easier. The natural frequency of the hydraulic cylinder with coupled mass, is dependent on the position of the rod $y(t)$ (see equations 3.25 and 3.26). If the rod is on half of the stroke of the cylinder (at mid stroke), the natural frequency becomes minimal. The hydraulic stiffness of the hydraulic cylinder equals

$$Co(t) = E_{oil}A_{eff}^2 \left(\frac{1}{V_1(t)} + \frac{1}{V_2(t)} \right) \tag{3.28}$$

$$= \frac{E_{oil}A_{eff}L}{\frac{L^2}{4} - y(t)^2} \tag{3.29}$$

with $y(t)$ defined as a displacement from mid stroke. So the theoretical natural frequency of the hydraulic cylinder equals

$$\omega_o = \sqrt{\frac{Co(t)}{m}} \tag{3.30}$$

Only the influence of the position of the rod on the natural frequency is shown. Validation using measurements is discussed in the next section. In Figure 3.10 the pressure transfer function of the hydraulic system is shown at three different positions of the rod. The positions are $y = 0$ mm, $y = 10$ mm and $y = 13$ mm. From equations 3.29 and 3.30 the theoretical natural frequency of the hydraulic cylinder can be calculated. For these positions, this natural frequency equals 95 Hz, 129 Hz respectively 192 Hz. Figure 3.10 shows that the results of the white box model correspond well to these values.
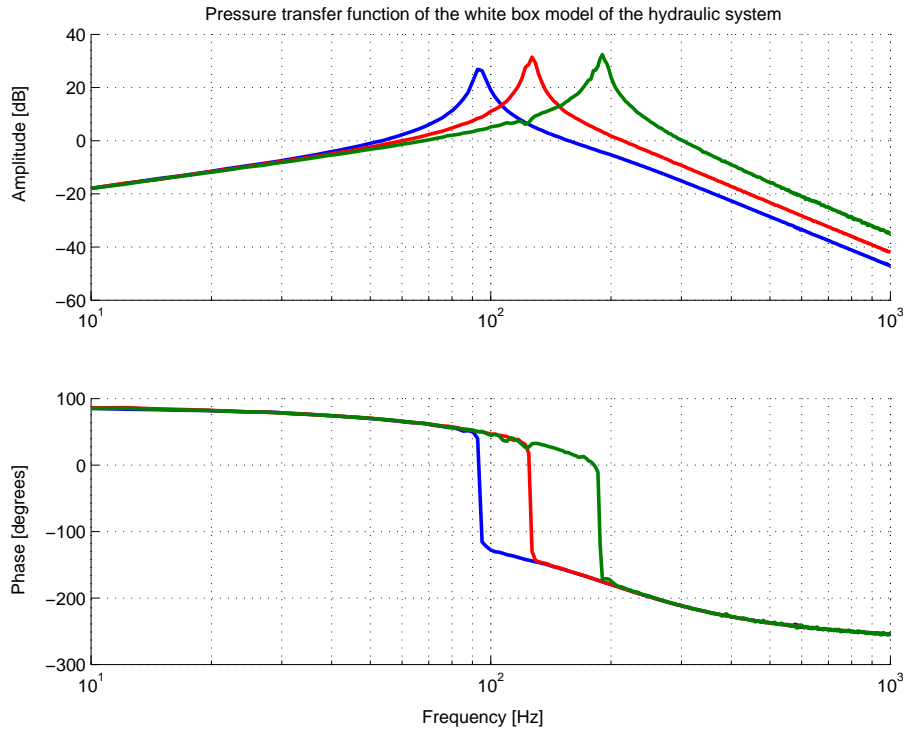

Figure 3.10: pressure transfer functions of the hydraulic system resulting from the white box model at various rod positions y.

3.6.3   Measurements and black box modelling

The techniques described in section C.2 of Appendix C are used to determine the transfer functions of the hydraulic servo system of the setup. The pressure as well as the displacement resulting from the hydraulic system are of importance in the weld process. So two distinctive transfer functions are determined. The transfer function estimates of the pressure and of the displacement are shown in Figure 3.11. The measurements at the setup to determine these transfer functions, are performed with the rod positioned at mid stroke. Using CDesign [MCDesign, 2005] a black box model is fitted over the measurement results (see also Figure 3.11). In fitting the black box model, the restrictions determined in section C.3 of Appendix C are taken into account. This black box model is off course only valid for this rod position. The transfer functions resulting from the linearised white box model are show in Figure 3.11 as well. A mechanical model of the welding machine including its mass and static friction is used as external mechanics in the white box model. This mechanical model is discussed in more detail in section 3.4 and section C.1.3.

(a) pressure transfer function   (b) position transfer function
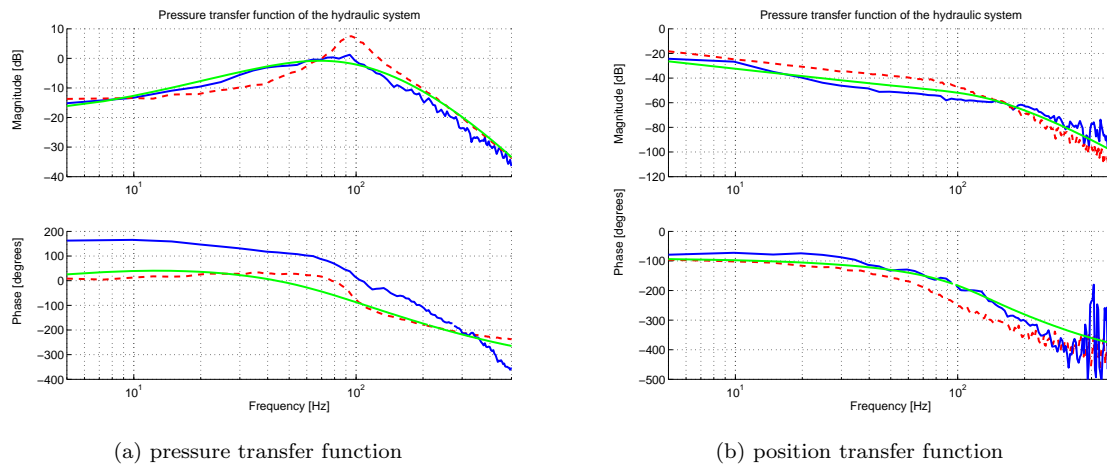
Figure 3.11: transfer functions of the white box model (the dashed red plots), resulting from measurements (the blue plots), and the black box model (the (light) green plots on top of the others). (a): transfer function of the pressure. (b): transfer functions of the position.

Because the measurements are performed with the rod positioned at mid stoke, the transfer function estimates of these measurements show the lowest natural frequency of the system. The lower the natural frequency, the smaller the bandwidth of the system will be. Consequently, the working point with the lowest natural frequency has to be used in modelling, considering robustness of the controlled system. In this way, the developed controllers will be robust for other working points as well. Hence the fitted black box model is used in further development of a new controller for the hydraulic system (see section 3.6.4). Because of the position dependent characteristics, the white box model is used in further modelling of the total weld process.

3.6.4   Control of the hydraulic system

The hydraulic system is used to control the position of the rod as well as the welding force. During the weld process, the upset force has to be controlled. Before and after the actual weld process, the system is position controlled. The design of a position controller is not further discussed at this point. More details on the control of the position can be found in Wijnheijmer & Naus [2005]. In Figure 3.12(a) the characteristic progress of the demanded force and of the actual force during a weld process are depicted. The controller used, is the present force controller of WELD2001. This controller is dependent on the speed of displacement. In Figure 3.13, the controllers corresponding

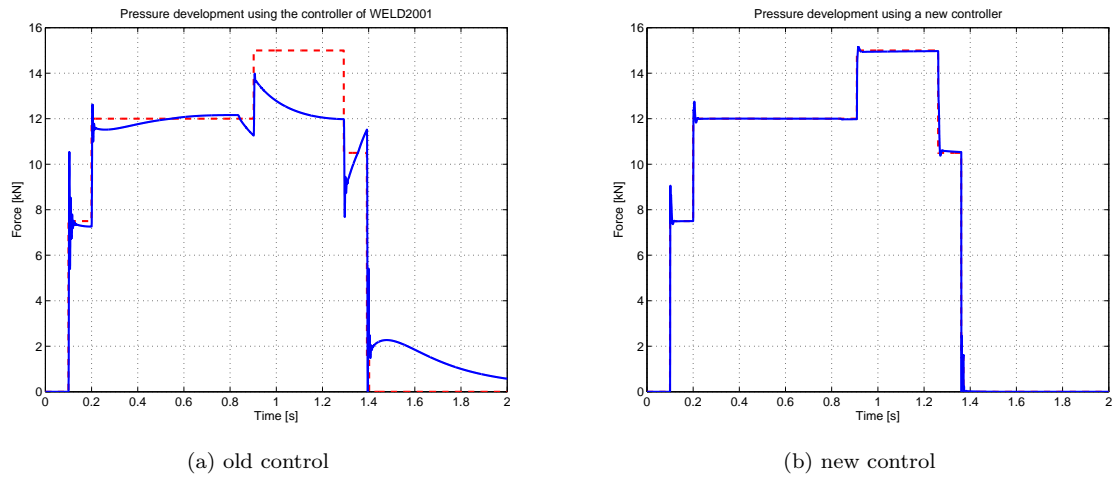(a) old control   (b) new control

Figure 3.12: (a): the old control of the force in the weld process and a (b) new controller. The dotted plot indicates the setpoint signal and the solid plot the actual force.

to a speed of 0 mms^{-1} and of 15 mms^{-1} are shown. In the yielding phase, an extra boost in the reference trajectory of the force is present. This boost is prescribed to overcome the sudden drop in compression at the welding seam. Its purpose is not to increase the force, but to keep it relatively constant, which, as can be seen in Figure 3.12(a), is the case. At the end of the boost, nothing is left of it in the actual force. Consequently a new controller is developed apart from the study to a new control strategy for the total weld process. The fitted black box models are used to apply loop shaping techniques using CDesign [MCDesign, 2005]. The developed controller is shown in Figure 3.13. A clear distinction between the present controllers and the new controller can be noticed. The new controller damps the natural frequency of the system, where the old controllers only have an integrating action. In this way, the bandwidth of the controlled system can be increased. In Figure 3.12(b), a simulation result using the newly designed controller is shown. Comparing this figure to Figure 3.12(a) indicates the adequacy of the new controller.

3.7 Modelling results

All modelled parts of the weld process, as discussed before, are now combined to a single model. This results in a complete model, which can be used to simulate the weld process off-line, see `SimulationModel.mdl` in Appendix F. The model is developed using Simulink. To facilitate working with this model, a Simulink Library is written, see Appendix B. Models of the hydraulic system and of the converter system are already validated separately (see sections 3.5 and 3.6). So the main attention in this section lies on the results of the weld process part, the thermodynamical and mechanical parts of the model. The progress of the electrical current, of the pressure and of the displacement are measured during the weld process. These measurement results are compared to the results of simulations to test the validity of the model. The progress of the modelled pressure and electrical current follow from the combination of the weld program and the hydraulic system respectively the converter system. So the displacement is the only variable that can be used to validate these parts directly. The temperature is an important variable in the weld process too, but it is not measured. However, some experiments using thermocouples and an infrared camera are performed. In this way an indication of the real temperature progress during the weld process is obtained. The results of these experiments are compared to the temperature progress resulting from the model. In Figures 3.14 and 3.15 the results of several experiments with varying magnitude of the electrical current and of the force are compared to the results of simulations. The simulation
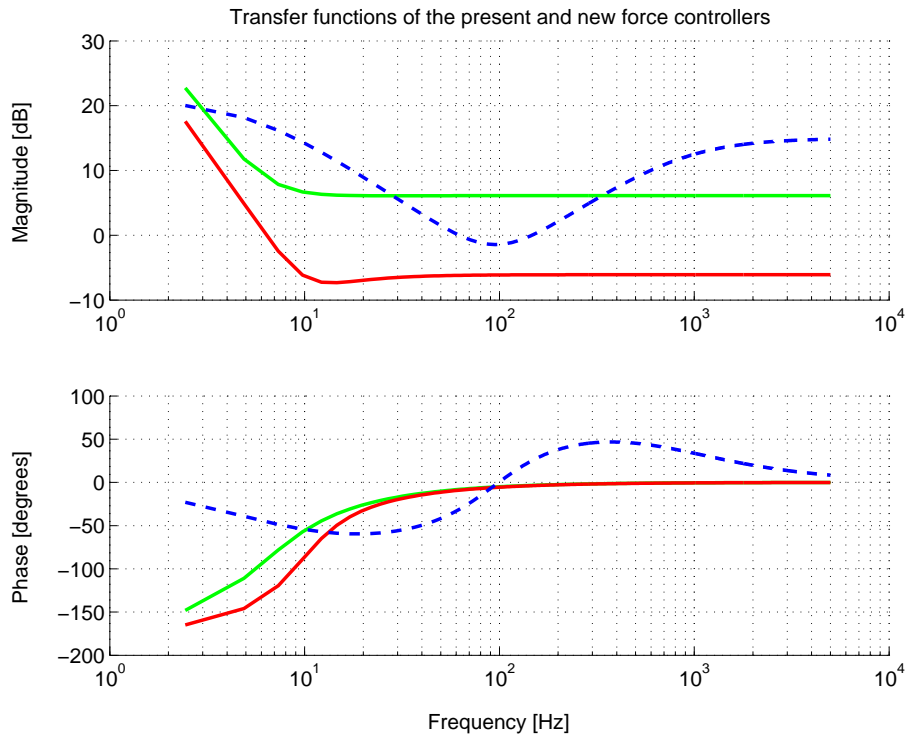
Figure 3.13: the force feedback controllers of the hydraulic system as implemented in WELD2001 (the solid red and green plots) and a newly designed controller based on the black box model (the dashed blue plot).

model used for these experiments did not include the models of the hydraulic system and converter system yet. Hence, the setpoints for these variables are used instead of the controlled variables. The weld programs used in the simulations are the same as those used in the experiments.

The switching moments between the various phases can be determined from the progress of the electrical current and of the force. They correspond good as can be seen in Figures 3.14 and 3.15. The amplitude of the displacement progress of the model also corresponds well to the experiments. So from these results, it may be concluded that the thermodynamical and mechanical part of the weld process are modelled well enough to provide a good representation of the progress of the displacement during the actual weld process.

The displacement progress is dependent on both the thermodynamics and mechanics of the process. Consequently the temperature progress resulting from the model is assumed to give a good indication of the real temperature progress. In Figure 3.16 the results of measurements using a thermo couple and an infrared camera are compared to the temperature progress resulting from simulations. A comment on these measurements is that both measurements are random samples instead of results of a series of tests. Consequently, the weld programs of Figure 3.16(a) and 3.16(b) differ. Besides, the measurements give an indication of the temperature at a single point in the welding seam. The temperature values resulting from the simulations however, represent an average temperature over the welding seam. From the results can be concluded that the time intervals of the heating and of the yielding are comparable. The same applies for the maximum temperature reached during the process. The actual progress of the temperature however can be better registered by the measurements of the infrared camera. The temperature progress during cooling down is better represented by the thermo couple measurement. So an indication of the temperature resulting from the simulation model is given. But no unambiguous conclusions can be drawn concerning the validity of this progress with respect to the performed measurements.
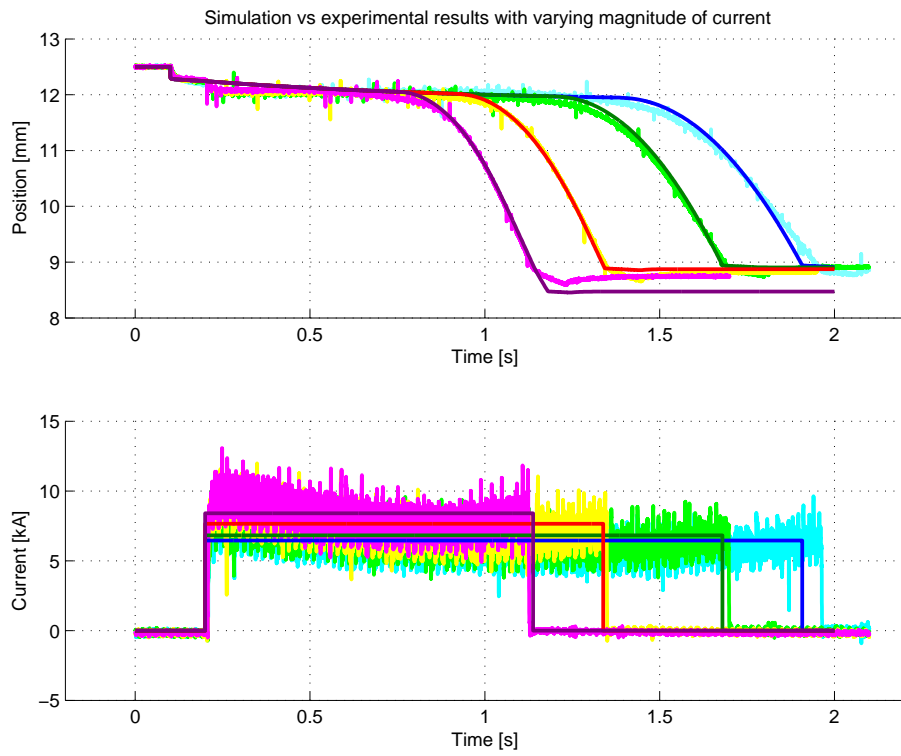
Figure 3.14: displacement and electrical current progress of simulations compared to experiments with varying current.
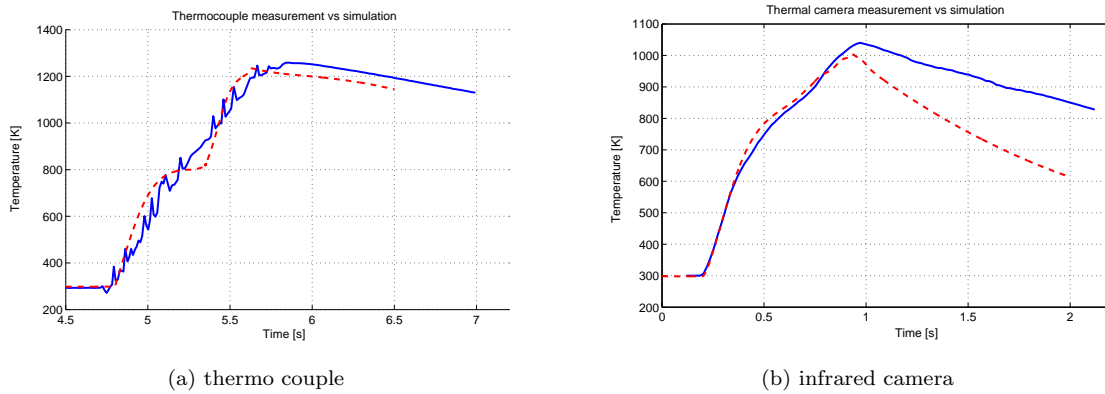

(a) thermo couple

(b) infrared camera

Figure 3.16: temperature progress during the weld process resulting from the simulation model (dashed red plot) compared to (a): a measurement using a thermo couple (solid blue plot), (b): a measurement using an infrared camera (solid blue plot).
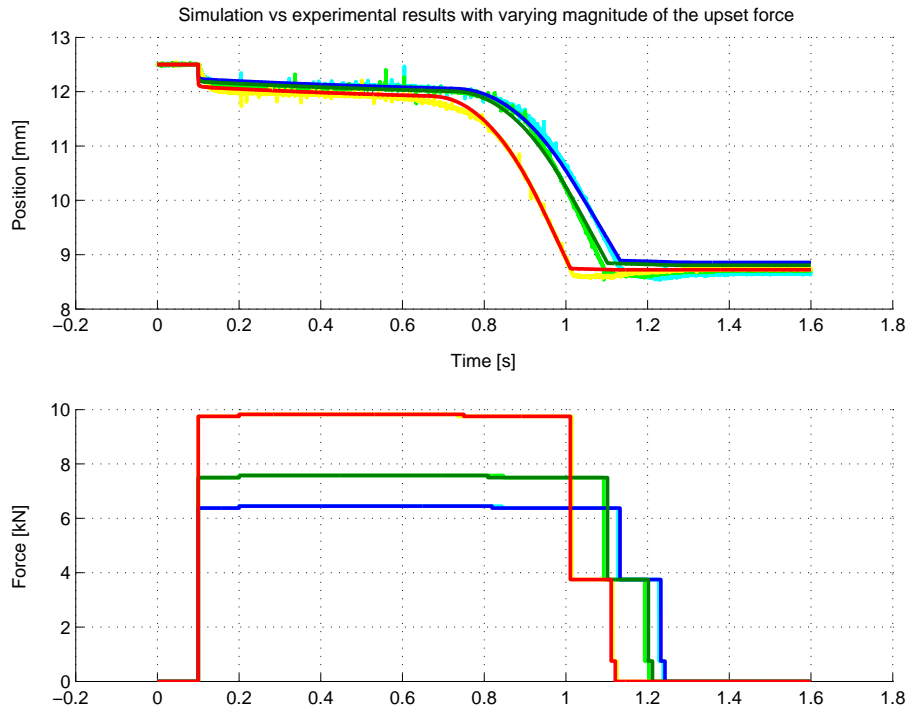
Figure 3.15: displacement and force progress of simulations compared to experiments with varying force.

Chapter 4

Control

The aim of this study is to develop a more robust and reliable control strategy based on good insight in the weld process. The development of the controller is presented in this chapter. First the demands to the controller and the possible control strategies to apply, are discussed. From this a new control strategy, including an on-line temperature calculation, reference trajectories and the actual controller design, follows. Finally the implementation of the controller and the results are discussed.

4.1 Demands to the controller

The demands to the new control strategy are derived mainly from the advantages and disadvantages of the present control strategy. The present control of the weld process is based on a discrete steering of the force and electrical current. The process is divided into 5 phases based on position and time restrictions. Consequently the position is a restriction, limiting the amount of displacement per phase instead of really prescribing the position progress during the weld process. Most of the welding machines are part of an automated rim production line and thus only have a predefined amount of time to perform the weld process. Moreover, the weld process often is one of the time restricting processes (see section 1.3). The time the process takes however, is only limited per phase. So the process time is not predefined and can only be tuned via trial and error. Consequently the magnitude of the electrical current and the force are based on trial and error instead of being dependent on material parameters. Setting these variables during switching between different materials or rim sizes takes a lot of time and experience. The quality of the weld depends on the resulting christalline structure of the material in the weld. This structure in particular depends on the temperature progress of the material during welding. As this temperature is not measured nor coupled to the weld program, nothing can be said about the weld quality with respect to the weld program. The most important demands to the controller thus are:

- a reproducible weld process

- execution of the weld process within a previously defined time interval

- the demanded amount of upset has to be reached exactly

- if possible, some control of the temperature is desirable. In this way the resulting crystalline structure of the material of the weld may be influenced.

Apart from these demands, practical advantages for the customer are also of importance. Failure of rims by cracking seems to happen arbitrarily at the moment. If the weld process is controlled

43

better, this may be solved. Customers off course have the wish for shorter weld times and shorter setup times. The setup of the weld program is done by trial and error at the moment. The new control strategy is based on insight in the process and most of the tuning of the controller is done in advance. The process time thus is defined in advance and setup times may be decreased.

The development of a new control strategy based on the foregoing demands, is discussed in the next section.

4.2   Control strategy

The weld process is a nonlinear process, which can be divided into a heating and a yielding part. The characteristics of the process are different for each part, so the controller has to be process dependent. The question arises whether a model-based controller can be developed. First of all the model of the weld process as derived in Chapter 3 has only limited accuracy. Secondly, parts of the model are rather extensive, which makes it difficult to use in a model-based controller. Because of these rather extensive parts, the total order of the model is large. This also puts a restriction to the choice of a suitable control strategy. So a model-based controller is not the first choice at this point.

A second option is to examine both parts of the weld process separately and split up the control problem into two separate parts. This seems to be a good choice regarding the weld process. In the heating part, the mechanics of the weld process are rather steady. In the yielding part, the thermodynamics are of less importance while the mechanics of the process become more important. This indicates that a linearisation of both parts of the process should be possible. Thus, the development of the controller can be simplified. If the weld process is split up into two linear models, the two separate controllers can be designed using loop shaping techniques. Linearising the first part of the weld process, assuming the mechanics of the process to be constant, probably will be not to hard. Linearisation of the yielding part, including the transition from elastic to plastic material behaviour however, may be more difficult. A solution may be to use a gain scheduling controller for this part of the process. The controller becomes process dependent in applying a gain scheduling controller. Due to the linearisation used, this may not be a problem nevertheless. If two separate controllers are developed, these have to be linked. So besides the two controllers, a strategy to switch from the first to the second controller has to be developed.

The temperature and pressure are the variables to be controlled during the heating part of the weld process. In the second part the displacement is the variable to be controlled. The temperature progress during the heating part as well as the position progress during the yielding part are known in advance. They are determined by the yield temperature of the material, the total process time and the amount of upset demanded. The pressure is needed to assure good contact of the metal sheets and catalyses the yielding. So for all three variables, a reference trajectory can be designed. This leads to the development of a tracking controller. A schematic representation of the setup of the new control strategy as defined till now is shown in Figure 4.1.

Unlike the pressure and displacement, the temperature is not measured. The developed model from which the temperature follows, is too extensive to use for on-line calculation. If the model is simplified, the calculation of the temperature may be possible nevertheless. The switching moment of the two controllers will lie at the start of the yielding region. At that moment, the temperature equals the momentarily (force dependent) yield temperature of the material. So the calculation of the temperature has to be good relative to the calculation of the yield temperature. Using a simplified model, this calculation may be suitable for on-line implementation.

The controller shown in Figure 4.1 is a MIMO controller. It has three inputs: the error in the pressure, the displacement and the temperature and two outputs: the control signals of the converter system and the hydraulic system. In developing the controller, it has to be taken into account that this way of control is new to the customers. Till now they could adjust the amount of pressure and electrical current very straightforwardly. With this new control strategy the actual controller is hidden in the design. This means it will become more difficult for the customer to adjust the controller. The intention is to preserve the customer adjusting the controller, but this
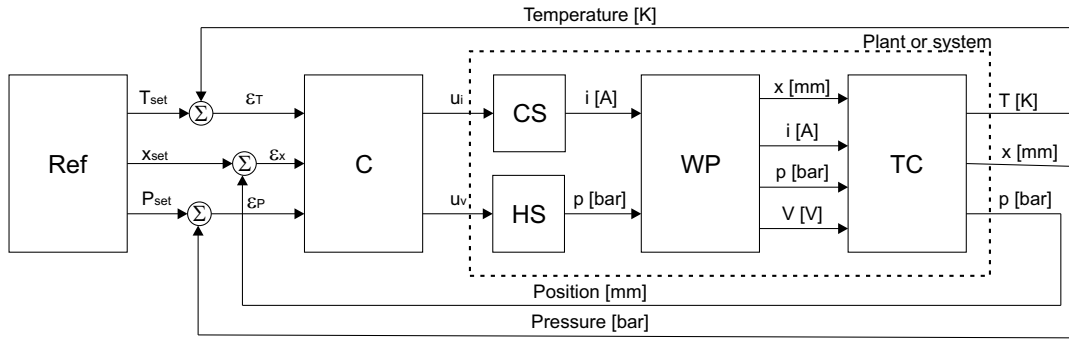
Figure 4.1: schematic overview of the new control strategy with the reference trajectories Ref, a MIMO controller C, the converter system CS, the hydraulic system HS, the weld process WP and the temperature calculation TC.

may not always be possible. To overcome this problem partly, controllers only using gains are designed in the first place. Application of gains only, makes it easier to understand the operation of the controller. Secondly, also controllers that are more dedicated to their purpose are designed. Thus the possibilities of the new control strategy are examined. Taking into account that two linear models of the weld process will be used, loop shaping techniques are very suitable.

So first a simplified model of the weld process is derived, leading to a temperature calculation suitable for on-line implementation. The model developed in Chapter 3 is used as a base for this model. Next, the model is split up into two parts, which are linearised separately. Two rather simple and two more sophisticated tracking controllers are designed. Loop shaping techniques are used to design these controllers. Besides that, a switching strategy is developed and three reference trajectories are designed. The controllers and trajectories are tested using simulations. Finally they are implemented on the setup and tested experimentally.

4.3 Temperature calculation and simplified model

The temperature of the welding seam is one of the variables to be controlled. The temperature is not measured, so it has to be calculated on-line. For this calculation a simplified model of the model developed in Chapter 3 is derived. Assumptions made to simplify this model are:

- The material in between the clamps is regarded as two pieces of material instead of a number of sections in formulating the balance of energy. The same holds for the upset parts.

- Energy loss through radiation is neglected because of the very small contribution with respect to energy loss through conduction for example. The loss through radiation is of the order $O(10 \cdot 10^{-2})$, while the loss through conduction is of the order $O(10 \cdot 10^2)$

- Using measurement results of an infrared camera, heating of the electrodes is shown to be minimal. Hence, heating of the electrodes is neglected.

- The transition region of elastic to plastic behaviour of the material is not approximated completely. The damping during the yielding phase remains temperature dependent. The transition from the elastic to the plastic stiffness and damping however, is defined by a switch.

Furthermore, the assumptions made throughout Chapter 3 are taken into account.

Defining the state vector $\underline{x}(t)$

$$\underline{x}(t) = \begin{bmatrix} x_1 & = & \text{normalised spool valve position } x_n(t) \\ x_2 & = & \text{velocity of the normalised spool valve movement } \dot{x}_n(t) \\ x_3 & = & \text{normalised pressure } p_n(t) \\ x_4 & = & \text{welding seam temperature } T(t) \\ x_5 & = & \text{displacement of the right clamp } y(t) \\ x_6 & = & \text{velocity of the right clamp } \dot{y}(t) \\ x_7 & = & \text{electrical current } i(t) \\ x_8 & = & \text{time derivative of the electrical current } \dot{i}(t) \end{bmatrix} \tag{4.1}$$

the input vector $\underline{u}(t)$

$$\underline{u}(t) = \begin{bmatrix} u_1 & = & \text{inverter control signal } u_i(t) \\ u_2 & = & \text{servo valve control signal } u_v(t) \end{bmatrix} \tag{4.2}$$

and the output vector $\underline{y}(t)$

$$\underline{y}(t) = \begin{bmatrix} y_1 & = & \text{displacement } y(t) \\ y_2 & = & \text{temperature } T(t) \\ y_3 & = & \text{normalised pressure } p_n(t) \end{bmatrix} \tag{4.3}$$

the nonlinear state-space representation of the model becomes

$$\begin{aligned} \dot{\underline{x}}(t) &= \underline{f}(\underline{x}(t), \underline{u}(t)) \\ \underline{y}(t) &= \underline{g}(\underline{x}(t), \underline{u}(t)) \end{aligned} \tag{4.4}$$

An overview of the resulting set of nonlinear differential equations $\underline{f}(\underline{x}(t), \underline{u}(t))$ and $\underline{g}(\underline{x}(t), \underline{u}(t))$ is given in Appendix D.

The temperature progress influences the quality of the resulting weld. Consequently the temperature calculation has be a good approximation of the real temperature progress during the weld process. As far as good control is considered however, it should be a good fit with respect to the calculation of the yield temperature. The yield temperature of the material is dependent on the upset force and the characteristic yield stress at room temperature (see equation 2.5). The yield temperature is calculated on-line as well. It defines the switch from the heating phase to the yielding phase and consequently a switch in control strategy.

The model derived in Chapter 3 was validated by the progress of the displacement (see section 3.7). Taking into account the assumptions made at the start of this section, this is not possible for this simplified model. The progress of the displacement is used as the main validation variable in section 3.7. The transition region is not taken into account in this simplified model, so the progress of the displacement is not representative. However, the calculation of the temperature with respect to the calculation of the yield temperature can be validated. The switch from elastic to plastic material behaviour is defined by reaching the yield temperature. This moment in the weld process is calculated by the model and can be determined from the measured pressure or position progress as well. Experimental results show that the simplified and the temperature calculation meet their purpose.

The temperature progress resulting from a simulation is compared to the measurement as used in Figure 3.16(b) (see Figure 4.2). The progress of the temperature while heating the material is the main goal of this model. Hence, the measurement using a thermo couple (see Figure 3.16(a)) is not used in this case. The temperature progress resulting from the model reaches the same maximum value as the measured temperature. The amount of time the total heating takes is also comparable.
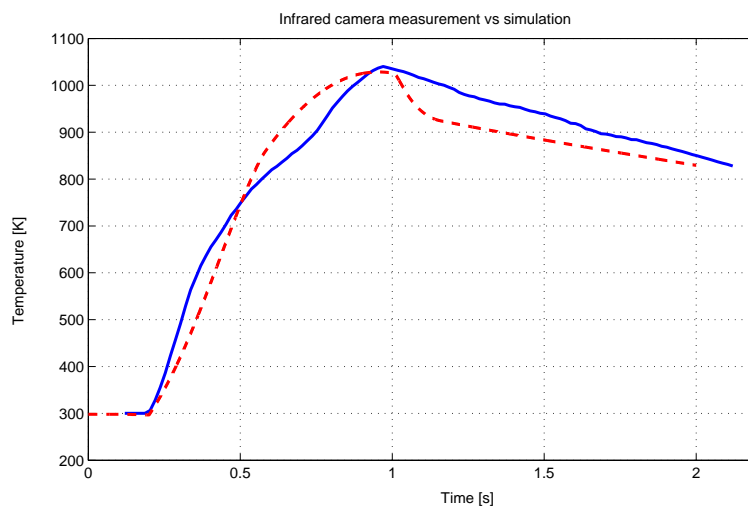
Figure 4.2: temperature progress during the weld process resulting from the model to calculate the temperature on-line (dashed red plot) compared to a measurement using an infrared camera (solid blue plot).

Instead of the modelled bulk resistance and contact resistance, the measured potential over the clamps may be used. The resulting model is discussed in Appendix D. In this way the model is simplified yet more. Consequently several material parameters can be omitted. This increases the reliability of the model. In implementing the controller, this potential measurement is applied besides the model developed at the start of this section. The latter one is compared to the results of the potential measurement. In this way a better validation of this part of the model is obtained.

4.4 Linearisation

To apply loop shaping techniques, a linear model of the system is needed. However, the model derived in Chapter 3 as well as the simplified model derived in section 4.3 are nonlinear. Hence a linearisation has to be applied to get a linear model. The model derived in section 4.3 will be used as a basis for this linearisation, because this model will also be used for the on-line calculation of the temperature.

The characteristics of the system change significantly when the yielding point of the material is reached (see section 3.4). Consequently at least two linear models are needed to describe the dynamics of the system. The corresponding linearised models are H_1 and H_2. The process is divided into two parts: a heating and a yielding part. To notice whether a single linearisation point per phase satisfy, the moment in time of the linearisation points is varied and the resulting transfer functions are compared.

4.4.1 Theory

In linearising a model, a specific point in the process is used as an equilibrium point. In this point, all the variables of interest behave in a linear way [Franklin, 1994]. Consequently the model can be approximated by a linear model at this point, $\underline{x} = \underline{x}_0$. Because of the linear behaviour of the system, for this point holds

$$\underline{\dot{x}} \quad = \quad \underline{f}(\underline{x}, \underline{u}) = \underline{0} \tag{4.5}$$

with $\underline{u}$ the vector of inputs and $\underline{f}$ the system of nonlinear differential equations (equation D.6). With $\delta\underline{x}$ a vector of (small) variations around this linearisation point follows

$$\underline{x} = \underline{x}_0 + \delta\underline{x} \tag{4.6}$$

The same holds for the input vector $\underline{u} = \underline{u}_0 + \delta\underline{u}$, which results in

$$\begin{aligned}
\underline{\dot{x}} &= \underline{\dot{x}}_0 + \delta\underline{\dot{x}} & (4.7) \\
&\cong \underline{f}(\underline{x}_0, \underline{u}_0) + \mathbf{A}\delta\underline{x} + \mathbf{B}\delta\underline{u} & (4.8)
\end{aligned}$$

with $\mathbf{A}$ and $\mathbf{B}$ the best linear fits to the system of nonlinear differential equations D.6 at $\underline{x}_0$ and $\underline{u}_0$, the so-called the Jacobian of the system

$$\begin{aligned}
\mathbf{A} &= \left.\frac{d\underline{f}(\underline{x}, \underline{u})}{d\underline{x}}\right|_{\underline{x}=\underline{x}_0, \underline{u}=\underline{u}_0} & (4.9) \\
\mathbf{B} &= \left.\frac{d\underline{f}(\underline{x}, \underline{u})}{d\underline{u}}\right|_{\underline{x}=\underline{x}_0, \underline{u}=\underline{u}_0} & (4.10)
\end{aligned}$$

The resulting linear model describing the nonlinear model with $\underline{x} = \underline{x}_0$ as the center to vary around is

$$\delta\underline{\dot{x}} = \mathbf{A}\delta\underline{x} + \mathbf{B}\delta\underline{u} \qquad (4.11)$$

The linearisation point is the new origin, so the bias of the linear model with respect to the nonlinear model is given by $\underline{x}_0$.

4.4.2   Implementation

Using equation 4.4, the state-space representation of the linear model becomes

$$\begin{aligned}
\underline{\dot{x}}(t) &= \mathbf{A}\underline{x}(t) + \mathbf{B}\underline{u}(t) & (4.12) \\
\underline{y}(t) &= \mathbf{C}\underline{x}(t) + \mathbf{D}\underline{u}(t)
\end{aligned}$$

with $\underline{x}$, $\underline{u}$ and $\underline{y}$ as defined in section 4.3 and A, B, C and D constant matrices. Applying the linearisation as defined in section 4.4.1, A and B are calculated. The other matrices result from the demanded output of the model as defined in section 4.3.

Some restrictions have to be taken into account in linearising the model. The spool valve position $x_n(t)$ may not be chosen zero for example (see section 3.6).

To simplify implementation of the linearisation, a graphical tool is developed (see also Appendix F). The operation of the tool is as follows: first the process is simulated using the nonlinear model and an user-defined weld program. The resulting progress of the displacement, of the temperature and of the pressure are presented in a graph. Next, the linearisation points have to be chosen by indicating these points in this figure. Figure 4.3 shows an example in which the black circles indicate the chosen linearisation points. The number of linearisation points can be chosen arbitrarily with at least one point in both parts of the process. After that, the model is linearised per point. The resulting linear models are simulated and the results are plotted in the same graph. An example of the results using 5 linearisation points is given in Figure 4.3. The starting conditions of the linearised models depend on the end state of the preceding model. In this way the entire process is covered.
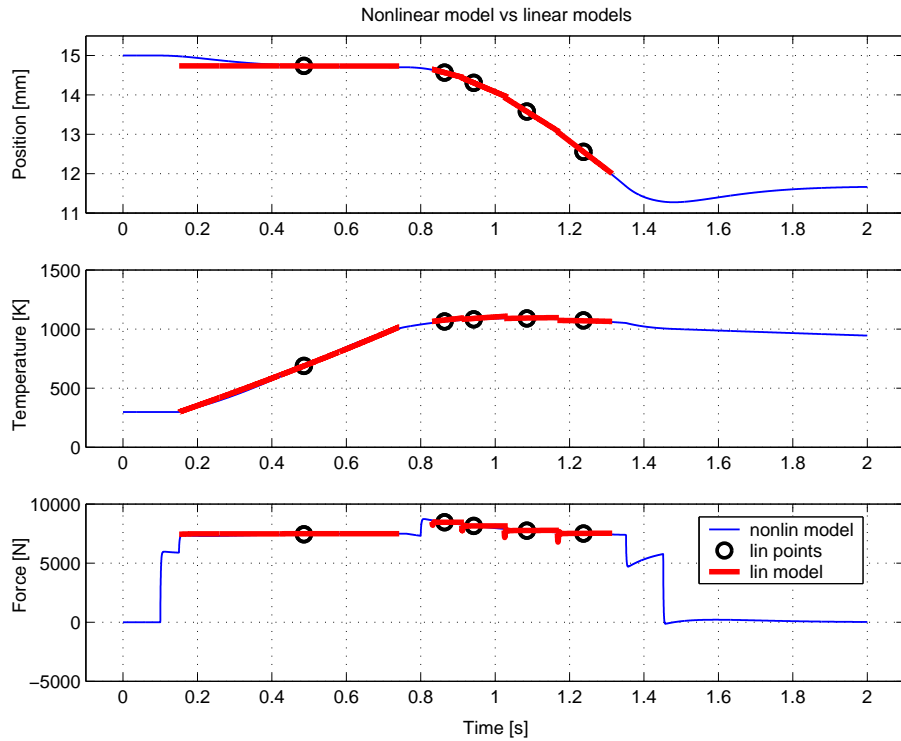
Figure 4.3: resulting displacement, temperature and pressure progress of a simulation using both the nonlinear model and the linear models resulting from the linearisation tool.

4.4.3   Results

The influence of varying the position of the linearisation points on the resulting linear models is examined. Small variations in the characteristics of the system can best be noticed in the transfer functions of a system.

Frequency domain results of simulations are examined These results show that variation of the linearisation point in the first part of the process does not have significant influence on the characteristics of the linear model. Consequently a single linearisation point in the middle of this phase is used to determine a linear model for this phase. The time domain result is shown in Figure 4.3. Due to the transition region from elastic to plastic material behaviour, the characteristics of the linear models vary during the yielding phase. This phase is split up into several parts, which have to be linearised separately (see Figure 4.3). Just the transition region is not taken into account if the yielding phase is approximated by a single well-chosen linearisation point. The major part of the yielding phase can be described relatively good by a single linear model. In designing a robust controller however, the model with the lowest natural frequency is of importance instead of the one describing the major part of the process. The lower the natural frequency of a system, the harder it is to design a stable controller with a demanded bandwidth. If this stable design succeeds for the linear model with the lowest bandwidth, the same controller often is suitable for the other models as well.

In Figure 4.4 one of the transfer function of H_2 is shown for a linear model determined by choosing a linearisation point at the start of the yielding phase and one with a linearisation point at the end of the yielding phase. This is a representative example of the influence of the variation in the characteristics of the other transfer functions. The variation in the characteristics of the linear models are small, especially in the working region, which starts at about $1 \cdot 10^{-2}$ Hz. The more the linearisation points are chosen close to the start of the yielding phase, the lower the natural frequency of the models. Hence the transfer functions of the linear model closest to the

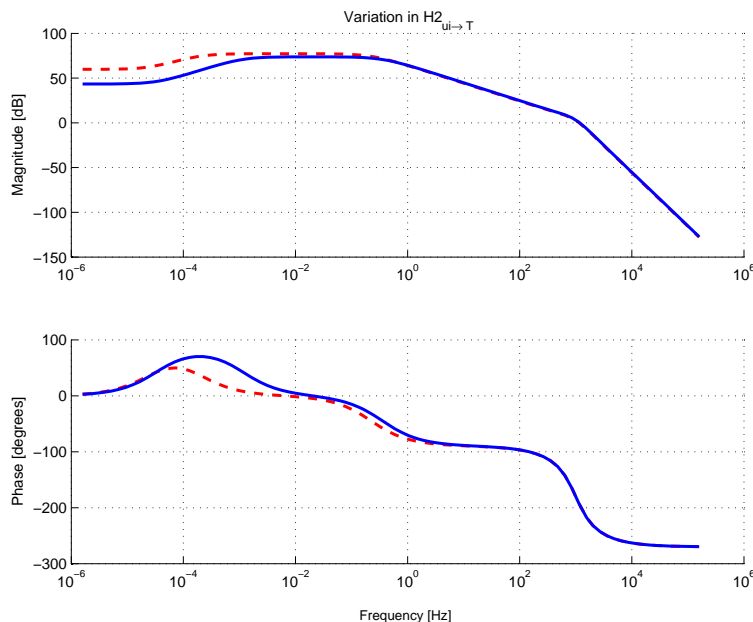start of the yielding phase is used for this phase.

Figure 4.4: difference in the resulting transfer function of $H_2|_{u_i \to T}$ if the linearisation point to determine the linear model is chosen at the start (the red dashed plot) or the end (the solid blue plot) of the yielding phase.

As shown in Figure 4.1 the total system has two inputs and three outputs. The inputs are the servo valve control signal u_v and the inverter control signal u_i and the outputs are the position x, the temperature T and the pressure p. This means 6 separate input-output relations and thus 6 transfer functions can be defined. In Figures D.1 and D.2 of section D.2 of Appendix D, the transfer functions H_1 and H_2 for the heating, respectively the yielding phase are shown. These figures show that during the heating phase the pressure as well as the position are not influenced by the magnitude of the electrical current. So no transfer functions for $H_1|_{u_i \to x}$ and $H_1|_{u_i \to p}$ are present.

4.5   Reference trajectories

As discussed in section 4.2, reference trajectories for the temperature, pressure and displacement are designed. The trajectories for the temperature and pressure are only of importance for the heating phase. The position trajectory is to be followed during yielding. In future the temperature may be prescribed during yielding or during curing as well to prescribe the speed of cooling down. No good indication of this speed with respect to the quality of the resulting weld is present yet, but it is studied by the NIMR (see section 1.2). In this section first the design of the reference trajectories is discussed after which an example of the resulting trajectories using different materials is given.

4.5.1   Design of the reference trajectories

The reference trajectories for the temperature, pressure and displacement are based on the characteristics of the the weld process and the material used. However the main process variables like the process time or amount of upset can be adjusted within bounds. Hence the parameters used are split up into 3 categories

1. **process variables** like the the process time and the amount of upset demanded. These variables influence the progress of the trajectories.

2. **setup variables** like the magnitude of the supply pressure of the hydraulic system or the size of the cross section of the material used

3. **material parameters** like the stiffness, electrical conductivity, etc.

The material parameters are furthermore split up into parameters that are or can be identified experimentally and parameters that follow from literature. The first ones may become learning in future by monitoring the progress of these parameters in subsequent processes. In this way drifting of the quality of the implemented controller during numerous process due to material variations can be overcome. See also section 4.5.2. In Figure 4.5 an example of three characteristic reference trajectories is given. The main process variables used to design the reference trajectories are
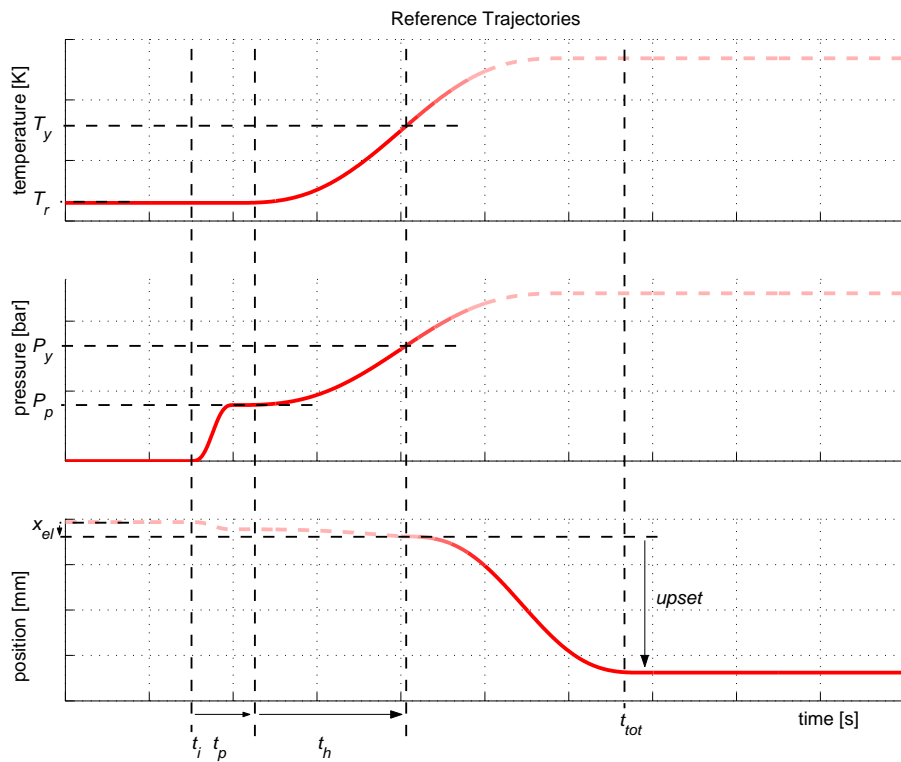

Figure 4.5: reference trajectories for the temperature, pressure and position including the main process variables.

depicted in this figure as well. These variables can be adjusted within bounds to adjust the trajectories to the material used and the demanded process specifications.

   Temperature progress
A skew sine function is used for the increase in temperature to assure a smooth progress of the process. This facilitates control of the process. The initial temperature T_r equals the room temperature. The temperature at the start of the transition to position control equals the pressure dependent yield temperature T_y. To assure the process does not stop heating if the yield temperature is reached, the temperature reference keeps on increasing during the transition region. The duration of the heating phase t_h, heating the material from $T = T_r$ to $T = T_y$, is user defined.

Pressure progress

As well as for the temperature, a skew sine function is used for the increases in pressure. The magnitude of the initial pressure P_p is user defined. It is needed to close the gap between the sheet ends and form a contact surface. The duration t_p of this initial gap-closing is user defined. The pressure at the start of the transition region P_y is also user defined but if chosen too low, the pressure during yielding will be too low and spattering will occur. Hence the pressure reference keeps on increasing during the transition region as well. It is examined if a constant force at the welding seam assures good welding so that this pressure will be dependent on the size of the cross section of the material.

Position progress

The start of the position trajectory is determined by the size of the initial gap, the slip and the elastic stiffness of the material. In combination with the pressure reference trajectory this latter one yields an elastic deformation. All three are defined using experimental results. The transition region present in the position trajectory is approached again by a skew sine function. The accurateness of this skew sine describing the transition region is validated using the results of section 3.4.2). Besides that, the resulting progress is compared to experiments to design a reference trajectory best suited. The end position is dependent on the user defined amount of upset.

4.5.2   Material determination

In producing wheel rims, numerous types of steel and even aluminium are used. Because the reference trajectories of the previous section are based on material parameters, these parameters have to be determined in advance. Often suppliers of materials are not very generous in indicating the exact composition and characteristics of their materials. The materials fulfill a prescribed standard and furthermore some general parameters are provided. Some specific parameters however like the yield temperature T_y or the electrical resistivity ρ_e are hard to find. Parameters like the stiffness and damping of the material k respectively d are just modelling parameters, but are also material specific.

Therefore the first version of a tool to determine some of these parameters is developed. In future the tool may be automated by implementation of for example iterative learning techniques, see section 4.6.4. In Table 4.1 some of the major parameters used in the design of the reference trajectories are summarised and a way to determine them is given.

The resulting reference trajectories after parameter identification of two types of steel are shown in Figure 4.6. Three different types of steel were used from which only one was definitely HR45. Both the other types were assumed to be QSTE and because the parameter variation between these latter was not significant enough to be noticed in the resulting reference trajectories, only one of the results is shown.

4.6   Controller design

Based on the linear models derived in section 4.4 the requested controllers are designed. For the heating phase, denoted by H_1, a controller C_1 is designed to control the temperature and pressure. For the yielding part H_2, a controller C_2 is designed to control the position progress. Via steering of the control signals of the inverter and servo valve, u_i respectively u_v, the electrical current respectively the upset force needed in the weld process are prescribed. Loop shaping techniques [Steinbuch, 2005] are used and because of the MIMO structure of the controller, also sequential loop closing is applied. To facilitate working with these techniques the tool MCDesign [MCDesign, 2005] specialised in managing MIMO control problems is developed, see Appendix C. Besides the design of the controllers and a strategy to switch from C_1 to C_2, the application of learning techniques are examined.

Quantity		Importance	Determination
yield temperature	T_y	used to determine the switching point between (the controllers of) the heating and yielding phase	apply of a constant electrical current till yielding starts, determined by a displacement, speed or pressure drop
yield temperature calculation	$E * \alpha_{th}$	used in calculating the pressure dependence of the yield temperature	several experiments with varying yield pressure P_y
electrical resistivity	ρ_e	used in calculating the resistance in the material to determine the heat generation	varying distance between the clamps, applying a constant electrical current and using one and two sheets of metal (see section 2.3.4)
elastic material stiffness	k_{el}	part of the total displacement at the yield point at which the position control starts	varying magnitude of the gap-closing pressure P_p, taking into account the initial $SlipGap$
average size of slip and initial gap	$SlipGap$	part of the total displacement at the yield point at which the position control starts	varying gap-closing pressure P_p, up and down

Table 4.1: overview of material dependent parameters, significant in the design of the reference trajectories.

4.6.1 Sequential loop closing

In MIMO systems, various interacting loops exist. This means that a controller designed for one loop, may influence the system's behaviour of other loops as well. When a second controller is designed for another loop, this controller does not only "feel" the original system, but also the influence of the controller of the first closed loop. Consequently in designing a second controller, the first controller designed influences the second closed loop when evaluating the stability, robustness, etc. This can be extended to more controllers and is indicated as sequential loop closing.

The sequential loop closing system H_{sl}, which is the system including at least one closed loop, can be calculated. This is the system "felt" by the next controller to be designed. The MIMO controller is split up into two parts (see Figure 4.7). The first part containing the already designed controllers substituting a zero for the controller to be designed next, C_a. And the second part with zeros substituted for all controllers except for the controller to be designed next, C_b. The control signal $\underline{u}$ now is built up of two separate parts (see Figure 4.7). Treating the input $\underline{r}$ as a disturbance considered to be zero, H_{sl} can be determined using the process sensitivity PS (see Figure 4.7)

$$\underline{\epsilon} = \underline{y} \quad \text{for } r \simeq 0 \tag{4.13}$$

$$PS = \frac{Y}{U_a} = \frac{H}{1 + C_a H} \tag{4.14}$$

$$= \frac{E}{U_a} = H_{sl} \tag{4.15}$$

Y, U_a and E are the Laplace transforms of y, u_a and ϵ. Using $H_{sl,i}$ instead of H_i in designing C_i, stability can be guaranteed for this second loop. For each following controller to be designed $H_{sl,i}$ can be determined.

In this case, sequential loop closing is useful to some extent. In the heating phase both the temperature and the pressure have to be controlled. As follows from the transfer functions
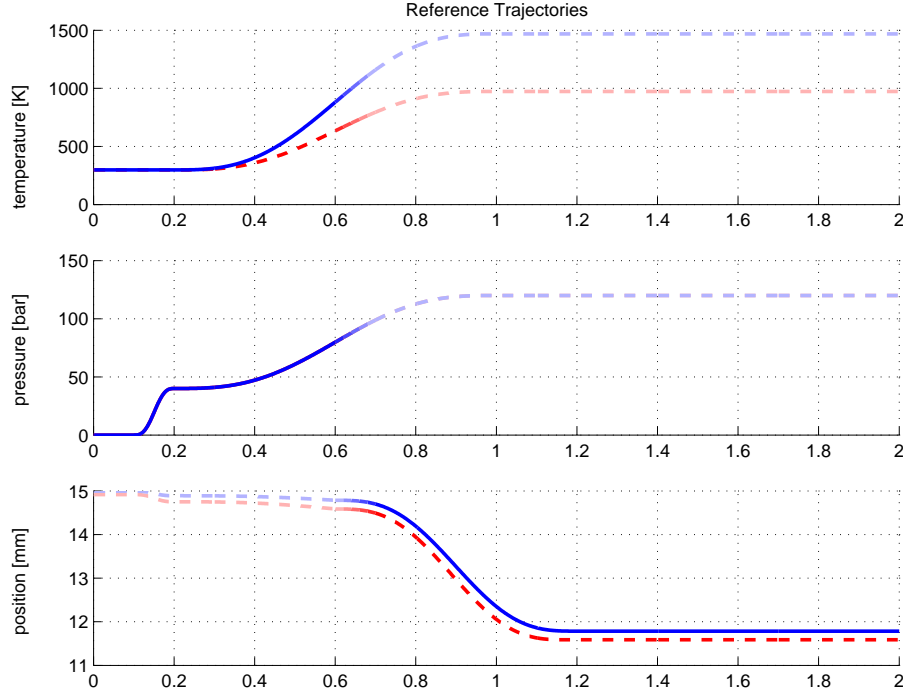
Figure 4.6: reference trajectories for two different types of steel. The dashed red plots are resulting from HR45, the solid blue plots from material assumed to be QSTE.

of this first part of the weld process (see Figure D.1), the pressure seems to have no influence on the temperature and vice versa. This holds even if the temperature is only controlled by steering the inverter control signal u_i and not by steering the servo valve control signal u_v. The temperature is influenced by the servo valve control signal, $H_1|_{u_v \to T}$ in Figure D.1, but this does not affect the transfer function from u_i to the temperature error. This can be checked by calculating both possible sequential loop closing systems and comparing them with the original system. Implementing a controller $C_1|_{\epsilon_p \to u_v}$ to control the pressure by steering the servo valve control signal, $H_{1,sl}|_{u_i \to T}$ does not change. The same holds for the controller $C_1|_{\epsilon_T \to u_i}$ and $H_{1,sl}|_{u_v \to x}$. So for the heating phase, two SISO controllers can be designed using loop shaping techniques, see section 4.6.2.

In designing the position controllers for the yielding phase, the first controller to be designed influences the system "felt" by the second one. If the position is controlled using u_v, the transfer function from u_i to the position error is influenced and vice versa. Starting with a controller $C_2|_{\epsilon_x \to u_v}$ to control the position steering the servo valve control signal, the system "felt" by the controller $C_2|_{\epsilon_x \to u_i}$ becomes

$$H_{2,sl}|_{u_i \to x} = \frac{H_2|_{u_i \to x}}{1 + H_2|_{u_v \to x} C_2|_{\epsilon_x \to u_v}} \tag{4.16}$$

and vice versa if $C_2|_{\epsilon_x \to u_i}$ is designed first, the system "felt" by $C_2|_{\epsilon_x \to u_v}$ becomes

$$H_{2,sl}|_{u_v \to x} = \frac{H_2|_{u_v \to x}}{1 + H_2|_{u_i \to x} C_2|_{\epsilon_x \to u_i}} \tag{4.17}$$

In Figure 4.8 the original system and the sequential loop closing system of $H_2|_{u_i \to x}$ are shown with the control loop of $H_2|_{u_v \to x}$ already closed. At low frequencies the latter has a relatively
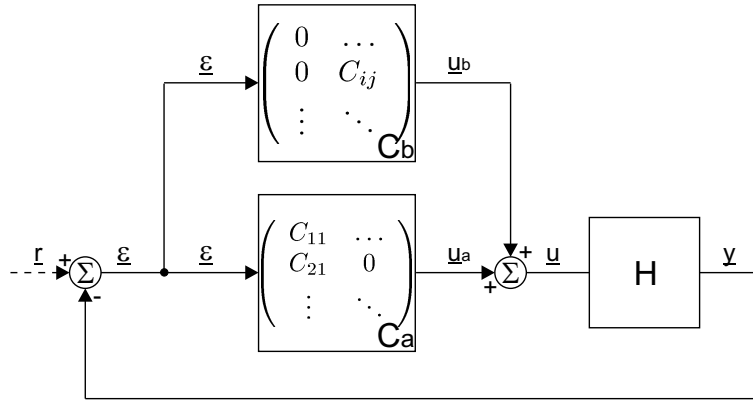
Figure 4.7: schematic representation of the setup to determine the sequential loop closing system H_{sl}. With the weld process H and controller parts of a MIMO controller C_{ij}.

large magnitude as results from Figure D.2. Consequently the influence on $H_2|_{u_i \to x}$ is significant in this region and the larger the magnitude of $C_2|_{\epsilon_x \to u_v}$, the larger this influence will be. The other way around the influence is smaller and although $H_{2,sl}|_{u_v \to x}$ also differs from $H_2|_{u_v \to x}$ at low frequencies, this has not the most significance.

In this case first controller $C_2|_{\epsilon_x \to u_v}$ is designed, because $H_2|_{u_v \to x}$ is a more reliable transfer function than $H_2|_{u_i \to x}$. Therefore the influence of this first closed loop on $H_s l$ calculated for the design of the second controller is assumed more reliable as well. So $H_s l$ as defined in equation 4.16 is used in designing the second controller $C_2|_{\epsilon_x \to u_i}$. The design of these controllers is discussed in section 4.6.2.

4.6.2 Loop shaping

As concluded in section 4.2, two separate controllers for the heating respectively the yielding phase of the weld process are required. Besides that, a set of controllers using only gains and a set using more advanced control actions have to be designed. Using the transfer functions derived in section 4.4 and taking into account the sequential loop closing techniques of section 4.6.1 these controllers are designed using loop shaping techniques. To start with the controllers based on gains only, a gain for which the controllers show good results and an upper bound for these gains are defined. The upper bounds are used for as safety gains in implementation. CDesign in combination with MCDesign is used for this purpose.

Starting with the heating phase 2 SISO controllers, $C_1|_{\epsilon_T \to u_i}$ and $C_1|_{\epsilon_p \to u_v}$, are designed. The first one controlling the temperature by steering the control signal of the inverter and the second one controlling the pressure by steering the control signal of the servo valve. The duration of heating is defined to be in between 0.3 to 1.0 s. Consequently the bandwidth of the corresponding closed loop has to be in the order of $O(10)$ Hz. About 0.1 s is allowed for the duration of the setup of pressure changes. Hence, the bandwidth of the corresponding closed loop has to be of at least the same order as the first closed loop.

During the yielding phase the position is controlled by $C_2|_{\epsilon_x \to u_i}$ and $C_2|_{\epsilon_x \to u_v}$. As discussed in section 4.6.1 the latter controller is designed first. The average time of yielding is about the same as the heating time, so the bandwidth of the corresponding parts of the controlled system using these controllers has to be in the order of $O(10)$ Hz too.

In Table 4.2 the controller gains designed are shown. A striking result is the large difference between the upper bounding value and the working value for $C_1|_{\epsilon_T \to u_i}$. From this result may be concluded that the converter system is oversized for this setup. However the capacity of the hydraulic system is too small. The capacity of the converter system is suited to weld cross sections up to 500 mm^2 instead of the 150 to 200 mm^2 the the hydraulic system is suited for.
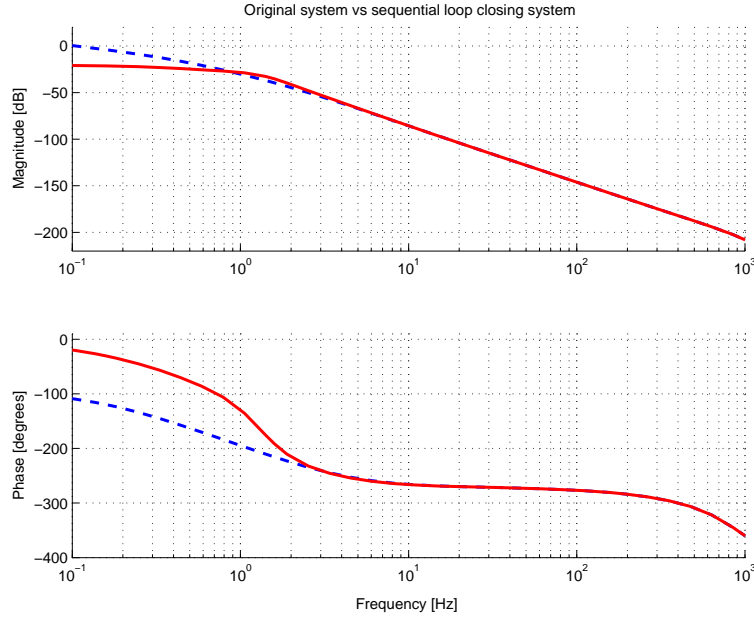
Figure 4.8: the original system versus the system resulting from sequential loop closing. The dashed blue plot shows the original transfer function $H_2|_{u_i \to x}$ and the solid red plot the system actually "felt" by $C_2|_{\epsilon_x \to u_i}$ with the control loop of $H_2|_{u_v \to x}$ already closed.

Controller	Upper bound		Working value	
$C_1|_{\epsilon_T \to u_i}$	0.1	400 Hz	0.004	6 Hz
$C_1|_{\epsilon_p \to u_v}$	1.2	100 Hz	0.8	65 Hz
$C_2|_{\epsilon_x \to u_v}$	0.6	2 Hz	0.3	1 Hz
$C_2|_{\epsilon_x \to u_i}$	15	0.7 Hz	10	0.5 Hz

Table 4.2: feedback controllers, designed using only a gain. The upper bounds as well as working values for the gains are given.

Controller $C_2|_{\epsilon_x \to u_i}$ is designed using a gain of 0.05 for $C_2|_{\epsilon_x \to u_v}$. The higher this gain, the higher the bandwidth of the open loop system $H_2|_{u_i \to x} C_2|_{\epsilon_x \to u_i}$ if the gain of $C_2|_{\epsilon_x \to u_i}$ is increased simultaneously.

Some demands to the closed loop system are not met using the controllers presented in Table 4.2. First, not all demanded bandwidths are reached. Besides that, simulation and experimental results show small steady state errors. This can not be solved by controllers using only gains. Consequently controllers using more advanced control techniques have been designed.

The closed loops corresponding to the controllers $C_1|_{\epsilon_T \to u_i}$ and $C_1|_{\epsilon_p \to u_v}$ satisfy the demanded bandwidth (see Table 4.2). Moreover, if necessary, the bandwidths can be increased yet. However simulation and experimental results show small steady state errors. So for both cases application of an I-action may be useful. However the present working gain of $C_1|_{\epsilon_T \to u_i}$ can be increased that much before it reaches its upper bound, that an I-action is only applied in $C_1|_{\epsilon_p \to u_v}$. This already is discussed in section 3.6.4.

An exact amount of upset resulting after yielding is one of the demands to the controller. However after implementation of the controllers $C_2|_{\epsilon_x \to u_v}$ and $C_2|_{\epsilon_T \to u_v}$, a small steady state error in the position response results. Besides that, the demands to the bandwidths of the corresponding closed loops are only nearly met. First an I-action is applied in $C_2|_{\epsilon_x \to u_v}$. In order to increase the bandwidth, also damping is added. The open loop system using the original controller as presented in Table 4.2 and the new controller for two different gains is shown in Figure 4.9. Using a gain of $7 \cdot 10^{-5}$, the corresponding open loop has a bandwidth of 1 Hz and a phase margin of 90 deg. Increasing the gain to $6.5 \cdot 10^{-4}$ this bandwidth increases to 5.5 Hz. The phase margin however decreases to 45 deg (see Figure 4.9). During this study a paper on the modelling and position control of hydraulic systems has been written [Wijnheijmer & Naus, 2005]. This paper can be used as a guide for this part of the control problem.
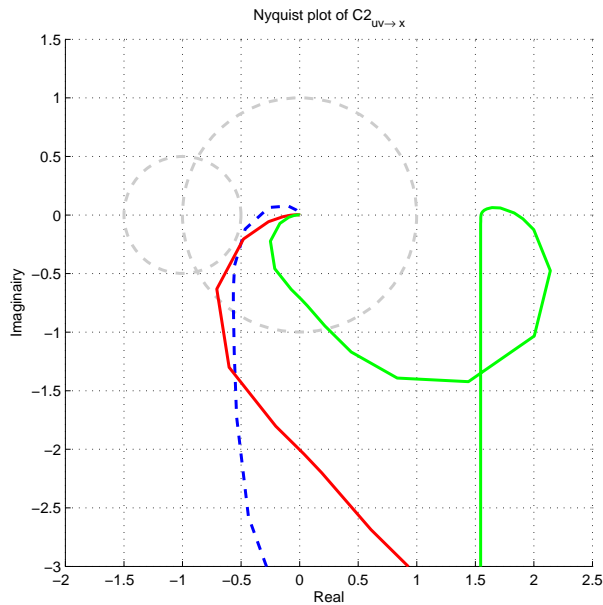

Figure 4.9: open loop responses of $H_2|_{u_v \to x} C_2|_{\epsilon_x \to u_v}$. The dashed blue response shows the open loop using only a gain for $C_2|_{\epsilon_x \to u_v}$. I-action as well as damping is applied in both the other two responses. The difference between them is a varying gain. The bandwidths of the responses are 2 Hz, 1 Hz and 5.5 Hz.

In designing $C_2|_{\epsilon_x \to u_i}$, the sequential loop closing system $H_{2,sl}|_{u_i \to x}$ is used. In the closed loop present in $H_{2,sl}|_{u_i \to x}$, $C_2|_{\epsilon_x \to u_v}$ of Table 4.3 with a gain of $7 \cdot 10^{-5}$ is used. The higher the gain of $C_2|_{\epsilon_x \to u_v}$, the more the gain of $C_2|_{\epsilon_x \to u_i}$ can be increased in order to increase the bandwidth

Controller	textrmDesigned controller	textrmBandwidth
$C_1\|_{\epsilon_T \to u_i}$	$G_1\|_{\epsilon_T \to u_i}$	6 Hz
$C_1\|_{\epsilon_p \to u_v}$	I-action at 0.3 Hz and a gain varying in between 1 and 2.7	$40 \ldots 100$ Hz
$C_2\|_{\epsilon_x \to u_v}$	I-action at $1.6 \cdot 10^{-4}$ Hz, D-action at 1.6 Hz, extra pole at 1300 Hz and a gain varying in between $7.5 \cdot 10^{-5}$ and $3.2 \cdot 10^{-4}$	$1 \ldots 4$ Hz
$C_2\|_{\epsilon_x \to u_i}$	D-action at 0.5 Hz, an extra pole at 100 Hz and a gain varying in between 17 and 90	$0.5 \ldots 4$ Hz

Table 4.3: feedback controllers, designed using more advanced control techniques.

of the corresponding open loop. For the design of $C_2|_{\epsilon_x \to u_i}$ the same holds as for $C_2|_{\epsilon_x \to u_v}$. The bandwidth of the corresponding open loop can be increased to almost 4 Hz by the application of damping. However no I-action is applied, because this may lead to reheating of the material if the demanded amount of uset is not reached quick enough. In future this may be compensated by a switchable electrical current.

The implementation of these controllers and the results are discussed in section 4.7.

4.6.3   Switching control

Now two successive MIMO controllers for the two parts of the weld process are designed. Consequently a transition between these controllers has to be developed. An often applied strategy to obtain a varying controller is gain scheduling. However, gain scheduling rather is applied to nonlinear systems for which the nonlinearity can be described by a single varying parameter or variable. Switching control in which a real switch in control strategy is present, is an other often applied strategy. The switching usually consist of a transition region in which the switching takes place gradually. In this case a switching strategy is implemented. During the transition region a switch between the MIMO temperature and pressure control and the MIMO position control takes place.

As an example the control of injection molding machines was examined. This actually is the reverse of the weld process. First, the melt is liquid and behaves plastic. Next the injection of the material into the mould takes place and the material solidifies. Consequently the material behaviour becomes elastic. Simple PID-controllers, robust enough to cope with this transition are used. Besides that, implementation of iterative learning control is an often used strategy. In this way the duration of the transition region and the control effort needed during the transition region are determined on-line [Havlicsek, 1999], [Zheng, 2001]. Because of the complexity of implementation and the need for a relatively simple controller, which has be tested thoroughly at this stage, iterative learning control is not implemented yet.

An often used, more straightforward but effective method is the gradually transition from the first to the second controller. A decreasing and an increasing switching gain are used. Stability of the controlled system during the transition region has to be taken care of in applying this strategy. Besides, it is of importance that the steering signals resulting from the second controller are not of a different order than those of the first controller. This technique is applied at the weld process. The start of the transition region wherein the material behaviour changes from elastic to plastic, is also used as the start of the switching between the controllers. This is already taken into account in the design of the reference trajectories, (see section 4.5). The start of the transition region t_1 and the switching gain ζ are defined:

$$\zeta = \frac{t - t_1}{t_{sw}} \tag{4.18}$$

with t_{sw} the duration of the transition region. The controller during switching now becomes

$$C_{1\to2} = \zeta C_2 + (1-\zeta)C_1 \qquad \text{for } t_1 \leq t \leq t_1 + t_{sw} \tag{4.19}$$

C_1 controls the temperature and pressure progress and C_2 the position progress. Hence, different parts of the MIMO controller $C_{1\to2}$ are used. Consequently, the decrease and increase in switching gains during the transition region does not lead to stability problems if the controllers are considered separately. However, although different input-output responses are used, the closed loops influence each other nevertheless because of the MIMO nature of the system (see section 4.6.1). Stability during the transition region is guaranteed if all open loops, based on the appropriate sequential loop closing system rather than the original system, are stable. Consequently the sequential loop closing systems of the various parts of $C_{1\to2}$ are determined. The concerning open loops are taken as the last ones to close. In this way stability is guaranteed. This is done for the controllers defined in Table 4.2 as well as for the controllers presented in Table 4.3.

Using the controllers as defined in Table 4.2, the MIMO switching controller $C_{1\to2}$ is stable $\forall t$ during switching. In Figure 4.10 the open loop $C_{1\to2}|_{\epsilon P\to u_v} H_{1\to2,sl}|_{u_v\to P}$ is shown for varying t. For $C_{1\to2}|_{\epsilon P\to u_v}$ only the gains of Table 4.2 are used, so the increasing influence of the position controllers with increasing t is obvious. The open loop system remains stable $\forall t$ all the same.
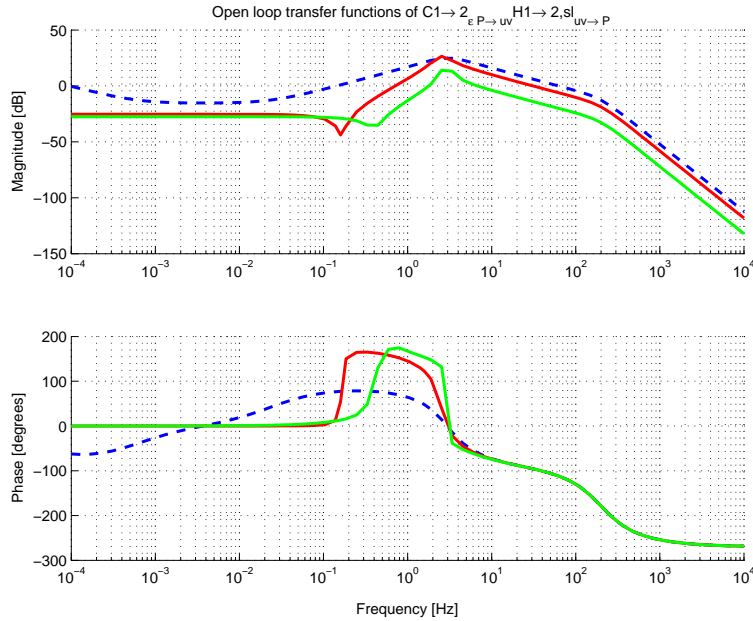

Figure 4.10: progress of the open loop system $C_{1\to2}|_{\epsilon P\to u_v} H_{1\to2,sl}|_{u_v\to P}$ during the transition region using the controllers defined in Table 4.2. $t = t_1$ yields the dashed blue plot, $t = t_1 + 0.5t_{sw}$ yields the solid red plot and $t = t_1 + 0.9t_{sw}$ the (light) green plot.

Next the more advanced controllers as defined in Table 4.3 are tested using average gains. The MIMO switching controller $C_{1\to2}$ again appears to be stable $\forall t$ during the transition region. In Figure 4.11 the Nyquist responses of $C_{1\to2}|_{\epsilon x\to u_v} H_{1\to2,sl}|_{u_v\to x}$ are shown for varying t (see also Figure 4.9). The dash-dotted black plot shows the final controller $C_2|_{\epsilon_x\to u_v}$. The dashed blue to the solid (light) green plot show $C_{1\to2}|_{\epsilon x\to u_v}$ for various t. From this is concluded that the switching controller $C_{1\to2}$ (see equation 4.19) is stable $\forall t$ during the transition region.

4.6.4 Learning control

In the original assignment learning control was proposed as part of the new strategy because of the high level of repetition of the process. Within the framework of this study only time was
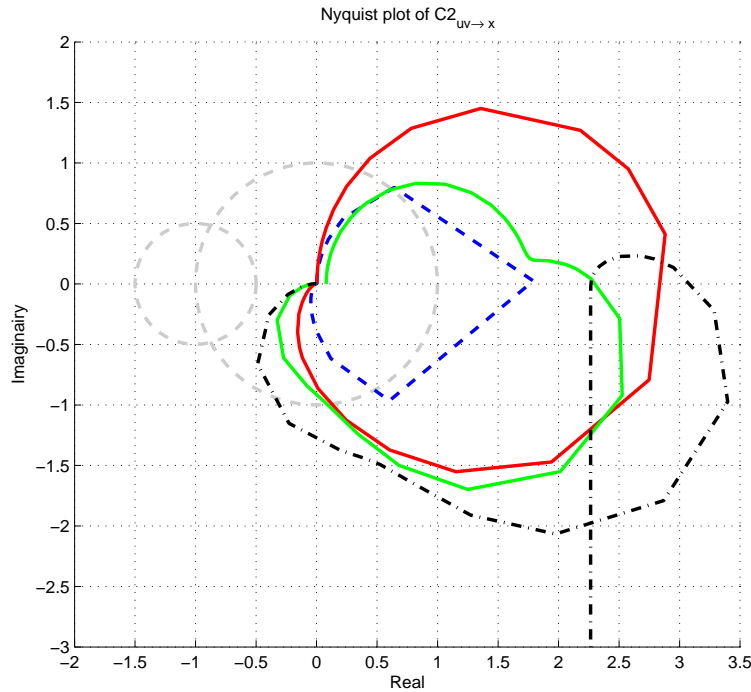
Figure 4.11: progress of the open loop system $C_{1\to2}|_{\epsilon x\to u_v}H_{1\to2,sl}|_{u_v\to x}$ during the transition region using the controllers defined in Table 4.3. The start of the transition region at $t = t_1 + 0.1t_{sw}$ yields the dashed blue plot, $t = t_1 + 0.5t_{sw}$ yields the solid red plot and the end at $t = t_1 + 0.99t_{sw}$ yields the solid green plot. The dash-dotted black plot represents the final $C_2|_{\epsilon x\to u_v}$.

found to examine the possibilities of implementation of learning control. Using the new control strategy as a basis learning control may be applied and implemented in future. In this section a short outline of some interesting results found till now is given. Yet a thoroughly examination to the possibilities of the implementation of learning control has to be performed.

The possibilities of the implementation of learning control with respect to the weld proces as discussed in this study, is bipartite. First the initialisation of the reference trajectories and parameters used in the new control strategy of the weld process is of importance in starting up the process. Secondly variation in the characteristics of the material used, is of importance during the process. With respect to the initialisation of the process an iterative learning process may be implemented to determine the new material characteristics used in the reference trajectories and the on-line calculation of the temperature, see section 4.5. An initialisation sequence of for example 5 to 10 welds may be performed to determine the right parameter values after which the process is started up. With respect to the variation in the characteristics of the material used, on-line feed forward compensation of repetitive errors during the process may be implemented. In this way relatively small variations in material characteristics may be overcome. These variations for example may origin from the difference in material at the inner and outer side of a coil of supplied steel. Moreover a more reliable tracking of the predefined trajectories will be the result.

In learning control several different strategies can be distinguished with as main purpose to add feed forward control action to the system. Jian-Xin and Ying [2003] give a structured overview of various implementations. Learning controllers based on accurate white box nonlinear models of a system can be distinguished, see for example Tinsel [2001]. Besides that, learning controllers based on black box models of a system can be distinguished. For example Gorinevsky [2002] not taking into account extensive modelling of the system, uses a black box model of the repeating error as a feed forward parameter updating the reference trajectory.

The final model used as a base for the controller in this study, suffices for the purpose it is meant for. However parts of it are not validated thoroughly enough to define it accurate on all levels. The hydraulic system in combination with the mechanical part may be used as a base for repetitive learning control for example. The accuracy of the model of the hydraulic system is good and the mechanical model of the welding machine and the mechanical behaviour of the material is defined simple but good to apply learning techniques. Seunghyeokk [2004] applies this technique to control an electric hydraulic servo valve resulting in addition of a feed forward control signal to the steering signal of the system.

The way of implementation as proposed by Gorinevsky is of interest to compensate for errors in the initially identified material parameters forcing the system to follow trajectories that are not optimal. Using several iteration steps a good estimate for the average compensating signal may be determined. On-line application may help the controller to adept to small variations in the parameters over numerous processes. The possibilities of implementation of this kind of learning control will be examined in future.

4.7 Implementation and results

The controllers listed in Table 4.2 of section 4.6.2 are implemented and tested at the setup. For this purpose the complete controller is modelled as a single block using Simulink. This controller block can be implemented directly into WELD2001 and consists of 4 parts, a signal modification block, the reference signals, the on-line temperature and yield temperature calculation and the MIMO tracking controller. Using this revised version of WELD2001 and a dSpace system the connection to the setup is made. The temperature calculation as discussed in section 4.3 and the switching controller as defined in section 4.6.3 are used. Because of limitations to the capacity of the processor present in the setup, the reference trajectories can not be calculated on-line. Therefore an automated tool is developed to design the trajectories in advance and uploading them to the weld program. Results of this program are discussed in section 4.5. The initialisation parameters for the on-line calculations and the tracking controller are uploaded at the same time. In Figure 4.12 the results of an experiment on the setup with this new control strategy implemented are given.

In the first part of the process the pressure as well as the temperature are controlled. When the calculated temperature reaches the yield temperature, which is calculated on-line as well, the controller switches to position control using the switching strategy as defined before. The moment of switching is indicated in the position figure as well to show that this resembles the moment the material actually starts yielding. This can also be verified using the pressure response.

Two different ways of calculating the temperature are present (see section 4.3). The first one makes use of a model of the bulk resistance and contact resistance present in the material, while the second one uses a potential measurement. In combination with the electrical current the generation of heat can be calculated for both cases, see section 3.3.2. The potential measurement however is not standard implemented on the welding machines currently in the field. Hence it is of importance that the calculation using the bulk and contact resistance of the material is correct. Furthermore the installation of a potential measurement is not that hard. The temperature calculation using the potential measurement is more reliable than that using the resistance calculations because the model is less extensive and less material parameters are used. Using the test setup the latter one can be validated as far as possible using the calculation in which the potential measurement is used. From experiments the electrical conductivity of the material, ρ_{er}, appears to be particularly significant in this validation. A small error in this value already makes the calculation fail. The quantitative accuracy of the temperature calculation is validated, examining the switching point with respect to the position and pressure progress . In Figure 4.12 the temperature progress calculated using a model of the material resistance is depicted with the dotted red plot, the solid red plot shows the temperature progress calculated using the potential measurement. Among many other experiments the results of this experiment prove both calculations to correspond very well, especially during the heating phase. The calculations sometimes differ during the yielding
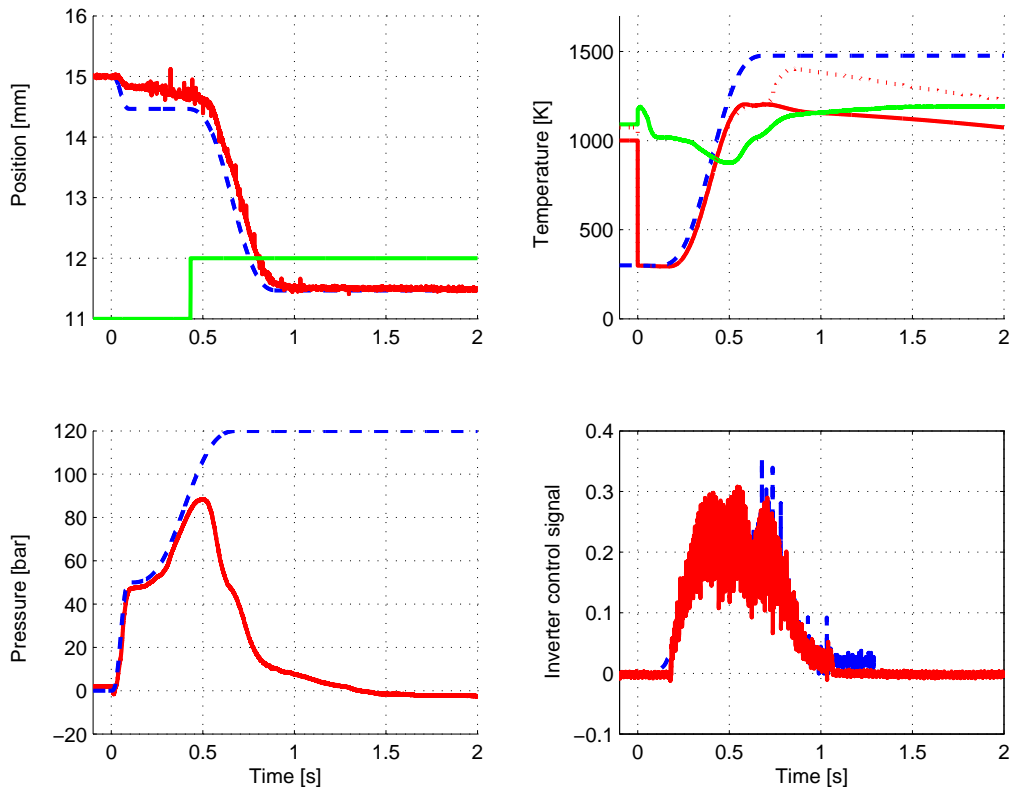
Figure 4.12: resulting position, temperature, pressure and inverter control signal progress during the weld process after implementation of the new control strategy. The dashed blue plots indicate the reference trajectories and in case of the inverter control signal the command signal to the inverter. The solid red plots show the actual progress of the various parameters and the (light) green plots in the upper right and left Figures show the on-line calculated force dependent yield temperature respectively the switch moment when crossing the calculated temperature. The dotted red plot in the temperature figure results from the second temperature calculation.

phase and further on as is also the matter in this case. However, they resemble very well during heating, which is the part of the process that is temperature controlled, so for the moment these results suffice.

Relatively small gains are used in this example, as can be seen in Figure 4.12. Larger gains as listed in Table 4.2 are successfully tested as well. A lot of experiments are performed, but the more advanced controllers listed in Table 4.3 are not implemented and tested yet. These controllers are tested off-line using a simulation model, `ProcessSimulation.mdl` in which the developed controller block can be implemented (see Appendix F). The reference trajectories are still being improved, see for example the trajectories of section 4.5, which are already of a next generation than those used in this example, and as from experiments result, improvement is still needed. Especially the transition region from elastic to plastic material behaviour has to be levelled more to assure a smooth position progress. The transition from elastic to plastic deformation in the position reference trajectory is not smooth enough yet. Consequently for example dips in the progress of the electrical current and the pressure are present in the switching region.

The results of the experiment depicted in Figure 4.12 among many other experiments show that the developed controller performs well. The reference trajectories however, are still being improved and the more advanced controllers have to be implemented and tested on-line. Because of the highly repetitive character of the process, learning control as outlined in section 4.6.4 is

of great interest to be implemented as well. The on-line temperature calculation used has shown to suffice so far. However the model used has to be validated thoroughly using more reliable temperature measurements. Furthermore the control strategy is being adapted to suit control of the FRW-series welding machines.

Chapter 5

Conclusions and recommendations

In this chapter the conclusions and recommendations concerning the assignment are given.

Conclusions

To overcome limitations of the current control of the DC upset resistance weld process, a new control strategy is developed. Consequently a good insight in the process was needed. The theoretical insight in the process is renewed and has expanded. The validity of this theory is founded by experimental results. In this way the theory and assumptions made with respect to the systems and equilibria present in the process, are shown to be correct. A complete overview of the systems present in the weld process is given.

As a base for the new control strategy and to validate the expanded insight in the system, a model of the weld process has been developed. This has resulted in a simulation model, which can be used for off-line simulation of the weld process. The model and the theory have been validated by experimental results. The corresponding progress of position, of electrical current and of pressure exhibit good agreement. The model also gives a good indication of the progress of the temperature during the weld process. Special attention is given to the modelling and control of the hydraulic system. This has resulted in a relatively easy model-based controller development that suits the possibilities of the hydraulic system better than the previous controller. A paper on the modelling and control of hydraulic systems focussing on position control has been written during this study [Wijnheijmer & Naus, 2005].

The simulation model is simplified to suit on-line calculation of the temperature and yield temperature. Validation of the on-line calculation shows that the resulting model satisfies this purpose. In two different ways a good on-line calculation of the temperature progress can be made now. Linearised frequency responses are determined using the simplified model as a base. These responses are used in further controller development to enable application of loop shaping techniques. From the linearisation follows that a good approximation of the model can be made using two separate linear models. Each model has two inputs and three outputs. Application of these linear models shows that only the transfer functions involving the temperature-dependent material behaviour ($H_2|_{u_i \to x}$ and $H_2|_{u_i \to p}$) are less reliable. The remaining transfer functions are good representations of the process.

For the first and second part of the weld process, a MIMO controller for both temperature and pressure tracking, respectively for position tracking are designed. A switching strategy controls the transition between the two controllers assuring stability during switching. Furthermore sequential loop closing is used to assure stability of each of the MIMO controllers. The reference trajectories are based on the results of the developed theory and modelling as well as on practical experience. Consequently, they prescribe a representative progress of the involved variables. Loop shaping techniques are used to design two sets of controllers satisfying the demanded bandwidths. The first set of controllers is implemented and tested successfully. The second set is implemented only

partly yet, but experimental and simulation show good correspondence. To facilitate working with the MIMO control problem, MCDesign, a tool for MIMO controller design, has been developed [Wijnheijmer & Naus, 2005].

The resulting controller satisfies the stated requirements: the weld process now is completed within a predefined time interval in which a predefined amount of upset is achieved exactly. Moreover, the temperature progress during the first part of the process is controlled as well. In the future these results can be combined with the NIMR research, which should give rise to an indication of the quality of the weld in advance. The controller is sensitive for some material properties due to the dependence of the on-line calculation of the temperature and yield temperature on these properties. Because of the highly repetitive character of the process, application of learning control may be useful in solving this problem. A first start to future implementation of learning techniques in the controller or reference trajectories has been made.

Recommendations

Recommendations are distinguished concerning the results of the assignment and the setup. The recommendations concerning the results of the assignment:

- More extensive modelling of the mechanics of the material may be performed, especially during the transition from elastic to plastic material behaviour. This may result in an improved design of the corresponding controllers.

- The models used for on-line temperature calculation have to be validated better using several reliable temperature measurements.

- The force needed during the weld process is still determined by trial and error. The influence of the size and the material of the coiled sheets on this force has to be examined.

- Implementation and testing of the more advanced controllers and optimisation of these controllers by extensive testing has to be done.

- Based on literature, the possibilities for the implementation of iterative learning or updating techniques are promising. Examination and implementation of learning techniques may increase the reliability and robustness of the controller for changing material properties.

- Combining future results of the NIMR giving guidelines for the progress of the weld process with respect to the quality of a weld and the reference trajectories respectively the developed controllers.

The recommendations concerning the setup:

- When the material is clamped, the distance between the clamps instead of the pressure on the material is controlled This results in a considerable increase in pressure. Hence it may be replaced by a pressure controller including a position feedback with low gain to prevent drifting.

- Loading the setup and surface conditions of the sheet ends to be welded together have much influence on the resulting weld. So loading the welding machine has to become unambiguous. If the problems resulting from varying surface conditions remain, a study to insert an extra operation before the weld process to derive constant surface conditions of the sheet ends may be useful.

- The influence of a varying initial distance between the clamps has to be examined.

- Further development of the setup as used in this study may be useful to reduce upset and welding times in future.

Chapter 6

References

Books and notes

1   Bejan, A., *Heat transfer*, John Wiley & Sons, Inc, 1993.

2   Franklin, G.F., Powell, J.D. and Emami, A., *Feedback control of dynamic systems*, Addison-Wesley Publishing Company, Inc., third edition, 1994.

3   Jian-Xin Xu, Ying Tan, *Linear and Nonlinear Iterative Learning Control*, Springer, March 2003.

4   Kokernak, R.P., *Fluid power technology*, New York, US Imports & PHIPEs, second edition, 1998

5   Leijendeckers, P.H.H., Fortuin, J.B., Van Herwijnen, F. and Schwippert, G.A., *Poly technisch zakboek*, 49th edition, 2002, Elsevier Bedrijfsinformatie B.V., ISBN 90-6228-358-6 geb.

6   Merrit, H., *Hydraulic Control Systems*, New York US: John Wiley & Sons Inc, first edition, 1967.

7   Post, W.J.A.E.M. and Teerhuis, P.C., *Hydraulic servo control*, lecture notes, University of Technology Eindhoven, Mechanical Engineering, Control Systems Technology, 2004.

8   Skogestad, S. and Postlethwaite, I., *Multivariable feedback control - analysis and design*, 1996

9   Steinbuch, M. *Digital Motion Control*, lecture notes, University of Technology Eindhoven, Mechanical Engineering, Control Systems Technology, 2004.

10   Tochtermann, Bodenstein, *Konstruktionselemente des Maschinenbaues*, 8th edition, first part, 1968.

11   Viersma, T.J., *Analysis, Synthesis and Design of Hydraulic Servosystems and Pipelines*, Delft University of Technology, revised edition, 1990.

12   Zwolsman, J.O. and Vroomans, H.M., *Der Kontakwiderstand beim Widerstandsschweissen*, DVS Berichte no 124, 1987, p. 122-127.

13   Zwolsman, J.O., *Quality in resistance welding: an analysis of the process and its control*, Cambridge: Abinton, 1991, ISBN 1-85576-033-2.

Reports and papers

14 Allersma, et al, *Plan van aanpak*, graduation report on the start of building the setup, WA0023, September 2003.

15 Elassal, M.E.H., *Modelvorming en krachtregeling van de FHL400 lasmachine*, internship report on the modelling and control of the weld process as per formed on the FHL series, March 1996.

16 Feng, Z., Gould, J.E., et al, *An incrementally coupled electrical-thermal-mechanical model for resistance spot welding*, 5th International Conference on Trends in Welding Research, Pine Mountain, GA, 1-5 June 1998.

17 Fontijne Grotnes B.V., *Improved technology to DC butt welding*, DC-press butt welding for car and truck rims, called FRW-series since 2001

18 Gorinevsky, Dimitry, *Loop Shaping for Iterative Control of Batch Processes*, IEEE Control Systems Magazine, December 2002.

19 Havlicsek, H. and A. Alleyne, *Nonlinear Control of an Electrohydraulic Injection Molding Machine via Iterative Adaptive Learning*, IEEE/ASME Transactions on Mechatronics, Vol. 4, No. 3, pp. 312-323, September 1999.

20 Kucklick, F.C., *Flashless DC welding of rims offers advantages*, Welding Journal, July, 1996.

21 Ledeuil, M., *FHL300 - Een nieuw concept*, internship report on the concept of the setup, WA0024, November 1998.

22 Legemaate, R., *Dynamisch gedrag van een lasproces*, internship report on the weld process as performed on the FHL series, May 1997.

23 Legemaate, R., *Beheersing van het lasproces op de Fontijne Holland Lasmachine*, graduation report on modelling and control of the DC upset resistance weld process, March 1998.

24 Louter, R., *De bepaling van meetspecificaties en selectie van sensoren voor een experimentele lasmachine*, internship report on the specifications and measurement equipment of the setup, WA0022, December 1999.

25 Mast, S.E.P., *Analyse van het weerstandstuiklasproces*, internship report on the quality of a weld, May 2000.

26 Meulenberg, R., *De beschrijving van het weerstandstuiklasproces van wielvelgen*, graduation report, August 2002.

27 Put, R.P., *De invloed van de stuikweg bij het weerstanddruklassen van R-St37-2*, graduation report on the modelling of the weld process as performed on the FHL series, August 1999.

28 Seunghyeokk James Lee, Tsu-Chin Tsao, *Repetitive learning of backstepping controlled nonlinear electrohydraulic material testing system*, Control Engineering Practive 12, 1393-1408, 2004.

29 Tinsel, R.B.G., *Iterative Learning Control for a Gantry type manipulator*, graduation report, April 2001

30 Wijnheijmer, F.P. and Naus, G.J.L., *On the modelling and control of hydraulic systems*, paper, 2005.

31 Zheng, D. and A. Alleyne, Modeling and Control of an Electrohydraulic Injection Molding Machine with Smoothed Fill-to-Pack Transition, ASME Journal of Manufacturing Science and Engineering, October, 2001.

Applications

32   Convert, *Convert*, http://www.joshmadison.com/software, version 4.08, 1998.

33   DIET, *Do It Easy Tool, DIET*, http://www.dct.tue.nl/home_of_diet.htm, University of Technology Eindhoven, Mechanical Engineering, Control Systems Technology Group, 2003.

34   MCDesign, *MCDesign, MIMO controller design tool including MDesign, CDesign and FDesign*, Wijnheijmer, F.P., and Naus, G.J.L., version 2.0β, 2005.

35   WELD2000, *WELD2000, the DC Weld control retrofit package*, Fontijne Grotnes B.V., software package, 2000.

Internet pages

36   aluSELECT, *http://aluminium.matter.org.uk/aluselect*, computer-based reference database containing technical information on the most widely used aluminium alloys, partnership between the European Aluminium Association and the MATTER project, 2001.

37   Automation International Inc., *http://www.automation-intl.com/*, automated welding and metalworking machines.

38   Bosch Rexroth AG, *www.boschrexroth.com/.../products/brc/ProductDirectory/ CurrentProducts/Welding/PSQ/087004-101-de+en-ws.pdf*, Electric Drives and Controls Division.

39   Fontijne Grotnes B.V., *http://www.fontijnegrotnes.com*, homepage of the Fontijne Grotnes B.V. company.

40   Hess Industries inc., *http://www.hess-eng.com/pages/wrttech.html*, Sabre weld control, Wheel and Rim Technologies, Hess Engineering.

41   Infrared Servics Inc., *http://www.infrared-thermography.com/material.htm*, emissivity values for common materials.

42   Key to steel, *http://www.key-to-steel.com/articles/art75.htm*, steel database - weld processes, INI International, 2003.

43   Matweb, *http://www.matweb.com*, material property data for metals, plastics ceramics and composites.

44   Medar, *http://www.medar.com/controls/index.html*, Welding Technology Corporation.

45   MOOG Inc., *http://www.moog.com*, manufacturer of precision control components and systems, 2005.

46   NIMR, *http://www.nimr.nl*, Netherlands Institute *for* Metal Research, 2005.

47   Nonferrous Products, Inc., *http://www.nonferrousproducts.com/material%20selection.htm*, nonferrous materials database, 2004.

48   NSRW, *http://www.nsrw.com/components/weldcomputer.htm 2004*, new southern resistance welding, Pelham, Alabama.

49   Wolfram research, *http://scienceworld.wolfram.com/physics*, Eric Weisstein's world of science.

Appendix A

FRW-series welding machine

The FRW-series welding machines are the welding machines developed and produced by Fontijne [Fontijne, 2001]. The FRW-series is the successor of the FHL-series Fontijne used to build. In Figure A.1(a) a picture of a FRW-series welding machine is shown. In Figure A.1(b) a schematic overview of this welding machine is given.
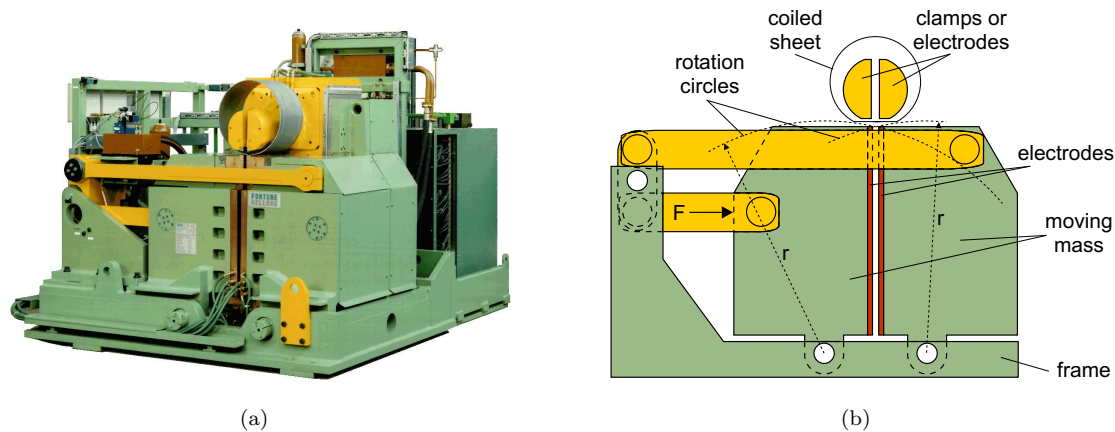

(a)   (b)

Figure A.1: (a): a FRW series welding machine [Fontijne, 2001]. (b): schematic representation of the FRW welding machine with F the force delivered by the hydraulic system.

The upper and lower electrodes clamp the coiled sheet. The two masses onto which these clamping mechanisms are mounted can move towards each other. A system of bars, driven by the hydraulic system, initiates this movement. The force delivered by the hydraulic system is indicated with a F in Figure A.1(b). In this way the ends of the coiled sheet are pushed together. When the coiled sheet is clamped and an initial force is applied, an electrical current is directed through the material. The temperature of the butt-joined material increases due to the electrical resistance. This resistance is highest at the seam between the two sheets. When the temperature is high enough, the sheet ends start to yield, an upset is formed and the sheets are welded together.

Because of the system of bars driving the masses, the clamping mechanisms carry out a rotation instead of a linear motion. They move over a circle with a radius r (see Figure A.1(b)). Besides that, the bar system introduces hysteresis and loss of stiffness. The displacement of the clamps is derived from the measured displacement of the rod. The hysteresis, stiffness of the bars and rotation instead of a linear motion are not taken into account. Hence, the displacement of the electrodes is not determined accurately. It is assumed that the minimal upset needed for a good weld may be much smaller then used at this moment. A large upset is used however, which is

73

partly due to the inaccuracy of the position measurement.

Appendix B

Simulation models and URW Library

From Chapter 3 an extensive model of the weld process results, `SimulationModel.mdl` (see Appendix F). This model can be used to simulate the weld process controlled by WELD2001 off-line. A second less precise model of the weld process results from section 4.3, `WeldProcess.mdl` which is included in `ProcessSimulation.mdl` (see Appendix F). This model is used in the new control strategy to calculate the temperature progress on-line. Therefore this model can be used to simulate the weld process controlled by the new control strategy. Both models are developed in the Simulink environment.

The first simulation model makes use of the Upset Resistance Welding Library (URW Library), `URW_Library.mdl`, and an accompanying m-file for initial parameter definition, `parameters.m` (see Appendix F). The URW library makes it possible to change the separate parts of the model straightforward, keeps the model orderly and easy to expand or reduce.
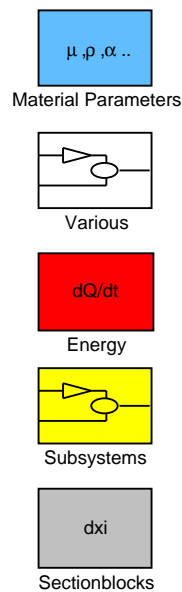
Figure B.1: Upset Resistance Welding Library developed in Simulink.

The URW Library consists of 5 parts

75

- **Material Parameters**   light blue blocks containing models for the temperature dependent parameters.

- **Energy**   red blocks including the energy terms are used in the balances of energy of every section. Each term described in section 3.3 is built-in in this library.

- **Subsystems**   yellow blocks containing various frequently used larger groups of blocks.

- **Section blocks**   grey blocks representing the sections in the working area. The sections as resulting from the discretisation of the various parts in the working area (see section 3.3.1) and including the accompanying balances of energy and mechanics.

- **Various**   various small user-defined functions.

The weld program WELD2001 is categorised in the section blocks of the URW Library. Geometrical, process and temperature independent material parameters are defined in the accompanying m-file `parameters.m` and included in the model by cyan colored blocks.

Appendix C

Modelling of the hydraulic system

In this Appendix the modelling of the hydraulic system is discussed. A parametric white box model and a fitted black box model are developed. Results of the modelling are discussed in section 3.6.

C.1   White box modelling

The main parts of the hydraulic system are an electric hydraulic servo valve and a hydraulic cylinder. A schematic representation of the complete hydraulic system is given in Figure C.1. The controller C in this figure is a MISO controller. In case only a single reference signal is used, this becomes a SISO controller.
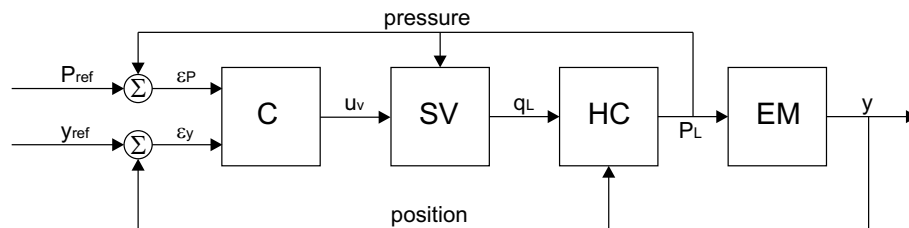

Figure C.1: schematic representation of the hydraulic system of the setup: a MISO feedback controller C, partly used to control the pressure $P_L(t)$ and partly to control the displacement $x(t)$, the electric hydraulic servo valve SV, the hydraulic cylinder HC and the external mechanics EM, coupled to the hydraulic system.

A parametric white box model of the system is developed using supplier data and insight in the system. In the next sections the servo valve and the hydraulic cylinder are discussed in more detail. The external mechanics are discussed briefly in the last section. A more detailed discussion about the mechanics of the weld process and the effects on the dynamics of the hydraulic system is given in section 3.4.

C.1.1   Electric hydraulic servo valve

In Figure C.2 a cross section of the electric hydraulic servo valve used is depicted. The servo valve consists of 3 main parts: the torque motor, the flapper-nozzle system and the spool valve.
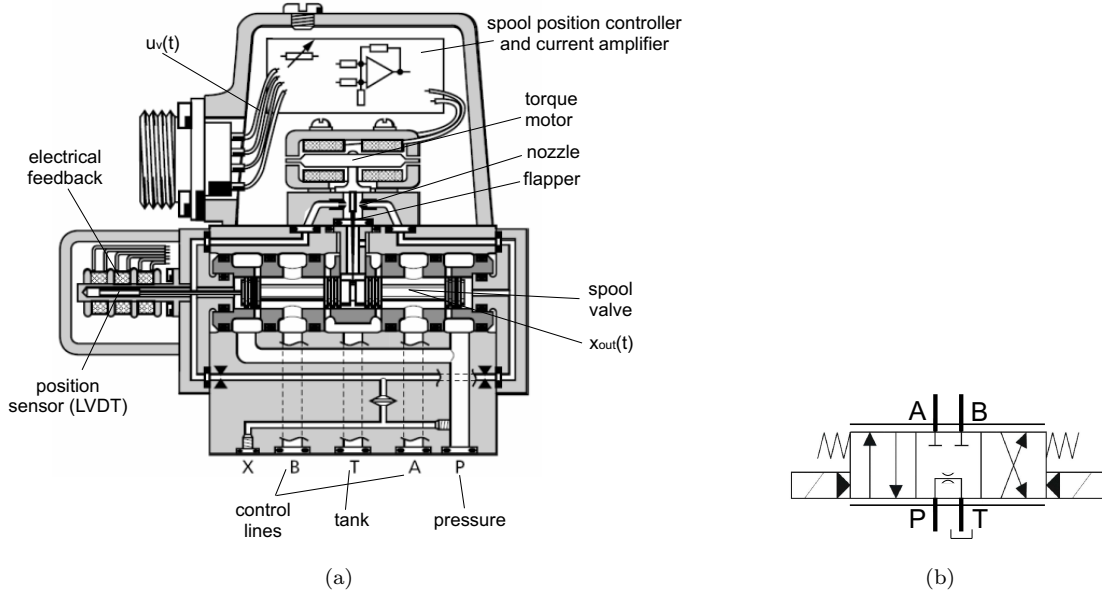
Figure C.2: the electric hydraulic servo valve used of the D765 Series manufactured by MOOG [(web)]. In Figure (a) a cross section of the servo valve and its components is shown, in Figure (b) the schematic symbol for this type of servo valve is shown.

The servo valve control signal $u_v(t)$ represents the incoming voltage signal to the current amplifier. The torque motor transforms this current to a mechanical displacement $x_{in}(t)$. This movement drives the flapper-nozzle system (in the middle of Figure C.2(a)). The flapper-nozzle system drives the movement $x_{out}(t)$ of the spool valve (the lower part of Figure C.2(a)). The spool valve controls the flow that is directed to and from the hydraulic actuator. A position feedback is included in this latter part. This feedback can be mechanical, electrical or both, as in this particular type of servo valve. The transfer function from the voltage input signal to the mechanical displacement of the spool, equals 1 till a certain bandwidth. This bandwidth is specified in the manufacturer's specifications of the servo valve. In this case a D765 series servo valve, manufactured by MOOG [(web)] is used. It is a so-called 3 position 4 port, high response servo valve with electrical and mechanical feedback. See Table C.1 for a more detailed list of specifications. Plots of the transfer functions for this servo valve are shown in Figure C.3.

From Figure C.3 follows that different behaviour of the servo valve exists for different inputs. The input is given in percentages of the maximal input voltage. These percentages correspond to nominal flows through the valve. In further modelling, the behaviour according to an input voltage of in between 40% and 90% of the maximal input voltage, is used. This is the operating point of the servo valve most used in this application. Moreover, the bandwidth of the servo valve is relatively small for these input values. This negatively influences the total system's bandwidth and behaviour. Considering robustness of the controlled system, this is desirable if the model is used for further control development. In this way, the developed controllers will be robust for other working points as well. In Figure C.3(b) also a fitted model of this transfer function is shown. The phase of the transfer function of the servo valve has the most significant effect on the frequency response of the total hydraulic system. Consequently good modelling of the phase of the transfer function is emphasised in fitting the model. The poles and damping of the fit are used to determine the natural frequency $\omega_{v,o}$ and damping ξ_v of the servo valve. This results in the following transfer function, describing the dynamics of the servo valve:

$$\frac{X_{out}}{U_v} = \frac{1}{\frac{1}{\omega_{v,o}^2}s^2 + 2\frac{\xi_v}{\omega_{v,o}}s + 1} \tag{C.1}$$

D765 Series servo valve, type designation: H10-JOGMEURAO

high response behaviour
rated flow of $q_n = 10$ l/min at $\Delta p_n = 35$ bar per land
maximum operating pressure $p_p = 315$ bar
body material is aluminium
bushing spool type: axis cut and linear characteristic
the pilot stage is with mechanical feedback
the mid position is the spool position without electrical supply
the pilot connections are internal and the pressure equals 15 to 315 bar
the valve connector is a 6 + PE pole DIN 43563 over port A
the command signal as well as the output signal for 100% spool stroke are ± 10 V
the electrical supply is ± 15 VDC $\pm 3\%$ with a ripple < 50 mV$_{\text{pp}}$

Table C.1: main specifications of the servo valve used, manufactured by MOOG [(web)].

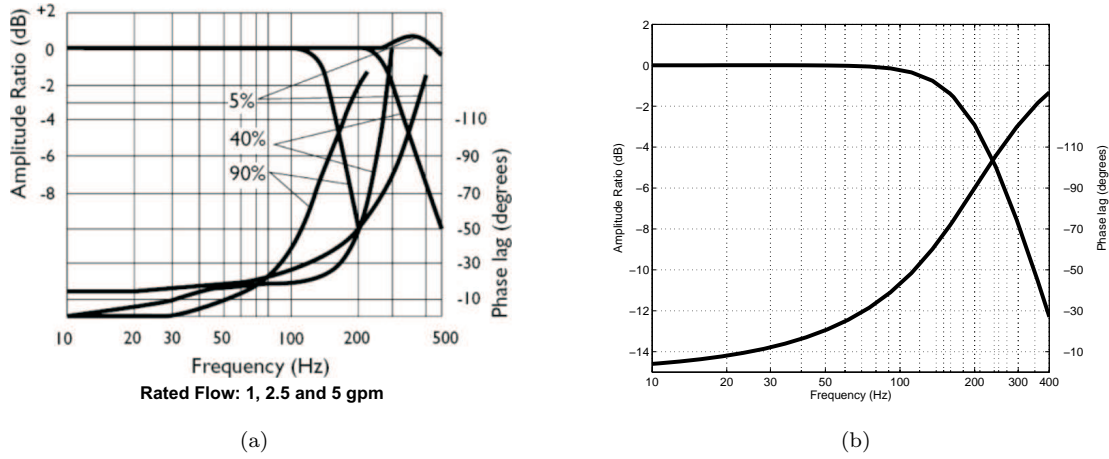(a)   (b)

Figure C.3: (a): the transfer function for the D765 Series servo valve of MOOG, type H10-JOGMEURAO. (b): fitted model of the specification data of Figure A at 40% to 90% of the maximal input voltage.

with

$$\omega_{v,o} = 2\pi * 200 \text{ rads}^{-1}$$
$$\xi_v = 0.7 \text{ }[-]$$

This transfer function is used as a representation of the servo valve further on. Instead of the real displacement $x_{out}(t)$ often the normalised output $x_n(t)$ is used

$$x_n(t) = \frac{x_{out}(t)}{x_{max}} \tag{C.2}$$

with x_{max} the maximum stroke of the spool valve.

Next the dynamics of the spool valve are modelled. First it is assumed the edges in the spool valve are sharp, so the flow can be modelled as turbulent. This corresponds to an orifice flow, which yields:

$$\Delta p(t) \propto q(t)^2 \tag{C.3}$$

The volume flow $q(t)$ through the control piston then equals [Viersma, 1990], [Merrit, 1967]:

$$q(t) = bx(t)c_d\sqrt{\Delta p(t)} \tag{C.4}$$

with b the diameter, c_d a compensation factor and $x(t)$ the length of the gap. This length is controlled by the flapper-nozzle system. From Figure C.4 it follows that

$$p_1(t) = \frac{1}{2}p_s + \frac{1}{2}p_l(t) = p_{pump} = p_s \tag{C.5}$$

$$p_2(t) = \frac{1}{2}p_s - \frac{1}{2}p_l(t) = p_{tank} = 0 \tag{C.6}$$

with p_s the supply pressure. The servo valve used is a critical center valve, so the overlap $\epsilon = 0$. Solving equation C.4 for $x \leq 0$ and $x \geq 0$ and using equations C.5 and C.6, yields

$$q_l(t) = \begin{cases} q_n x_n(t)\sqrt{1 + p_n(t)} & \text{for } x > 0 \\ 0 & \text{for } x = 0 \\ q_n x_n(t)\sqrt{1 - p_n(t)} & \text{for } x < 0 \end{cases} \tag{C.7}$$

$$\tag{C.8}$$

with $x_n(t)$ the normalised position of the spool valve as defined in equation C.2, and $q_n(t)$ the normalised flow through the servo valve at the normalised pressure $p_n(t)$.

$$q_n = bx_{max}c_d\sqrt{\frac{p_s}{2}} \tag{C.9}$$

$$= q|_{x=x_{max}}\omega\Delta p \tag{C.10}$$

$$p_n(t) = \frac{p_l}{p_s} \tag{C.11}$$

Assuming the sign of p_n and x_n to correspond, the result is a nonlinear equation describing the flow to the hydraulic cylinder

$$\frac{q_l(t)}{q_n} = x_n(t)\sqrt{1 - p_n(t)sign(x_n(t))} \tag{C.12}$$

Equation C.12 is linearised for small variations (x_e, p_e) around $(x_o, p_o) = (\eta, 0)$. The equation can not be linearised around $x = 0$, since it only holds for turbulent flows. For very small values of x the flow becomes laminar. The following linearised equation results

$$\frac{q_l(t)}{q_n} = x_n - \frac{p_n(t)}{2}sign(x_n(t)) \tag{C.13}$$

Besides that, linearisation of the *sign*-function is not possible. It is thus approached by an *atan*-function:

$$\frac{q_l(t)}{q_n} = x_n(t) - \frac{p_n(t)}{\pi}atan(Gx_n(t)) \tag{C.14}$$

The higher gain G, the better equation C.14 resembles equation C.13.

C.1.2   Hydraulic cylinder

The hydraulic cylinder used in the setup is a double acting, double end-rod cylinder.
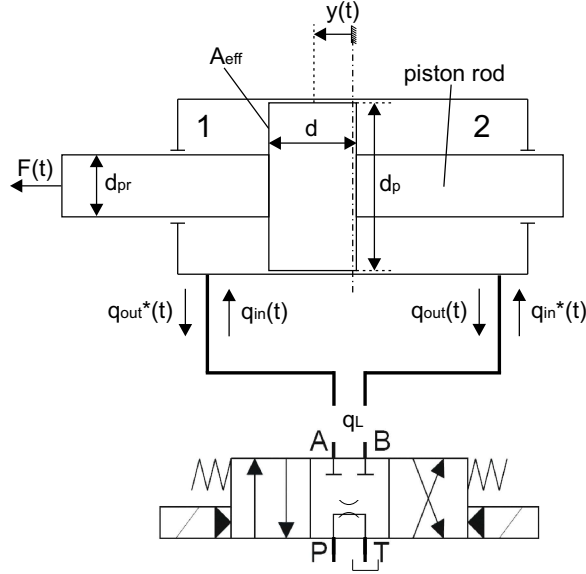
Figure C.4: schematic representation of the hydraulic servo system.

In Figure C.4 a schematic representation of the hydraulic cylinder in combination with the servo valve is shown. The leak flow over the rod bearings is neglected. Some properties of the hydraulic cylinder are listed in Table C.2. The rod is attached to the setup, driving the horizontal movement of the clamping mechanism (see Figure 2.1(a)). The displacement of the rod is measured using a linear variable differential transducer (LVDT), which is attached to one end of the rod. The pressure difference between the two cylinder chambers is measured by a differential pressure gauge. The resulting displacement $y(t)$ and pressure $p_L(t)$ is controlled by the flow, which is controlled by the servo valve.

description	quantity	magnitude	unity
maximum stroke	L	$30 \cdot 10^{-3}$	m
oil stiffness [Meulenberg, 2002]	E_{oil}	$8 \cdot 10^8$	Nm^{-1}
piston diameter	d_p	$65 \cdot 10^{-3}$	m
rod diameter	d_{pr}	$40 \cdot 10^{-3}$	m

Table C.2: properties of the hydraulic cylinder.

A dynamic model of the hydraulic cylinder is derived using the balance of mass. For a single cylinder chamber this balance equals

$$\frac{dM_i(t)}{dt} = \sum \Phi_i(t) \qquad (C.15)$$
$$= \Phi_{in,i}(t) - \Phi_{out,i}(t)$$

with $\Phi_i(t)$ the mass flow rate of cylinder chamber i:

$$\Phi_i(t) = \rho_i(t)q_i(t) \qquad (C.16)$$

with $q_i(t)$ the volume flow rate and $\rho_i(t)$ the density of the oil per cylinder chamber and

$$M_i(t) = \rho_i(t)V_i(t) \qquad (C.17)$$

with $V_i(t)$ the volume per cylinder chamber, this yields

$$\dot{\rho}(t)V_i(t) + \rho(t)\dot{V}_i(t) = \rho(t)\{q_{in,i}(t) - q_{out,i}(t)\} \tag{C.18}$$

For a Newtonian liquid like mineral oil the following holds

$$\rho(t) = \rho_0(1 + \frac{p(t)}{E_{oil}}) \tag{C.19}$$

$$\dot{\rho}(t) = \rho_0\frac{\dot{p}(t)}{E_{oil}} \tag{C.20}$$

with E_{oil} the stiffness of the oil used, ρ_0 the density of the oil at atmospheric pressure and $p_i(t)$ the pressure per cylinder chamber. The stiffness of the oil is negatively affected by the presence of air or vapour. The less air or vapour is present, the higher E_{oil}. Normally the stiffness of the oil is high enough and the pressure $p(t)$ is limited at a much lower value. In that case

$$\frac{p(t)}{E_{oil}} << 1 \tag{C.21}$$

holds, so

$$\rho(t) = \rho = \rho_0 \tag{C.22}$$

Combining equations C.18, C.20 and C.22 results in

$$\dot{p}_i(t) = \frac{E_{oil}}{V_i(t)}\{q_{in,i}(t) - q_{out,i}(t) - \dot{V}_i(t)\} \tag{C.23}$$

$q_{in,i}$ equals the volume flow from the servo valve into cylinder chamber i. $q_{out,i}$ consists of the leakages at the bearings and the leakage over the piston (directed from cylinder chamber 1 to chamber 2), $q_{Lb(earing)}$ and $q_{Lp(iston)}$ respectively. With $r_{b(earing)}$ and $r_{p(iston)}$ the leakage coefficients

$$q_{Lb,i}(t) = r_{b,i}(p_i(t) - p_\infty) \tag{C.24}$$

$$q_{Lp}(t) = r_p(p_1(t) - p_2(t)) \tag{C.25}$$

The effective force (the upset force) supplied by the hydraulic cylinder, follows from the balance of force

$$F(t) = p_1(t)A_1 - p_2(t)A_2 \tag{C.26}$$

with $A_1 = A_2 = A_{eff}$ the effective surface of the piston:

$$A_{eff} = A_p - A_r \tag{C.27}$$

with A_p the total surface of the piston and A_r the cross section of the rod. Using

$$p_l(t) = p_1(t) - p_2(t) \tag{C.28}$$

this results in

$$F(t) = A_{eff}p_l(t) \tag{C.29}$$

If the piston is in the utmost left position of the hydraulic cylinder, the actuator is in its initial position.

$$y(t)|_{t=0} = y_o = 0 \tag{C.30}$$

$$V_1(t)|_{t=0} = 0 \tag{C.31}$$

$$V_2(t)|_{t=0} = LA_{eff} \tag{C.32}$$

with

$$L = L^* - d - 2L_d \qquad \text{for } L_d \leq y(t) \leq L - L_d \tag{C.33}$$

with L_d the dead zone of both the cylinder chambers, d the height of the piston and L^* the total inner length of the hydraulic cylinder. From this follows

$$V_1(t) = A_{eff}y(t) \tag{C.34}$$
$$V_2(t) = A_{eff}(L - y(t)) \tag{C.35}$$

Using

$$\dot{V}_1(t) = -\dot{V}_2(t) = A_{eff}\dot{y}(t) \tag{C.36}$$
$$q_l(t) = q_{in,1}(t) - q_{in,2}(t) \tag{C.37}$$
$$q_{Lp,1}(t) = -q_{Lp,2}(t) = r_p p_l(t) \tag{C.38}$$

and assuming $q_{Lb,i}(t)$ to be zero, combination of equations C.23 and C.36 to C.38 result in

$$\dot{p}_l(t) = \left(\frac{E_{oil}}{V_1(t)} + \frac{E_{oil}}{V_2(t)}\right)(q_l(t) - A_{eff}\dot{y}(t) - r_p p_l(t)) \tag{C.39}$$

Because of the great difference in order between the pressure $p_l(t)$ and for example the displacement $y(t)$, numerical problems occur if equation C.39 is solved in this form. Therefore a scaling of the pressure is introduced as already used in equation C.11. Using this scaling, rearranging of some variables and equations C.34, C.35 yields

$$\dot{p}_n(t) = \frac{E_{oil}A_{eff}}{p_s}\left(\frac{1}{V_1(t)} + \frac{1}{V_2(t)}\right)\left(\frac{q_l(t)}{A_{eff}} - \dot{y}(t) - R_p p_n(t)\right) \tag{C.40}$$

with

$$R_p = \frac{r_p p_s}{A_{eff}} \tag{C.41}$$

Now the load pressure $p_l(t)$ can be calculated. Combining this result with equation C.29, this leads to the upset force generated by the hydraulic system.

C.1.3 External mechanics

Following from the previous section, the displacement as well as the velocity of the rod influences the force the hydraulic system generates. This means a feedback of these variables from the external mechanics to the hydraulic actuator and servo valve is necessary in modelling the system (see Figure C.1). When the hydraulic system is actuated without a real load, the only mechanics of interest are the moving mass of the piston and the friction inside the hydraulic cylinder. When the hydraulic system is coupled to the welding machine, a mass of about 300 kg has to be moved and static friction have to be overcome. Finally when the system is coupled to the mechanics of the weld process, the damping and stiffness of the material become significant. The damping of the material has the same effect on the total system as the viscous friction in the hydraulic cylinder. So the friction inside the cylinder and the mass of the piston alone, can be neglected with respect to those of the mechanical system.

Hence, in modelling the hydraulic system alone, a model of the mechanics as shown in Figure C.5(A) is used. The resulting model is:

$$F(t) = m\ddot{x}_A(t) \tag{C.42}$$

When the hydraulic system is coupled to the welding machine, a model as shown in C.5(B) is used, now including friction and the moving mass of the welding machine:

$$F(t) = m(\ddot{x}_B(t) - F_f sign(\dot{x}_B(t))) \tag{C.43}$$

When it is coupled to the model of the weld process finally, a model as shown in C.5(C) is used, now including the material stiffness and damping as well:

$$F(t) = m\left(\ddot{x}_C(t) - F_f sign(\dot{x}_C(t)) - b_m(t)\dot{x}_C(t) - k_m(t)x_C(t)\right) \tag{C.44}$$

with m the mass of the moving part of the setup, F_f the amount of static friction in the welding machine, dependent on the direction of the velocity (see section 3.4) and $k_m(t)$ and $d_m(t)$ the stiffness respectively the damping of the material. The combination of the hydraulic process and the mechanics of the weld process (Figure C.5(C)) is discussed in more detail in section 3.4.
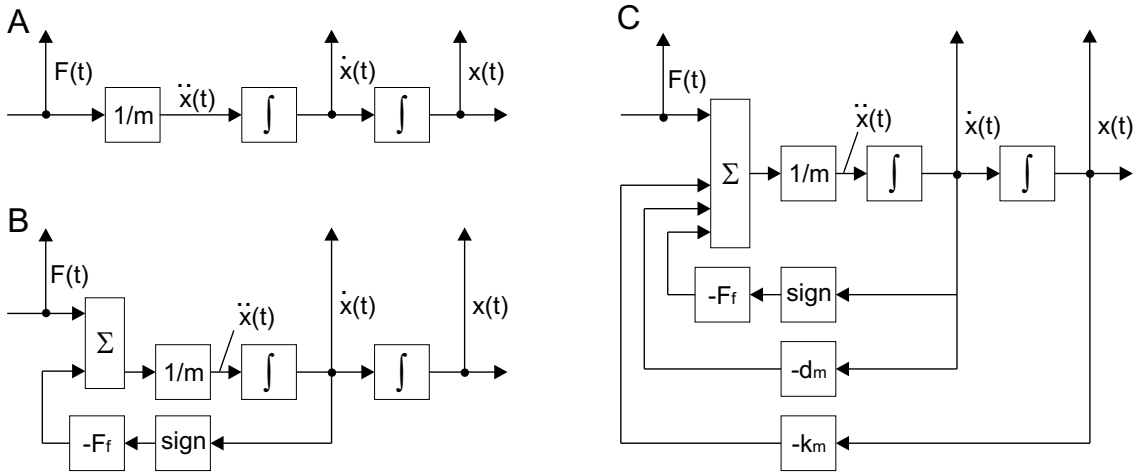

Figure C.5: schematic representation of three examples to model the external mechanics of the hydraulic system. The force $F(t)$ is generated by the hydraulic cylinder. $F(t)$, $x(t)$ and $\dot{x}(t)$ are used in modelling of the servo valve and the hydraulic cylinder.

C.2   Measurements

Validation of the white box model is done by performing measurements at the hydraulic system of the setup (see section 3.6). The relatively small allowable stroke of the hydraulic cylinder with respect to the amount of static friction present in the setup, the present electronic components and the relatively large moving mass of about 300 kg, made it delicate to perform measurements at the setup without damaging anything. Hence, experiments are also performed on another setup at the department of mechanical engineering at the University of Technology Eindhoven. In this way the insight in and conception of the behaviour of the hydraulic system is expanded. This setup included an electric hydraulic high performance servo valve. The valve was coupled to a one side single rod-end cylinder with hydrostatic bearings and a mass of about 130 kg. The mass was mounted onto a carriage. A paper on modelling and control of this hydraulic system is published [Wijnheijmer & Naus, 2005].
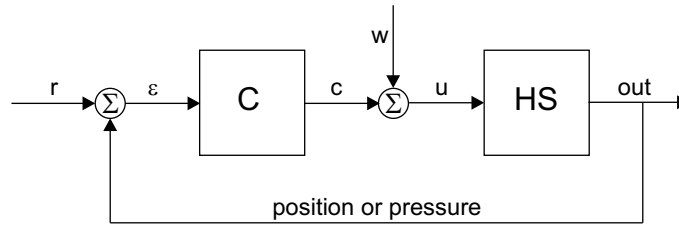
Figure C.6: schematic representation of the measurement setup for performing sensitivity or direct measurements to determine the transfer function of the hydraulic system HS with C a feedback controller.

To examine the characteristics of the system, the frequency responses of the system are determined using two techniques. A closed loop setup as depicted in Figure C.6 is used to prevent drifting of the system. Because of this, a sensitivity measurement is preferable for the determination of the position frequency response of the system. A direct measurement gives good results for the determination of the pressure frequency response of the system. The disturbance signal w in Figure C.6 is omitted in case of a direct measurement. The signal r is a reference signal, which in case of a direct measurement consists of two parts. Firstly it has to be a signal with enough frequency content to determine the frequency response of the system H over a large frequency range, for example a white noise-alike signal. Secondly it consists of a prescribed trajectory, for example a constant position or pressure, which prevents drifting of the system. The white noise-alike signal is added to this second reference signal. In case of a sensitivity measurement the disturbance signal w in Figure C.6 fulfils this function and the reference signal only consists of the reference trajectory to prevent drifting of the system. Instead of a white noise-alike signal a so-called chirp signal may be used. This introduces an input signal with increasing and decreasing frequency input in between a prescribed frequency range. Because of the integrating behaviour of the hydraulic system however, the magnitude of the chirp signal will decrease with increasing frequencies. In combination with the relatively large amount of static friction present in the setup and the limited stroke of the rod of the hydraulic cylinder, it is difficult to keep the system in jogging mode (moving) to overcome the static friction safe enough not to damage the setup. Some measurements using a chirp signal as input signal over a small frequency region are performed, especially in the frequency regions where a noise signal did not give good enough results. The results however were worse than those with a white noise-alike input signal. For the controller C in Figure C.6 a small gain was used, which has to keep the system in the vicinity of the prescribed trajectory and therefore prevent drifting of the system. For this gain is compensated in the calculations afterwards.

Using the direct measurement technique out and u are measured to determine the hydraulic system HS directly

$$HS = \frac{out}{u} \tag{C.45}$$

with out the force $F(t)$ or the displacement $y(t)$. If the measured signals are transformed to the frequency domain using a Laplace transformation, the transfer functions of the hydraulic system HS result

$$H_P = \frac{P}{U} \tag{C.46}$$

$$H_y = \frac{Y}{U} \tag{C.47}$$

Using the sensitivity measurement technique the sensitivity S of the system for a disturbance signal is measured from which the transfer functions of the system can be derived using the following equations.

$$u = w + C(r - out) \tag{C.48}$$

If a signal with only very small frequency content is chosen as a reference signal, the influence on the output signal will be negligible with respect to the influence of the disturbance signal w and r may be neglected and equation C.48 becomes

$$u = w - Cout \tag{C.49}$$

If the measured signals are transformed to the frequency domain using a Laplace transformation the sensitivity S results

$$S = \frac{U}{W} \tag{C.50}$$
$$= (1 + HC)^{-1} \tag{C.51}$$

From this the system H can be calculated

$$H = C^{-1}(S^{-1} - I) \tag{C.52}$$

The results of the measurements are shown and discussed in section 3.6.3.

C.3   Black box modelling

The transfer functions resulting from the measurements can be used to fit a black box model of the system. From the white box modelling however some restrictions to the black box fit can be determined. Combining the model of the hydraulic system and the external mechanics of Figure C.5(C) leaving the friction out, a representation of the total mechanics of the weld process results. To gain better understanding in the frequency responses of the total model, they are derived using the white box model. In this way the two resulting frequency responses are deducted. The effect of an input signal to the servo valve on the resulting pressure $p_l(t)$ and the effect of the input signal on the resulting displacement $y(t)$ are examined.

Summarising the pressure-based equations

$$P_n = \frac{\dot{p}_l}{sp_s} \tag{C.53}$$
$$\dot{p}_l = \frac{E_{oil}L}{\frac{L^2}{4} - y^2}\left(\frac{q_l}{A} - \dot{y}\right) \tag{C.54}$$
$$q_l = q_n x_n(1 - signx_n p_n) \tag{C.55}$$

Combining these equations and rearranging the variables results in the following equation for the frequency dependent pressure

$$P_n = \frac{E_{oil}L(X_n q_n - YsA)}{Asp_s(\frac{L^2}{4} - Y^2) + \frac{q_n}{2}signX_n E_{oil}L} \tag{C.56}$$

with P_n, Y and X_n the Laplace transformed frequency dependent variables based on $p_n(t)$, $y(t)$ and $x_n(t)$.

The position-based equations are

$$Y = \frac{\dot{y}}{s} \tag{C.57}$$
$$\dot{y} = \frac{\sum F}{s^2 m} \tag{C.58}$$
$$\sum F = p_n A - ky - d\dot{y} \tag{C.59}$$

which results in the following equation for the frequency dependent position

$$Y = \frac{P_n A}{ms^2 + ds + k} \tag{C.60}$$

Substitution of equation C.60 in equation C.56 yields

$$P_n(c_4 s^3 + c_5 s^2 + c_6 s + c_7) = X_n(c_1 s^2 + c_2 s + c_3) + c_a P_n^3 \tag{C.61}$$

and if variations around the working point $p_n(t_1) = 0$ are assumed to be very small, the higher order terms like $p_n(t)^3$ can be neglected. This results in the following expression for the frequency dependent pressure response

$$\frac{P_n}{X_n} = \frac{c_1 s^2 + c_2 s + c_3}{c_4 s^3 + c_5 s^2 + c_6 s + c_7} \tag{C.62}$$

with

$$\begin{cases} c_1 &= E_{oil} L q_n m \\ c_2 &= E_{oil} L q_n d \\ c_3 &= E_{oil} L q_n k \\ c_4 &= \frac{A}{4} L^2 m p_s \\ c_5 &= \frac{d}{4} A L^2 p_s + \frac{q_n}{2} sign(x_n) E_{oil} L m \\ c_6 &= \frac{k}{4} A L^2 p_s + \frac{q_n}{2} sign(x_n) E_{oil} L d + A^2 E_{oil} L \\ c_7 &= \frac{q_n}{2} sign(x_n) E_{oil} L k \end{cases} \tag{C.63}$$

Substitution of equation C.56 in equation C.60 yields

$$Y(c_9 s^3 + c_{10} s^2 + c_{11} s + c_{12}) = X_n(c_8) + c_b Y^3 \tag{C.64}$$

and if variations around the working point $y(t_1) = 0$ are assumed to be very small as well, the higher order terms like $y(t)^3$ may be neglected also. This results in the following equation for the frequency dependent position response

$$\frac{Y}{X_n} = \frac{c_8}{c_9 s^3 + c_{10} s^2 + c_{11} s + c_{12}} \tag{C.65}$$

with

$$\begin{cases} c_8 &= A E_{oil} L q_n \\ c_9 &= \frac{A}{4} L^2 m p_s \\ c_{10} &= \frac{d}{4} A L^2 p_s + \frac{q_n}{2} sign(x_n) E_{oil} L m \\ c_{11} &= \frac{k}{4} A L^2 p_s + \frac{q_n}{2} sign(x_n) E_{oil} L d - A^2 E_{oil} L \\ c_{12} &= \frac{q_n}{2} sign(x_n) E_{oil} L k \end{cases} \tag{C.66}$$

As follows from equations C.62 and C.65 both responses contain 3 poles. The definition of the constants c_i in equations C.63 and C.66 show that these poles correspond. So in fitting a black box model of the system using the transfer functions of the measurements, it has to be taken into account that the poles of both fits correspond to each other. From the equations describing both responses follows furthermore that the response of the pressure has two extra zeros. This can be explained by the fact that the pressure is proportional to the acceleration, which is the second derivative of the position.

At low frequencies, the pressure response as well as the position response (equations C.62 and C.65) start with zero phase due to the stiffness k and damping d of the material present. If the material is omitted, the pressure response will start with $+90$ deg and the position response with -90 deg. At high frequencies, the influence of the material's behaviour disappears. The pressure response ends with -90 deg and the position response with -270 deg as is the case if the material is omitted.

Appendix D

Weld process model

An overview of the model of the weld process based on the model developed in Chapter 3 and the assumptions made in section 4.3 is given in this Appendix. In the first section the nonlinear state-space representation of the model is given. In section D.2 the transfer functions resulting from a linearisation of this model discussed in section 4.4.

D.1 Nonlinear state-space model

Defining the state vector $\underline{x}(t)$

$$
\underline{x}(t) = \begin{bmatrix}
x_1 & = & \text{normalised spool valve position } x_n(t) \\
x_2 & = & \text{velocity of the normalised spool valve movement} \dot{x}_n(t) \\
x_3 & = & \text{normalised pressure } p_n(t) \\
x_4 & = & \text{welding seam temperature } T(t) \\
x_5 & = & \text{displacement of the right clamp } y(t) \\
x_6 & = & \text{velocity of the right clamp } \dot{y}(t) \\
x_7 & = & \text{electrical current } i(t) \\
x_8 & = & \text{time derivative of the electrical current } \dot{i}(t)
\end{bmatrix}
\tag{D.1}
$$

the input vector $\underline{u}(t)$

$$
\underline{u}(t) = \begin{bmatrix}
u_1 & = & \text{inverter control signal } u_i(t) \\
u_2 & = & \text{servo valve control signal } u_v(t)
\end{bmatrix}
\tag{D.2}
$$

and the output vector $\underline{y}(t)$

$$
\underline{y}(t) = \begin{bmatrix}
y_1 & = & \text{displacement } y(t) \\
y_2 & = & \text{temperature } T(t) \\
y_3 & = & \text{normalised pressure } p_n(t)
\end{bmatrix}
\tag{D.3}
$$

The nonlinear state-space model of the weld process becomes

$$
\begin{aligned}
\underline{\dot{x}}(t) &= \underline{f}(\underline{x}(t), \underline{u}(t)) \\
\underline{y}(t) &= \underline{g}(\underline{x}(t), \underline{u}(t))
\end{aligned}
\tag{D.4}
$$

with

$$
\underline{\dot{x}}(t) \quad = \quad \underline{f}(\underline{x}, \underline{u})
\tag{D.5}
$$

$$
= \begin{bmatrix}
\dot{x}_n(t) \\
\ddot{x}_n(t) \\
\dot{p}_n(t) \\
\dot{T}(t) \\
\dot{y}(t) \\
\ddot{y}(t) \\
\dot{i}(t) \\
\ddot{i}(t)
\end{bmatrix}
$$

The accompanying system of differential equations resulting from the modelling in Chapter 3 and the assumptions made in section 4.3 are

$$
\begin{aligned}
\dot{x}_1 &= x_2 \\
\dot{x}_2 &= c_1 u_2 + c_2 x_2 + c_3 x_1 \\
\dot{x}_3 &= c_4 q_l \left(c_5 + c_6 x_5^2 + c_7 x_6 + x_6 x_5^2 + c_8 x_3 + c_9 x_3 x_5^2 \right)^{-1} \\
\dot{x}_4 &= c_{10} \left(c_{11} + x_5 \right)^{-1} \left(c_{12} x_7^2 + c_{13} x_5 x_7^2 + c_{14} x_4 x_7^2 + \ldots \right. \\
&\quad + c_{15} x_4 x_5 x_7^2 + \left(T_y(t) + c_{17} \right)^{-1} \left(c_{16} x_7^2 F(t)^{-1} T_y(t) + \ldots \right. \\
&\quad + c_{18} x_7^2 F(t)^{-1} x_4 T_y(t) + c_{19} x_7^2 F(t)^{-1} x_4 + c_{20} x_7^2 F(t)^{-1} x_4^2 \left. \right) + \ldots \\
&\quad + c_{21} x_6 x_4 + c_{22} (c_{10} + x_5)^{-2} + c_{23} (c_{10} + x_5)^{-2} x_5 \\
&\quad \left. + c_{24} (c_{10} + x_5)^{-2} x_4 + c_{25} (c_{10} + x_5)^{-2} x_5 x_4 \right) \\
\dot{x}_5 &= x_6 \\
\dot{x}_6 &= c_{26} F(t) + c_{27} k(t) x_5 + c_{27} d(t) x_6 \\
\dot{x}_7 &= x_8 \\
\dot{x}_8 &= c_{28} u_1 + c_{29} x_8 + c_{30} x_7
\end{aligned}
\tag{D.6}
$$

with

$$
\begin{aligned}
F(t) &= c_{31} x_3 & &\text{(D.7)} \\
k(t) &= \begin{cases} k_{el} & \text{for } x_4 \leq T_y(t) \\ 0 & \text{for } x_4 > T_y(t) \end{cases} & &\text{(D.8)} \\
d(t) &= \begin{cases} d_{el} & \text{for } x_4 \leq T_y(t) \\ c_{32} x_4^{-1} + c_{33} F(t) x_4^{-1} & \text{for } x_4 > T_y(t) \end{cases} & &\text{(D.9)} \\
T_y(t) &= c_{34} + c_{35} F(t) & &\text{(D.10)} \\
q_l(t) &= q_n \left(c_1 - \frac{x_3}{2} \operatorname{sign}(x_1) \right) & &\text{(D.11)}
\end{aligned}
$$

and using

$$
\begin{aligned}
c_1 &= \omega_{v,o}^2 \\
c_2 &= -2\omega_{v,o}\xi_v \\
c_3 &= -c1 \\
c_4 &= \frac{E_{oil}L}{4p_s} \\
c_5 &= \tfrac{1}{4}A_{eff}L^2 \\
c_6 &= -A_{eff} \\
c_7 &= -\frac{L^2}{4} \\
c_8 &= c_7 R_p \\
c_9 &= R_p \\
c_{10} &= -\frac{1}{\rho C_p A} \\
c_{11} &= -x_{init} \\
c_{12} &= \frac{x_{init}\rho_{e,r}}{A}\left(1 - \alpha_\rho T_r\right) \\
c_{13} &= \frac{\rho_{e,r}}{A}\left(\alpha_\rho T_r - 1\right) \\
c_{14} &= \frac{x_{init}\rho_{e,r}\alpha_\rho}{A} \\
c_{15} &= -\frac{\rho_{e,r}\alpha_\rho}{A} \\
c_{16} &= \frac{\rho_{e,r}}{2}\frac{\pi}{3}HB_r\left(1 - \alpha_\rho T_r\right) \\
c_{17} &= -T_r \\
c_{18} &= \alpha_\rho \frac{\rho_{e,r}}{2}\frac{\pi}{3}HB_r
\end{aligned}
\qquad
\begin{aligned}
c_{19} &= -c_{16} \\
c_{20} &= -c18 \\
c_{21} &= -A\rho C_p \\
c_{22} &= -4x_{init}A\lambda_r T_r \\
c_{23} &= 4A\lambda_r T_r \\
c_{24} &= 4x_{init}A\lambda_r \\
c_{25} &= -4A\lambda_r \\
c_{26} &= \frac{1}{m} \\
c_{27} &= -c_{26} \\
c_{28} &= G_{cs}\omega_{cs,o}^2 \\
c_{29} &= -2\omega_{cs,o}\xi_{cs} \\
c_{30} &= -c_{28} \\
c_{31} &= 0.1p_s A_{eff} \\
c_{32} &= \frac{d_{pl,r}T_{y,r}}{AE_{oil}\alpha_{th}} \\
c_{33} &= -\frac{d_{pl,r}}{AE_{oil}\alpha_{th}} \\
c_{34} &= T_{y,r} \\
c_{35} &= -\frac{1}{AE_{oil}\alpha_{th}}
\end{aligned}
$$

The potential difference over the electrodes is measured in the setup used in this study. In combination with the electrical current the resistance of the material to be welded in between the electrodes can be calculated relatively easy. The calculation of the bulk and contact resistance in which a lot of material parameters and assumptions are present (see Section 2.3.4) then is substituted and the validation of the calculated temperature becomes more easily. The fourth equation in the system of differential equations D.6 then becomes

$$
\begin{aligned}
\dot{x}_4 &= c_{10}\left(c_{11} + x_5\right)^{-1}\left(x_7 x_9\right) + ... \\
&\quad + c_{21}x_6 x_4 + c_{22}(c_{10} + x_5)^{-2} + c_{23}(c_{10} + x_5)^{-2}x_5 \\
&\quad + c_{24}(c_{10} + x_5)^{-2}x_4 + c_{25}(c_{10} + x_5)^{-2}x_5 x_4\Big)
\end{aligned}
\tag{D.12}
$$

with the extra state

$$
x_9 = \text{potential difference over the clamps } U(t)
\tag{D.13}
$$

D.2 Transfer functions

In Figures D.1 and D.2 the transfer functions of the linearised models based on the model of the previous section are shown. Figures D.1 shows the transfer functions for the linear model H_1 describing the heating phase of the weld process. Figures D.2 shows the transfer functions for the linear model H_2 describing the yielding phase of the weld process.
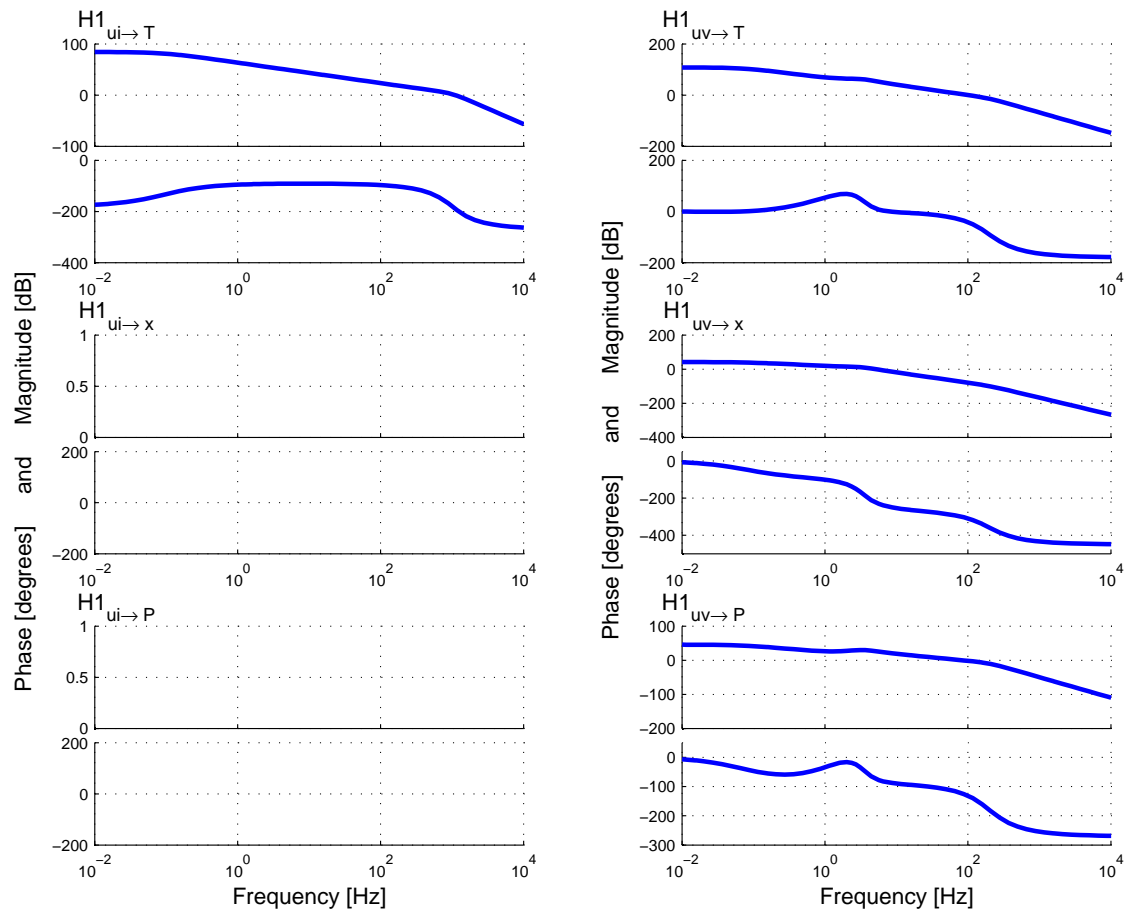
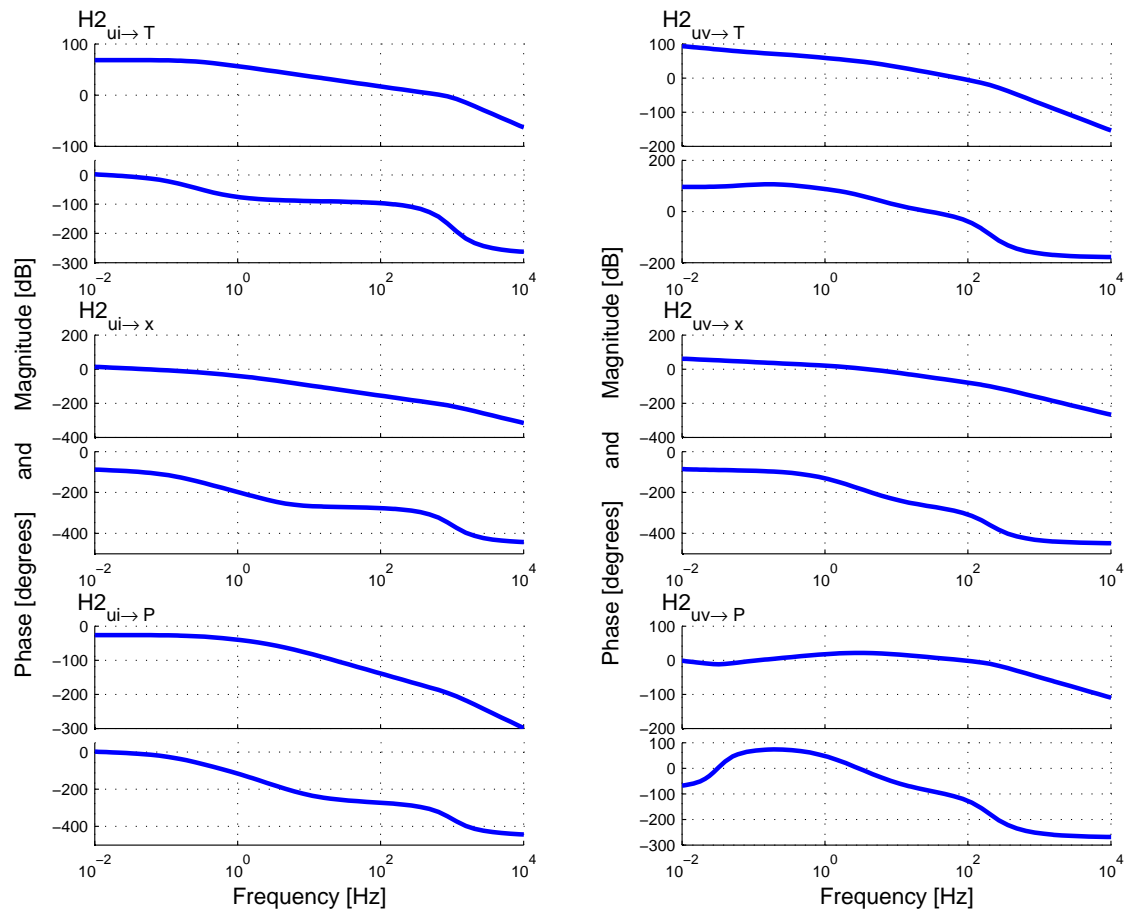Figure D.1: transfer functions for the linear model H_1 of the heating phase.

Figure D.2: transfer functions for the linear model H_2 of the yielding phase.

Appendix E

MCDesign

Various tools like DIET (Do It Easy Tool) [DIET, 2003] and SISOtool which is a tool of the control system toolbox of MatlabR13 exist for controller design using loop shaping techniques. Most of these tools are developed for controller design of SISO systems or models. For MIMO loop shaping no appropriate tool is at hands. Therefore MCDesign (MIMO Control Design) [MCDesign, 2005] was developed by G.J.L. Naus and F.P. Wijnheijmer to facilitate working with these systems and models.

MCDesign uses the MatlabR13 environment and consists of three main parts. The dtf-data object, which facilitates working with measurement data. Calculation with SISO as well as MIMO data and models is reduced to summation, multiplication, et cetera of the dtf object. CDesign is a tool to apply loop shaping and pole-zero placement techniques to SISO systems. Using CDesign, controllers can be designed as well as black box fits of measurement data can be made. MDesign is the command window controlling the data, especially suited for MIMO systems. In the main window, the various transfer functions of the system are shown from where controllers, fits of the data, et cetera can be designed. To simplify importing measurement data into MDesign, SDesign is developed. SDesign is a tool to convert measurement input output data to data-based transfer functions, which can be imported into MDesign. In the near future among other things, also MIMO system data fitting, which signifies 'grey' box fitting with fixed poles as well as $\mathcal{H}_\infty$ control will be implemented.

For a thorough description of the MCDesign tool, see the MCDesign Manual [MCDesign manual, 2005].

Appendix F

Matlab tools

An overview of the main Matlab tools developed during this study to support the various parts of the project is listed in this Appendix. The tools are all easy accessible and usable with a clear help file and included in corresponding folders.

Experiments

Modelling

`tellerfedern.m`	modelling of Belleville springs
`resistances.m`	modelling of temperature dependent bulk resistance and contact resistance (makes use of `temperatureprofile.mat`)
`Cv.m`	modelling of specific heat C_v
`specific_resistivity.mdl`	modelling of the specific resistivity $rho_e(T)$
`parameters.m`	geometrical and material parameters of the weld process used in modelling and simulation
`materials.m`	geometrical and material parameters of the weld process used in modelling and simulation
`weldprocess.mdl`	simplified nonlinear model of the weld process, which can be used for quick simulation to get a good indication of the weld process
`simulationmodel.mdl`	extensive nonlinear model of the weld process (makes use of blocks of the `URW_Library.mdl` and `materials.m`)
`plot_temp.m`	to make a 3D plot of the temperature profile resulting from the simulation model
`URW_Library.mdl`	Upset Resistance Welding Simulink library (makes use of `slblocks.m`, which is needed to include the URW-library to the general Simulink library)

Hydraulics

`valve.m`	modelling of the servo valve
`hydraulicsmdl.mdl`	model of the hydraulic actuator: servo valve, hydraulic cylinder and external mechanics (makes use of `HydParam.m`)
`hydraulicsm.m`	automated function to run `hydraulicsmdl_func.mdl`, which is the same model as `hydraulicsmdl.mdl`
`sensitivity.m`	frequency analysis of the hydraulic model or measurements (makes use of `hydraulicsm.m`)
`sensitivity_auto.m`	automated frequency analysis of 1. the hydraulic model of `hydraulicsmdl.mdl` (makes use of `sensitivity.m`) 2. measurement data (makes use of `overdracht.m`)

Control - control and linearisation

`WELD2001.mdl`	weld control program of the setup, based on WELD2000 [Fontijne, 2000]
`TempTest.m`	to simulate measurement data off-line and check for example the resistance calculation (makes use of `loaddata_TempTest.m` and `TempTestmdl.mdl`)
`ProcessSimulation.mdl`	simulation model of the controlled system including the nonlinear model and the new control block to implement (the temperature calculation and the controller)
`linearise.m`	automated linearisation of the model of the weld process (makes use of `../modelling/weldprocess.mdl`, `linear_part.mdl` and `../modelling/parameters.m`)
`linear_part.mdl`	part of the linearised weld process
`2PointLin.mat` and `5PointLin.mat`	linearised models, using 2 respectively 5 linearisation points (with the latter one 2 points are chosen in the heating phase)

Reference - reference trajectory (generator)

`refgen.c` and `refgen.dll`	original C-code and resulting .dll-file for the design of a crooked sine
`refger.c` and `refger.dll`	c-code and resulting .dll-file for the design of a crooked sine based on `refgen.c`
`testrefger.mdl`	model to test the operation of `refger.dll` (see also `testrefgen.mdl`)
`reftrajger.mdl`	reference trajectories based on model and material properties

Implementation

`param2mat.m`
`reftraj2mat.m`

Mtools - Matlab functions used in various files

`nearest.m`	to find a point in a data series closest to a given value